PEGGY KRISTINA TAYLOR
Study of Biologically Active Forms of Metalloproteins by Electrospray Ionization Fourier Transform Ion Cyclotron Resonance Mass Spectrometry
(Under the direction of IVES JONATHAN AMSTER)

Applications of high resolution mass spectrometry to the characterization of metalloproteins are developed. Metalloproteins in nondenaturing solutions are analyzed by electrospray ionization (ESI) mass spectrometry. ESI places a number of charges on the ion, reducing the mass-to-charge ratio of the ion and making it more easily studied by mass spectrometry. Fourier transform ion cyclotron resonance (FTICR) mass spectrometry is known for its high mass accuracy and high resolution, making it an ideal tool for the study of metalloproteins. By ESI-FTICR mass spectrometry, it is possible to determine the identity of the metal at the active site of a protein. ESI-FTICR was used to examine iron- and zinc-containing rubredoxins in a time-course study, examining the rate of incorporation of iron versus zinc into this protein.

Mass accuracy in ESI-FTICR depends on accurate measurement of the cyclotron frequency. However, the frequency is affected by space charge effects, caused by the coulombic interaction of the ions in the cell, which systematically reduce the observed frequency with increasing ion density in the FTICR cell. Prior research has characterized space charge-induced frequency shifts for singly-charged ions. ESI was used to characterize frequency shifts for multiply-charged ions.

The high resolution of FTICR was utilized in the study of bovine hemoglobin dimer and tetramer. In addition to peaks arising from sodium-proton exchange, low intensity peaks were observed in the mass spectrum. Overnight dialysis in oxygen-saturated buffer revealed the presence of two molecules of dioxygen bound to the dimer

and four molecules of dioxygen bound to the substrate, the first mass spectral evidence of oxygen binding to hemoglobin.

Noncovalent interactions play an important role in biology. Often the active site of the complex lies at the interface between the subunits. For this and a number of other reasons, it is important to apply the mass resolution and mass accuracy of FTICR to noncovalent complexes. However, these complexes are typically high mass molecules, stretching the limits of the technique. ESI-FTICR was used to characterize a range of biologically relevant noncovalent complexes, in order to determine the parameters necessary to achieve isotopic resolution of these molecules.

INDEX WORDS: Fourier Transform Mass Spectrometry, FTMS; Fourier Transform Ion Cyclotron Resonance Mass Spectrometry, FTICR; High Resolution Mass Spectrometry; Electrospray ionization, ESI; Metalloproteins; Rubredoxins; Overexpression; Metal Incorporation; Proteins; Space Charge Effects; Mass Accuracy; Quadrupolar Excitation, QE; Noncovalent Complexes; Substrate Binding; Isotopic Resolution

STUDY OF BIOLOGICALLY ACTIVE FORMS OF METALLOPROTEINS BY ELECTROSPRAY IONIZATION FOURIER TRANSFORM ION CYCLOTRON RESONANCE MASS SPECTROMETRY

by

PEGGY KRISTINA TAYLOR

B.S. degree earned 1994

A Dissertation Submitted to the Graduate Faculty

of The University of Georgia in Partial Fulfillment

of the Requirements for the Degree

DOCTOR OF PHILOSOPHY

ATHENS, GA

2000

STUDY OF BIOLOGICALLY ACTIVE FORMS OF METALLOPROTEINS BY ELECTROSPRAY IONIZATION FOURIER TRANSFORM ION CYCLOTRON RESONANCE MASS SPECTROMETRY

by

PEGGY KRISTINA TAYLOR

Approved:

Major Professor: I. Jonathan Amster

Committee: Rich Dluhy
Don Kurtz
Ron Orlando
John Stickney

Electronic Version Approved:

Gordhan L. Patel
Dean of the Graduate School
The University of Georgia
September 2000

DEDICATION

This work is dedicated first and foremost to God, as my life is dedicated to God. There have been dark moments in my graduate school career, and His peace and love have sustained me. There have been many moments of joy, as well, and I cherish them as gifts from God. Secondly, this work is dedicated to my parents, JoAnn and Ken Taylor. They have given me unquestioning support, ceaseless love, and boundless encouragement. I will never be able to thank them enough.

ACKNOWLEDGMENTS

Many different people have contributed many different things during my time of study. Most importantly, I must acknowledge my major professor, Dr. I. Jonathan Amster. From him I have learned many things far beyond equations and instruments, such as the value of stubbornness properly applied to a project which is not yielding results. I have learned the importance of curiosity, as each project inevitably leads to more questions and another project. And, of course, I have learned to always keep two tires on the asphalt.

To group members present and past, many thanks are owed. Dr. Paula Lei and Shubhada Kulkarni laid the groundwork for many of my experiments. Dr. Michael Easterling and Dr. Cindy Pitsenberger mentored me through my early graduate career. And to Keith Johnson, Todd Mize, Julia Swancy, Brad Swancy, and Bryan Parks, many thanks for maintaining a supportive and positive atmosphere in the lab, and for groaning at a vast array of bad puns.

Finally, to friends who reminded me that my graduate career is not my entire life, I appreciate you more than you know. Matt, Tiffany, Joyous, Chuck, Swigger, Cecilia, and Bryan, you guys are the greatest! Thanks for six years of laughs!

TABLE OF CONTENTS

INTRODUCTION AND LITERATURE REVIEW

This dissertation describes the development of mass spectrometric methods for the analysis of metalloproteins using Fourier transform ion cyclotron resonance (FTICR) mass spectrometry. This introduction will describe ionization methods suitable for protein analysis and basic concepts in FTICR mass spectrometry, and review the field of metalloprotein mass spectrometry.

There are two main components common to every mass spectrometer. First, an ionization source is necessary since all mass spectrometers act on charged molecules. Second, the mass analyzer separates the ions based on their mass-to-charge ratio. Extraneous components such as vacuum system and ion optics are similar in all systems; however, the choice of ionization method and mass analyzer greatly influences the appearance of the mass spectrum.

IONIZATION METHODS

The recent explosion in the field of mass spectrometry of biomolecules can be attributed to the advent of "soft" ionization techniques which are capable of producing intact biomolecular ions without fragmentation. The most commonly used of these techniques are matrix-assisted laser desorption/ionization (MALDI)[1-5] and electrospray ionization (ESI).[6-10] MALDI involves dissolving the sample of interest into a matrix which will absorb radiation of a particular wavelength. The mixture is crystallized onto a surface and irradiated with a laser. Energy is absorbed by the matrix and transferred to the sample, producing a plume of primarily singly-charged ions. MALDI produces singly-charged ions, yielding mass spectra which are relatively uncomplicated; however, high molecular-weight biomolecules may fall outside the practical range of most mass

spectrometers. ESI is a generally more useful technique for the production of ions from high mass biomolecules. The ionization process is represented schematically in Figure 1. For ESI, the sample is dissolved into a solvent, typically 49:49:2 H_2O:MeOH:NH_4OAc (v:v) for denaturing samples, pure water or ammonium acetate for nondenaturing samples. The sample is pumped at a flow rate on the order of 0.5-1.0 μL/min through a metal tip onto which voltage is applied, usually 4-5 kV. Ionization takes place at atmospheric pressure, often in a bath gas, close to the inlet of the mass spectrometer. The mechanism for ion formation is not well understood, but it has been observed that the solution forms a Taylor cone drawn out by electrostatic forces.[11] It is commonly accepted that multiply charged solution molecules exit the tip of the cone and move toward the mass spectrometer inlet. As the solution molecules move through the ambient bath gas, solvent begins to evaporate. Eventually, the charge on the droplet overcomes the surface tension maintaining the droplet, and a "coulombic explosion" produces smaller, multiply charged droplets. This process repeats, producing bare, multiply-charged biomolecular ions which enter the mass spectrometer. The multiple charging of the ions is crucial to the success of ESI as a bioanalytical ionization technique. Since mass spectrometers do not directly measure mass, but rather the ratio of mass-to-charge, multiple charging of the biomolecular ion lowers the mass-to-charge ratio, bringing it within the range of conventional mass spectrometers. ESI produces a range of multiply-charged ions, known as the charge state envelope, where the incremental range of charge states is related to the mass of the molecule. As the mass of the molecule increases, the number of sites available for protonation increases, and both the width and the centroid of the charge state

Figure 1. Electrospray ionization process. A) Voltage placed on a conducting liquid causes droplets to form. As the droplets desolvate, charge overcomes the surface tension, and the droplets undergo a coulombic explosion to form smaller charged droplets, eventually resulting in bare multiply-charged ions. B) Expansion of the Taylor cone formed at the electrospray tip. Adapted from reference 8.

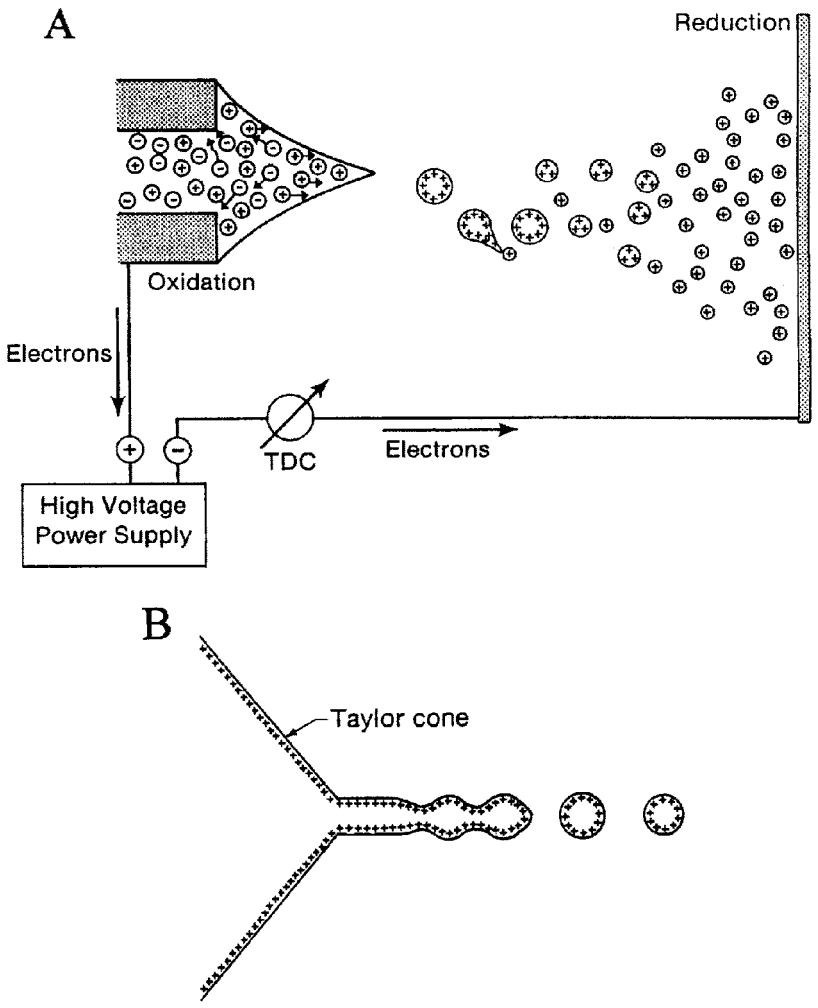
A
Reduction
Oxidation
Electrons
TDC
Electrons
High Voltage
Power Supply
B
Taylor cone

envelope increases. In addition, the choice of solvent influences the charge state distribution, in that denatured proteins have significantly wider charge state envelopes composed of higher charge states than nondenatured proteins, since more sites for protonation are accessible to the solvent.

Nanospray is a variation of electrospray which has proven to be highly effective for the analysis of biomolecules.[12, 13] Nanospray utilizes a micron diameter capillary, which can be produced by drawing fused silica capillary to a fine tip. Flow rates through these tips are greatly reduced compared to conventional ESI, 5-10 μL/hr vs 1-5 μL/min. The small diameter of the tip aids in the desolvation of proteins in aqueous solvents, as the original exit droplets are much smaller. Therefore, there is less total solvent to evaporate and no sheath gas is necessary. The tip is placed approximately 3 mm away from the capillary, allowing more efficient transfer of ions into the source. Lower electrospray voltages are used, aiding in the preservation of noncovalent interactions and metal attachment. Nanospray is useful for examining minimal amounts of protein, as less sample is consumed during the experiment. It has also been shown to be more robust than ESI for samples containing relatively high concentrations of sodium.[13] All of these factors make nanospray the ionization method of choice for the work discussed herein. A schematic of the nanospray setup is shown in Figure 2.

MASS ANALYSIS

A range of mass analyzers exists which can be coupled with various ionization methods. Fourier transform ion cyclotron resonance (FTICR) mass spectrometers, the focus of this work, separate ions based on their motion within a magnetic field.[14-17] An

Figure 2. Schematic of nanospray ionization source, not drawn to scale. A) Syringe pump B) Syringe C) High voltage connection, made on the syringe D) Teflon tubing E) Fused silica nanospray tip F) Heated metal capillary G) Connection to ground.

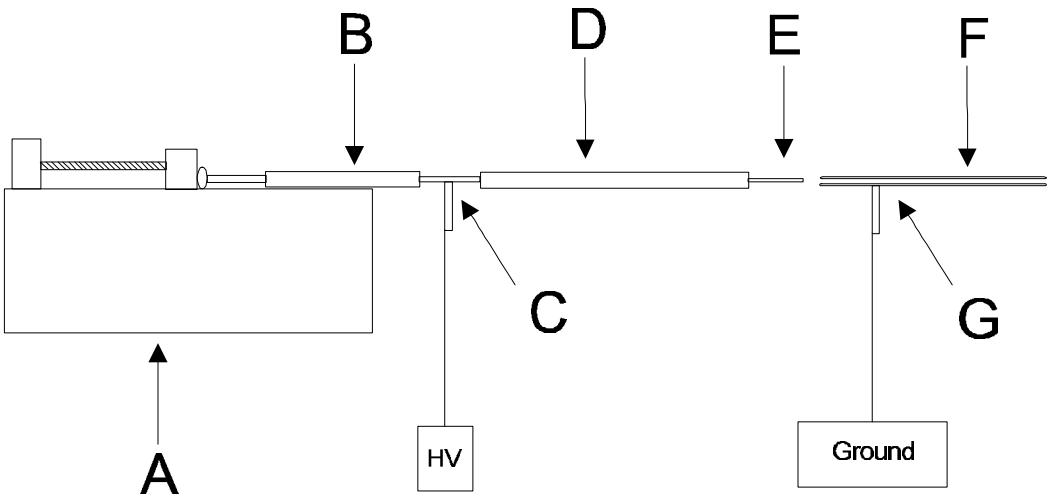
B
D
E
F
C
G
A
HV
Ground

ion in a magnetic field experiences a force defined by Equation 1 , where q is the charge of the ion, v is the velocity of the ion, and B is the strength of the magnetic field.

$$Force = qv \otimes B \qquad (1)$$

An ion with an initial velocity perpendicular to the magnetic field experiences a force constraining it in a circular orbit within the x-y plane around the magnetic field lines, Figure 3. The frequency of the orbit is based on the mass-to-charge ratio of the ion and is given by Equation 2, where w_c is the cyclotron frequency of the ion, q is the coulombic charge on the ion, B is the strength of the magnetic field in Tesla, and m is the mass of the ion in kilograms.

$$w_c = \frac{qB}{m} \qquad (2)$$

Ions of unique mass-to-charge have unique cyclotron frequencies, but ions of the same mass-to-charge with the same kinetic energy orbit the magnetic field lines as a coherent packet. For mass analysis, ions are introduced into an analyzer cell within the magnetic field. The cylindrical analyzer cell used in these experiments is composed of two excite plates and two detect plates, capped by two trap plates, Figure 4.[18] Ions are constrained in the x-y plane by the magnetic field, but free to move along the z-axis. In order to constrain the ions along the z-axis, a voltage is placed on the trap plates of the cell, creating a potential well in which the ions are held. When the ion first enters the cell, the radius of its cyclotron orbit is small, determined only by its initial kinetic energy. However, when a radio frequency (RF) pulse at a frequency in resonance with the cyclotron frequency of the ion is introduced through the excite plates, the orbit of the ion

Figure 3. Force experienced by an ion within a magnetic field. The magnetic field, *B*, extends into the plane of the page. An ion of initial velocity *V* experiences a force *F* causing it to orbit the magnetic field lines.

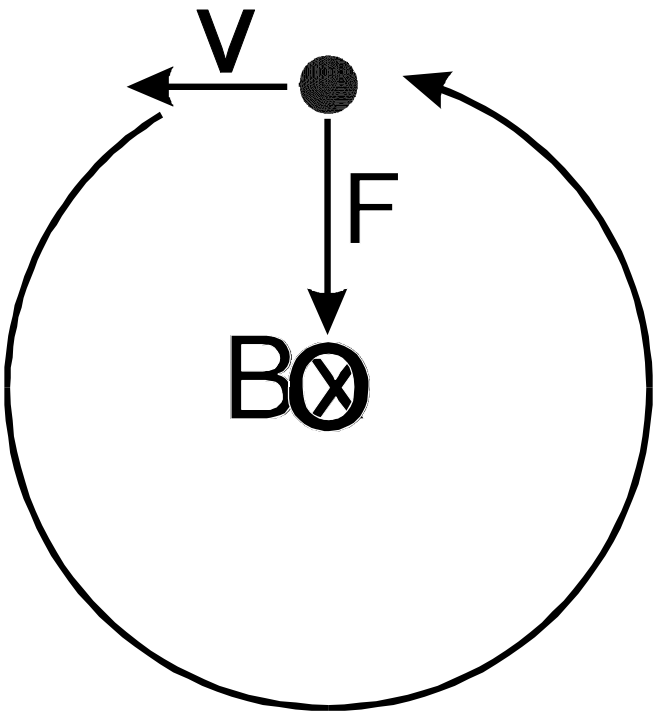
v
F
B⊗

Figure 4. Schematic of the Infinity cell. "E" indicates plates used for excitation. "D" indicates plates used for detection. "T" indicates plates used for trapping the ions. Adapted from reference 16.

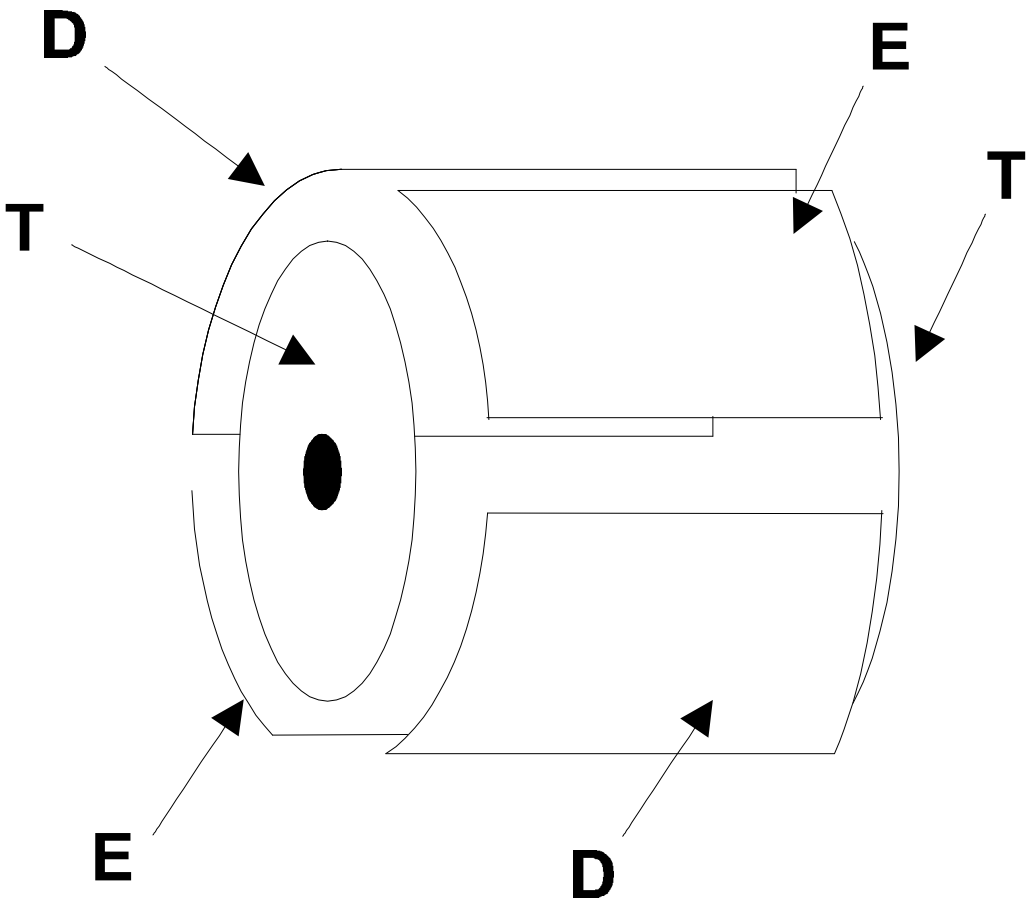
D
E
T
T
E
D

packet increases until the RF pulse is discontinued. Ions of the same mass-to-charge orbit as a coherent packet of charge. The rotating ion packet induces an image current in the detect plates. This image current is translated into a voltage, amplified, and digitized to a sinusoidal time-domain frequency signal of the ion, from which its mass-to-charge ratio can be derived by Equation 2. The actual experiment is somewhat more complex, however, since there are always multiple species of ions within the cell. In addition to the range of charge states produced by ESI, proteins have an isotopic distribution based on the statistical distribution of ^{13}C's within the molecule. Each of these species has a unique cyclotron frequency. Therefore, excitation is applied in such a way as to cause all species within the cell to achieve the same orbit radius. In the most common method of excitation, a frequency sweep known as an RF chirp is applied, moving rapidly through a wide range of frequencies. Although the RF chirp is the simplest way to excite ions, a Fourier transform of the RF chirp shows inequalities in the level of excitation, so that all ions do not get excited to exactly the same radius in the cell. A more uniform method of excitation is known as stored waveform inverse Fourier transform (SWIFT) excitation.[19-23] In this technique, a frequency function corresponding to the mass-to-charge range for desired excitation is defined and converted to an excitation signal by inverse Fourier transformation.

The detected signal, known as a transient or FID, is a composite of sinusoidal signals of different frequencies and amplitudes, based on the cyclotron frequencies of the ions within the cell and the number of ions of each individual cyclotron frequency. This data, after Fourier transformation, yields a frequency spectrum which is converted to a

mass spectrum by applying a calibration equation, Equation 3, where *A* and *B* are experimentally derived by fitting experimental calibrant peak frequencies to theoretically determined frequencies.

$$\frac{m}{z} = \frac{A}{f} + \frac{B}{f^2} \qquad (3)$$

A single ion within the cell, in a perfect vacuum, would produce a sinusoidal signal lasting forever. In practice, however, the signal has a finite lifetime with structure related to the complexity of the mass spectrum. ESI of proteins produces multiple species within the cell, namely a range of charge states, each of which, by Equation 2, has a unique cyclotron frequency. In addition, each charge state is made up of a distribution of isotope peaks, each of which also has a unique cyclotron frequency. Therefore, the resulting time domain signal is a composite of sinusoidal signals of differing amplitudes, based on the number of ions at each mass-to-charge, and differing frequencies. In the time domain signal, there is constructive interference producing a beat pattern, interspersed by regions where the signals interfere deconstructively, yielding noise.[24, 25] The spacing and width of these beats is based on the masses of the ions. As the mass of the ion increases, the spacing between the isotope frequencies decreases. The beats become sharper, and the spacing between them increases. The spacing between beats has been shown to be given by Equation 4, where Δt is the beat period, *m* is the molecular mass of the complex (in Da), *B* is the magnetic field strength in Tesla, and *z* is the charge state of the principal peak.[24]

$$\Delta t \cong \frac{2\pi m^2}{zB} x10^{-8} \qquad (4)$$

For example, a protein of mass 8500 Da with 10 charges at a magnetic field strength of 7 Tesla would have a beat spacing of approximately 65 msec, while a protein of mass 86 kDa with 15 charges at the same field strength would have a beat spacing of approximately 4.4 seconds. In addition to beats, the transient is complicated by damping. As the ion packets have collisions, coherence is lost, causing a decrease in the amplitude of the image current and a concurrent decrease in the strength of the transient. Since the achievable resolution depends on the length of the transient, the preservation of ion packet coherence through ultrahigh vacuum is essential.

There are two forms of motion in the FTICR cell which oppose the cyclotron motion and reduce cyclotron frequency.[16, 17] The first is magnetron motion, and its characteristic frequency is related to the magnitude of the trapping voltage as shown in Equation 5, where ω_m is the magnetron frequency, α is the geometry factor of the cell, V is the trapping potential in volts, a is the distance between the trap plates, and B is the strength of the magnetic field.

$$\omega_m = \frac{\alpha V}{2a^2 B} \qquad (5)$$

There is no mass dependence in Equation 5, indicating that ions of all mass-to-charge ratio exhibit the same magnetron frequency. Magnetron frequency increases with increased trap voltage and reduces with increasing magnetic field strength or increasing dimensions of the analyzer cell. A second perturbation to the cyclotron frequency arises from space charge effects.[26, 27] Space charge effects are caused by ion-ion interactions within the cell. Theory based on a simple model for singly-charged ions suggests that the observed

frequency is reduced by a value given in Equation 6, where ρ is the ion density, G_i is a constant related to the geometry of the ion cloud, q is the charge on the ion, and ε_0 is the permittivity of free space.

$$\delta = \frac{q\rho G_i}{\varepsilon_0 B} \qquad (6)$$

Equation 6 has no mass dependence, but is directly proportional to the charge on the ion. In addition, the effect of space charge is reduced with increased magnetic field strength. This equation has been developed and tested for singly-charged ions. A better understanding of space charge effects for multiply-charged ions is necessary, given the rising popularity of ESI. Taking these perturbations into account, the observed frequency is given by Equation 7.

$$\omega_{obs} = \omega_c - \omega_m - \delta \qquad (7)$$

The effect of magnetron motion on the observed frequency can be accounted for during calibration. The space charge effect on observed frequency is small, and can often be ignored. However, it is also possible to account for space charge, increasing the mass accuracy of the measurement, as discussed in Chapter 3.[28]

The advantages of FTICR consist of high mass resolution and high mass accuracy. The ability to achieve high resolution arises from the fact that FTICR is based on measuring the frequency of rotation of ions in the magnetic field. Advances in electronics over the last three decades have made it possible to measure frequency with a higher degree of accuracy than any other physical measurement. Because of the high resolution of FTICR, it is possible to detect peaks arising from the statistical distribution of isotopes

within each charge state. Figure 5 shows a theoretical mass spectrum of the 8+ charge state of ubiquitin. The binomial distribution is based on the statistical abundance of isotopes; i.e. each peak consists of incremental numbers of ^{13}C, with the intensity based on the 1.1% natural abundance of ^{13}C and the number of ^{13}C's in each peak. The isotope peaks can be used to determine charge state.[29] Since the mass difference between one ^{13}C and two ^{13}C's is 1.003, a singly charged ion would have isotope spacings of 1.003 mass unit divided by 1 charge unit, or roughly m/z 1. A doubly charged ion would have 1.003 mass unit divided by 2 charge units, or roughly m/z 0.5. Therefore, the charge state can be determined by measuring the spacing between the isotopes and inverting. The resolution of isotope peaks also contributes to mass accuracy.[29] Theoretically, the lowest mass peak in the isotope distribution, known as the monoisotopic mass peak (indicated by the arrow in Figure 5), consists of all elements present at their lowest mass isotope (^{12}C, ^{1}H, ^{14}N, ^{16}O, ^{32}S). However, as protein mass increases, the statistical likelihood of observing this monoisotopic mass peak decreases and the peak is lost in the noise region of the measurement. Monoisotopic mass is a more accurate way of reporting mass than average mass, the usual value that is reported. In order to determine monoisotopic mass, however, it is necessary to determine how many ^{13}C's are in each isotope peak. If the amino acid sequence of the protein is known, the elemental composition can be used to create a theoretical mass spectrum of the protein with a particular charge state. The experimentally determined isotope peak intensities can be matched with the theoretically determined peak intensities through a statistical χ^2 test.[29] The isotopic composition of each peak is known for the theoretical mass spectrum. The number of ^{13}C's in each

Figure 5. Theoretical isotopic distribution for the 8+ charge state of ubiquitin, 8565 Da. Arrow indicates the monoisotopic mass peak, arising from a molecule with zero ^{13}C's.

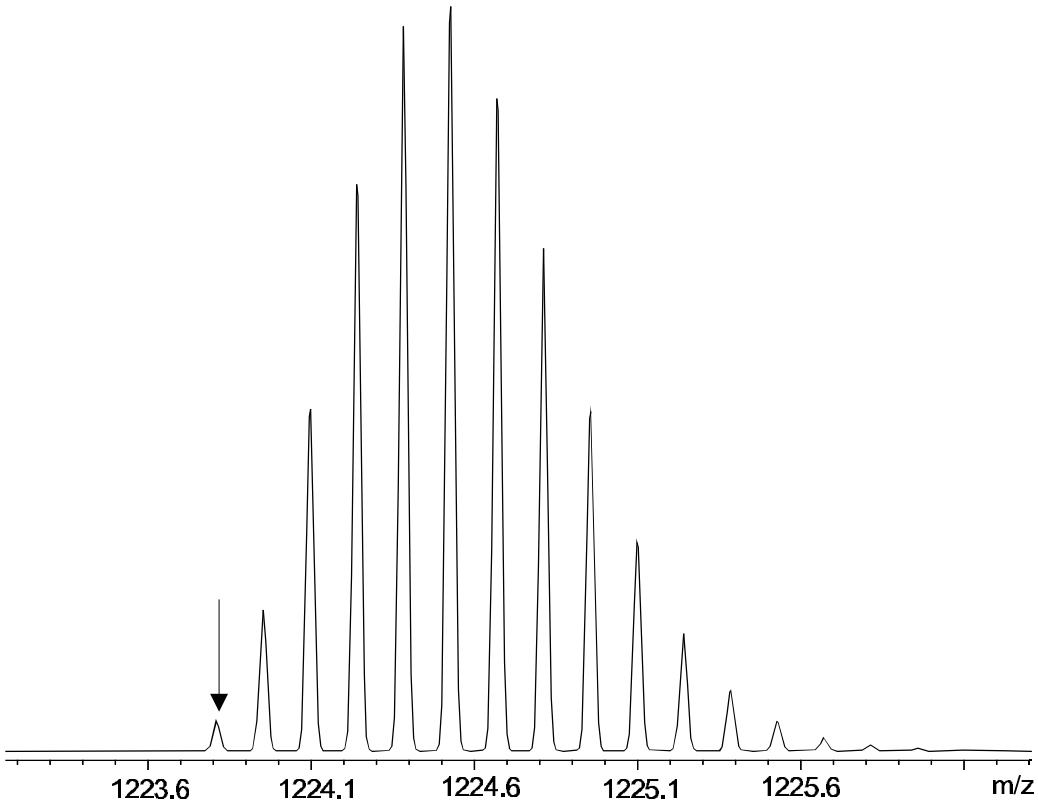
1223.6
1224.1
1224.6
1225.1
1225.6
m/z

experimental isotope peak can be determined by fitting the experimental distribution to the theoretical distribution. The mass of the extra ^{13}C's can be subtracted from the mass of the isotope peak to give the monoisotopic mass. Each isotope peak visible in the mass spectrum can be treated in the same manner, giving a large number of values for the monoisotopic mass. These values can be averaged together to give a highly statistically accurate value for the monoisotopic mass.

FTICR uses a nondestructive detection technique. Unless the ions are ejected from the cell through collisions or a programmed cell quench, they remain in the cell, although the ion packets themselves may lose coherence and produce undetectable signal. It is possible to take advantage of the nondestructive nature of FTICR ion detection to make further observations on already detected ions through an experimental technique known as quadrupolar excitation (QE).[30] In QE, a quadrupolar RF signal in resonance with a particular mass-to-charge ratio of interest is applied to the excite and detect plates, while a collision gas is introduced through a pulse valve. QE causes the interconversion of cyclotron and magnetron motion. Collisions with the background gas dampens cyclotron motion more rapidly than magnetron motion, causing the ions to move back into the center of the analyzer cell. QE prior to ion detection provides more uniform excitation conditions, since the ions are excited from the same point in the center of the cell. In addition, a single batch of ions can be excited and detected, subjected to QE, and excited and detected again in a process known as remeasurement.[31-33] Remeasurement eliminates the variation in the number of ions injected in a series of experiments and increases the signal-to-noise ratio. The disadvantage to QE is that the collision gas must be pumped

away, causing a delay of 20-90 seconds per scan, which greatly increases the experiment time.

Broadband excitation allows the experimenter to excite all species in the cell simultaneously and obtain information on a wide mass range. However, it may be desirable to focus on a narrow mass range containing one charge state, in order to obtain better isotope statistics or stronger signal-to-noise. In FTICR, the number of data points collected determines the length of the transient, given by Equation 8, where *T* is the length of the transient, *N* is the number of data points, and *S* is the sampling rate.

$$T = \frac{N}{S} \qquad (8)$$

The sampling rate is determined by the desired range of mass spectral detection, as the Nyquist criterion requires sampling at least twice the highest frequency detected; e.g. if the lowest mass selected for detection is m/z 500, then its cyclotron frequency given by Equation 2 is approximately 220 kHz, so the lowest sampling rate necessary would be 440 kHz. With a 500 kHz sampling rate, the length of a transient with 256k data points would be approximately 0.5 seconds. Resolution can be calculated according to Equation 9, where *R* is resolution, f_c is frequency, and *T* is transient length.

$$R = \frac{f_c T}{2} \qquad (9)$$

By Equation 9, the resolution for the 0.5 second transient of a peak at m/z 500 would be 55,000. A peak at m/z 3500, typical for high molecular weight biomolecules, with the

same 0.5 s transient length would have a resolution of only 8000. It is evident, therefore, that the transient length must increase as the mass-to-charge of the peak of interest increases, in order to achieve high resolution. It is possible to achieve longer transients by collecting larger datasets, however this is not always desirable. An alternative method of extending transient length is known as heterodyne mode, or narrowband detection.[16] In narrowband detection, the image signal is multiplied by a reference signal close in frequency to the signal of interest, giving a resultant signal containing components with frequencies equal to the sum and difference of the original signal frequencies. The high-frequency component can be removed with a low-pass filter, leaving only the difference frequency. The ion at m/z 3500 has a cyclotron frequency of approximately 32 kHz at 7T. If this frequency is multiplied by a reference frequency of 22 kHz, then the difference frequency is 10 kHz, which can be sampled at 20 kHz. At this sampling rate, a 256k dataset would produce a transient length of 13s, with a resolution of 208,000. Since by Equation 7, the time spacing between beats increases with the mass of the molecule, and it is necessary to detect two beats in order to achieve isotopic resolution,[25] narrowband is a useful tool for extending the observable transient length of high-mass molecules.

Much information about the structure and sequence of proteins can be gained from tandem mass spectrometry, or MS^n. Since FTICR is a non-destructive technique, product ions can be formed from the same packet of precursor ions already in the cell, through a wide variety of techniques. One such is collisionally-activated dissociation (CAD), typically via sustained off-resonance irradiation (SORI).[34-40] In SORI-CAD, an excitation frequency is applied which is slightly off-resonance with the cyclotron frequency of the

precursor ion of interest. Because the frequency is slightly off-resonance, the ion gains excitation energy only periodically. While the SORI pulse is applied, gas is allowed into the system through a pulse valve, raising the pressure and the probability of collisions. When the ion is not gaining excitation energy, it is collisionally cooled toward the center of the cell. The collisions, if they occur with sufficient energy, cause fragmentation, and the resulting product ions, after a suitable pumpdown time, are excited and detected. Two other methods of fragmentation are infrared multiple photon dissociation (IRMPD) and blackbody infrared radiative dissociation (BIRD). These two methods do not require a gas pulse with subsequent pumping delays. In IRMPD, an infrared laser is fired into the ion cloud prior to excitation.[41-45] The energy imparted by the laser causes fragmentation. In BIRD, the vacuum chamber (and the cell) are heated until blackbody radiation occurs, causing energy absorption and fragmentation of the ions.[46-51]

MASS SPECTRAL ANALYSIS OF METALLOPROTEINS

The research discussed in this work has focused on extending the capabilities of ESI-FTICR for the analysis of metalloproteins. The high mass accuracy and high resolution of this technique are valuable for the study of metal oxidation state and stoichiometry, specific binding of various species to metal-containing substrates, and the stoichiometry of metalloprotein noncovalent complexes. This body of research has been concerned with developing methods for sample handling and high-resolution mass analysis. The characterization of metalloproteins by mass spectrometry has been an active area of research, and a review of the existing work follows.

Metalloproteins play a vital role in various biochemical processes such as respiration, muscle contraction and relaxation, metabolism, signal transduction, blood coagulation, and photosynthesis. They contain a range of metals from aluminum to zinc which can either be bound to the protein or held in a noncovalent bond. The metal can serve several different purposes within the protein, including structural stabilization, electron transport, and catalytic function. Many different analytical methods have been applied to the study of metalloproteins; among them are NMR, resonance Raman spectroscopy, Mossbauer spectroscopy, x-ray crystallography, EPR, and mass spectrometry. Mass spectrometry has significant advantages over other analytical methods. It is possible to examine the protein in solution under nondenaturing conditions, retaining the functionality of the protein. Also, mass spectrometry does not require large amounts of sample, which is often a primary consideration in the study of wild type proteins. A variety of mass spectrometric techniques have been used to characterize metalloproteins, including inductively-coupled plasma mass spectrometry (ICP-MS), electrospray ionization (ESI), and matrix-assisted laser desorption ionization (MALDI). These techniques have also been combined with bioinorganic procedures such as proteolytic digestion and site-directed mutagenesis in order to achieve a more complete characterization of the metalloprotein. By exposing the protein to a range of metals and then examining the products by mass spectrometry, it is possible to study the binding abilities of metalloproteins. For metalloproteins in which the metal center is functional rather than structural, ESI is the primary tool for analysis. Several different procedures

have been used to probe the structure of metalloproteins, including HD exchange and examination of the shift of the charge state envelope in ESI.

I. Metalloprotein Binding Studies

A. Metallothioneins

Metallothioneins are small proteins weighing about 6000-7000 Da, consisting of around 60 amino acid residues in the mammalian form. Twenty of these residues are cysteines, giving rise to multiple metal binding sites, while the protein is completely lacking in aromatic amino acids or histidine.[52] Metallothioneins can bind up to seven divalent transition metal ions, typically cadmium, zinc, and copper.[53, 54] All twenty cysteine residues are considered to be involved in the binding of metals. In the native form, metallothionein is suggested to contain a two-cluster structure, with the amino terminal half of the protein binding three metals and the carboxyl terminal half of the protein binding four metals. The metal ions in each domain are bound in a cooperative manner, and are more exposed than metals in larger proteins.[54] Although zinc, cadmium, and copper are the primary metals bound to metallothionein, the protein is capable of binding a variety of heavy metals, and is thought to be involved in metal detoxification, transportation, and storage.[52] Yu et al. used electrospray ionization mass spectrometry (ESI-MS) to examine reconstituted metallothionein under native conditions, in order to quickly and accurately determine the nature and number of bound metals.[53] The metallothioneins were reconstituted with cadmium or zinc ions, and kept at pH 4 to avoid demetallation, and both the Cd_7 and Zn_7 species were observed. Using lower pH levels,

Yu obtained spectra of the protein bound to four cadmiums, indicating that the N-terminal cluster had lost its metals, while the C-terminal cluster possibly bound its metals more tightly. Fabris et al. examined the thiol protons of metallothioneins with ESI-MS.[55] Several different classes of metallothioneins were studied, including protein purified from the native strain, recombinant protein, and a synthetic protein. In all the samples, the observed molecular masses were higher than those expected with complete deprotonation. Only enough protons were lost in each case to balance the charges of the divalent zinc atoms, suggesting partial retention of protons within the metal clusters. Le Blanc et al. used ionspray mass spectrometry (IS-MS) to study metallothioneins which had been separated online with HPLC.[56] Although a Cd_4Zn_3MT was injected onto the column, several different species were observed by mass spectrometry, including a Cd_7MT and a Zn_7MT. Acid was added as a post-column modifier, allowing selective demetallation of the protein by change in the pH.

For the simple determination of metal identity and stoichiometry, ICP-MS is often the method of choice. This technique gives no information about the binding efficiency or structure of metallothionein, but it is a highly sensitive and metal-specific method of detection. Takatera and Watanabe used HPLC/ICP-MS to examine the synergistic effects of different heavy metals on the induction of metallothionein in a cyanobacterium.[57, 58] They noticed that zinc and cadmium each induced metallothionein, while copper alone did not. However, both copper and cadmium showed increased metallothionein induction in the presence of zinc. In addition, it was noted that mercury was seen almost entirely in a protein-bound form, indicating that the free (and therefore reactive) mercury ions were

detoxified by sequestration within the cells. The metallothionein induction by mercury dosing seemed to decrease after a period of 16 hours, in contrast to induction by other metals. Takatera suggested that the Hg-MT could be excreted from the cell. In addition to binding heavy metals, the overexpression of metallothionein seems to confer resistance to several anti-cancer drugs. Zaia et al. explored the existence of a binding site for the drug chlorambucil on metallothionein.[54] After allowing metallothionein to react with chlorambucil, the protein was digested with trypsin, and the fragments were analyzed with MALDI-TOF mass spectrometry. Modifications by chlorambucil were noted in several tryptic fragments. ESI-MS was also used to monitor the reaction between chlorambucil and metallothionein. After 60 minutes, most of the metallothionein was bound to chlorambucil, with no difference in the metal composition of the metallothionein.

B. Vitamin D receptor

The vitamin D receptor is a member of the nuclear hormone receptor family. These proteins contain a 66-70 amino acid DNA binding domain close to the N-terminus of the protein. The vitamin D receptor activates the transcription of over 60 genes. Its DNA binding domain contains two zinc-finger regions that are believed to bind to DNA sequences of vitamin D-responsive genes.[59] Two additional lower affinity binding sites are also postulated. Craig et al. used ESI-MS to examine the effects of zinc binding on the DNA binding domain of the vitamin D receptor.[60] The DNA binding domain of the vitamin D receptor was expressed in *E. coli* in order to produce enough protein for the experiments and reacted with $ZnCl_2$. The zinc stoichiometry was measured by ICP-MS, giving an average of 4 mol of zinc per mol of protein. ESI-MS was used to confirm the

zinc stoichiometry. The primary peak is that of the protein bound to two zinc metals. For the vitamin D receptor DNA binding domain in a 50-fold molar excess of zinc, peaks corresponding to the protein bound to 0-6 zinc metals were observed. These results agree with the presence of two high-affinity zinc finger regions in the protein, and suggest the presence of several lower affinity zinc binding sites. Veenstra et al. used ESI-MS to examine the zinc dependent binding of the vitamin D receptor DNA binding domain to the mouse osteopontin (mOP) vitamin D response element (VDRE).[59] In the presence of zinc, it was found that the vitamin D receptor bound the mOP VDRE in both a 1:1 and 2:1 stoichiometry. Both complexes contained two zinc atoms per protein. Addition of 100 μM zinc ion to the complex solution increased the amount of dimer/DNA complex relative to monomer/DNA complex, but addition of 200 μM zinc ion caused dissociation of the complex. In the absence of zinc, however, no binding to the mOP VDRE was observed. Cadmium, which also binds to zinc-finger domains, effected similar results. From these studies it is conjectured that metal binding to the two zinc-finger regions is necessary for DNA binding, but metal binding to the lower-affinity sites causes dissociation of the protein/DNA complexes.

C. Binding of different metals

Metalloproteins typically have one or two types of metals which they bind preferentially, and these specific metals are necessary for the proper functioning of the metalloprotein. However, it is often possible for the metalloprotein to bind other metals, although the affinity may be lower. It is also possible for proteins to interact with metals even though they are not primarily metalloproteins. One such protein is lysozyme.

Moreau et al. examined hen egg white lysozyme by ESI-MS in the presence of copper and zinc in order to determine the binding capacity of the protein.[61] The mass spectrum of the purified protein in the absence of metal was obtained as a reference. After an excess of copper had been added, the spectrum showed peaks containing up to eight copper atoms complexed with lysozyme, with the major peaks corresponding to 1-3 bound copper ions. These metal-bound proteins showed the same enzymatic activity as the native protein, indicating that the metal did not alter the enzyme structure. When an excess of zinc was added to the purified protein, complexes of the protein with up to six zinc atoms were observed. The primary peaks observed corresponded to the lysozyme-$(Zn)_1$ and lysozyme-$(Zn)_2$ complexes. Again, the enzyme activity was identical with the native protein. When the yeast *Candida glabrata* is exposed to copper, metallothionein proteins are induced by the activity of a copper-responsive transcription factor AMT1. Thorvaldsen et al. studied an AMT1 synthetic gene in the presence of copper and zinc with ESI-MS, among other methods, in order to examine the metal centers.[62] They found that AMT1 bound four copper ions and one zinc ion. After titrating apo-AMT1 with copper, only the AMT1-$(Cu)_4$ species was detected, indicating cooperative binding of the copper ions. Bacteriorhodopsin is a protein in the cell membrane of halobacteria that is involved in photosynthesis. It causes transport of a proton from the cytoplasm of the cell to the outside of the cell via several intermediates. In the native form, bacteriorhodopsin contains magnesium and calcium, and removal of these metal centers negates the activity of the protein. Griffiths et al. used ICP-MS to determine the identity and stoichiometry of the two high-affinity metal centers in native and structurally perturbed bacteriorhodopsin.[63]

It was found that two metal ions were bound per molecule of bacteriorhodopsin, and that there were 3-4 mol calcium per mol magnesium. For structurally perturbed protein, the total metal binding affinity decreased, with a constant ratio of calcium to magnesium, indicating that the decrease in binding affinity was not dependent on the metal identity. The Fur protein is involved in the uptake of iron in bacteria.[64] The presence of divalent metal atoms is necessary for the binding of Fur to DNA. Michaud-Soret et al. used ESI-MS to examine the identity and stoichiometry of metal ions in the Fur protein.[64] Under acidic conditions, each Fur monomer was found to bind either one cobalt or one manganese atom. Under biological conditions, a metal-containing dimer was detected, but it was not possible to identify the identity of the metal, whether one zinc and one manganese, two zinc, or two manganese atoms.

D. Metals in the presence of other metals

Although metalloproteins have an affinity for specific metals, that affinity may be affected by the presence of other metals. If the new metal is similar in size, it is possible for a metalloprotein to bind that metal preferentially. Or the presence of a new metal may increase or decrease the ability of the metalloprotein to bind its native metal. Calmodulin is a protein which binds calcium in a structural role. Calmodulin possesses two EF hand domains, each containing two high-affinity binding sites for calcium. In addition, six low-affinity calcium binding sites are located elsewhere on the protein. Lafitte et al. used ESI-MS to examine the calcium binding affinity of a synthetic calmodulin in the presence of magnesium and terbium.[65] Terbium has a similar ionic radius to calcium and is therefore expected to bind in a similar manner. When terbium was added to metal-free calmodulin,

up to six metals bound to the protein, indicating that not all metal binding sites were occupied. When calcium was added to apo-calmodulin followed by terbium, the observed peaks corresponded to the protein plus four calcium atoms plus a varying number of terbium atoms. When the apo-protein was treated with calcium and magnesium, peaks appeared corresponding to the protein bound to two magnesium atoms plus up to eight calcium atoms. It is suggested that only calcium binds to the main EF hand sites, but there is competition between the different metals for the lower-affinity binding sites.

Cytochrome *c* proteins are found in many organisms from bacteria to mammals. They contain at least one iron-binding heme group, and they are involved in electron transfer.[52] Although many studies have been performed on cytochrome *c*, little is known about the metal binding ability of the protein in the presence of other biologically useful or biologically toxic metals. Bond et al. used ESI-MS to study iron-bound cytochrome *c* in the presence of a wide range of metals.[66] The protein was examined in the presence of mercury, cadmium, zinc, nickel, cobalt, and lead. For all of these metals, it was found that several metal atoms adducted onto the cytochrome *c* peaks, indicating that the metal atoms were replacing protons on the amino acid side chains of the protein. The highest binding affinity was seen for the biologically toxic metal mercury, and at no point was loss of the iron-containing heme observed. These results indicate that cytochrome *c* is a robust protein in the presence of a wide variety of contaminating metals.

II. Metals in a Functional Role

A. Iron Proteins

Ferredoxins and rubredoxins are low molecular weight proteins involved in biological processes like photosynthesis and nitrogen fixation, containing one or two Fe-S centers coordinated by cysteine residues. Myoglobin is a somewhat larger protein (~17560 Da) containing an iron in a noncovalently bound heme group. It is found in the cytosol of muscle proteins and participates in oxygen storage. Both of these types of metalloproteins are a challenge to examine by ESI-MS, because the high voltages necessary to ionize and desolvate the proteins often cause disruption of the noncovalent bonds and loss of the metal centers. Van Dorsselaer et al. used ESI-MS to examine these proteins.[67] For rubredoxin in 50% methanol, peaks corresponding to both apo- and holorubredoxin were observed. For ferredoxin, however, it was necessary to use pure water as a solvent in order to obtain peaks for the holoprotein. The two major peaks corresponded to the protein with a [4Fe-4S] active center and a [4Fe-4S] active center plus one iron. There were also two minor peaks corresponding to a [2Fe-2S] active center and a [2Fe-2S] active center plus one iron. In both rubredoxin and ferredoxin, it was noted that the measured masses fit the expected masses of the proteins with iron and sulfur atoms complexed by cysteine thiolates. For myoglobin under nondenaturing conditions with a low extraction cone voltage, the major species detected was the holoprotein, containing both heme group and iron. A minor peak arising from the apo-protein was also detected. By raising the extraction cone voltage, it was possible to convert nearly all of the holoprotein to apo-protein. Rubredoxin is a small (MW~6000

Da) protein found in several different bacteria, including *Clostridium pasteurianum*. Although the function of rubredoxin is not known with certainty, it is thought to aid in electron transport. In its native state, rubredoxin contains an FeS_4 site. Petillot et al. used ESI-MS to examine rubredoxin purified from *C. pasteurianum* as well as rubredoxin which had been overexpressed in *E. coli*.[68] For rubredoxin purified from the bacterium, the identity and stoichiometry of the metal was confirmed. However, for rubredoxin overexpressed in *E. coli*, a zinc form of the protein was identified in addition to the iron form, with similar stoichiometry. Meyer et al. used ESI-MS to examine a [2Fe-2S] cluster in a variant of *C. pasteurianum* rubredoxin, wherein one of the cysteine residues had been altered to alanine.[69] The mass spectra for this sample showed that in addition to the apo-protein, a species existed whose mass matched the apo-protein plus two iron atoms and two sulfur atoms. The assembly of a [2Fe-2S] cluster was verified by other analytical methods. Ferredoxins are small molecular weight bacterial and plant proteins involved in electron transport, containing iron-sulfur clusters in a wide variety of stoichiometries.[52] Petillot et al. used ESI-MS to observe several different ferredoxins under nondenaturing conditions.[70] By careful manipulation of experimental techniques, they were able to observe a high potential [4Fe-4S] ferredoxin, a low potential 2[4Fe-4S] ferredoxin, and a [2Fe-2S] ferredoxin. Armengaud et al. used ESI-MS to examine a ferredoxin which had been expressed as an apo-protein, and then subjected to chemical insertion of the iron-sulfur cluster.[71] The ferredoxin isolated from *Rhodobacter capsulatus* contains one [3Fe-4S] cluster and one [4Fe-4S] cluster. However, overexpression of ferredoxin complete with metal centers yields only minimal amounts of protein. It was therefore necessary to

express the protein in the apo form and then reconstitute it with the metal centers. The mass of the overexpressed apo-ferredoxin was identical to that purified from the native bacteria. After insertion of the metal, ESI-MS was used to characterize the protein. The mass of the recombinant protein matched that of the apo-protein plus two [4Fe-4S] clusters, rather than containing one [3Fe-4S] cluster as in the native form. This recombinant protein also showed much weaker enzyme activity, added evidence for its erroneous composition. Remigy et al. used H/D exchange to examine the stability of mutated cyanobacterial ferredoxins versus the wild-type proteins.[72] The ferredoxin from *Anabaena* contains a [2Fe-2S] cluster. Two mutants of ferredoxin were examined, F65A and R42A, in order to discern their effects on the protein. ESI–MS was used to verify the presence of the metal cluster and the correct mutation. The replacement of arginine 42 caused a shift in the charge state distribution to higher charge states, indicating a less tightly folded structure. The F65A mutant showed few differences in the charge state distribution from the wild type. A comparison of H/D exchange rates showed that the two mutations had higher H/D exchange rates, and therefore a more open structure, than the wild-type protein. The wild-type protein and the two mutants were allowed to exchange for 12 hours, and then they were subjected to rapid proteolysis. A comparison of the masses of the fragments gave information about the changes in local structure of the protein due to the mutations. Many proteins contain iron which is not bound in an iron-sulfur cluster, and often the proteins must have a specific quaternary structure in order to function. Myoglobin is a protein found in muscle cells which participates in oxygen storage. It contains an iron held in a noncovalently bound heme group. ESI-MS is the

method of choice for the examination of noncovalent complexes, because of its soft ionization conditions. Jaquinod et al. used ESI-MS to examine myoglobin under nondenaturing conditions, in one of the earliest experiments on noncovalent complexes.[67] At low extraction cone voltage two peaks were measured, with the primary peak corresponding to the holo-protein and the minor peak corresponding to myoglobin without the heme or iron. It proved possible to convert all of the holo-protein to apo-protein through application of higher voltages. Lei et al. conducted further work on noncovalent complexes, examining recombinant rubrerythrin and hemerythrin, as well as native hemerythrin isolated from *Lingula reevii*.[73] Hemerythrin is found in some marine invertebrates and is involved in oxygen transport. It is composed of eight subunits, each containing an oxo-bridged diiron site. The native hemerythrin in these studies consists of a hetero-octamer of $\alpha_4\beta_4$ stoichiometry, while the recombinant hemerythrin consists of a homo-octamer. Rubrerythrin is found in anaerobic sulfate-reducing bacteria, and contains an FeS_4 center similar to that of rubredoxin as well as a diiron center similar to that of hemerythrin. Despite the name, hemerythrin does not contain a heme group. For the recombinant hemerythrin, two charge state distributions were observed, one corresponding to the monomer, and one which corresponded to the octameric holoprotein. At a higher nozzle-skimmer voltage, peaks corresponding to the heptamer appeared, and further increase of the nozzle-skimmer voltage gave rise to a hexamer, suggesting a stepwise loss of monomer. Closer examination of the deconvoluted monomer charge state distribution revealed peaks corresponding to the apo form of hemerythrin as well as peaks corresponding to the apo-protein plus one and two iron

atoms, and indicated that the irons were in the 3+ oxidation state. The peak arising from the apo-protein plus one iron atom was seen only at a high nozzle-skimmer voltage and was of very low abundance, indicating that hemerythrin binds two iron atoms in a cooperative manner. Hemerythrin isolated from *L. reevii* was also examined under nondenaturing conditions, and again, two charge state distributions were observed. Deconvolution of the higher mass-to-charge distribution gave a peak corresponding to an octamer composed of $\alpha_4\beta_4$ subunit stoichiometry. At higher nozzle-skimmer voltages, it was possible to remove the monomers in a stepwise fashion to achieve heptamer peaks composed of $\alpha_3\beta_4$ and $\alpha_4\beta_3$ stoichiometries. Examination of the monomer charge state distribution revealed both the α and β subunits, each containing two iron atoms. In the same manner as recombinant hemerythrin, the peaks corresponding to the subunit plus a single iron atom were of much lower abundance, consistent with cooperative binding of the metals. For *D. vulgaris* rubrerythrin under nondenaturing conditions, only peaks corresponding to the tetrameric holoprotein appeared. At increased nozzle-skimmer voltages, the tetramer dissociated into monomer and trimer. The monomer peaks corresponded to the apo-protein plus up to three iron atoms. These experiments definitively demonstrated the ability of mass spectrometry to examine metalloproteins in their oligomeric native state.

B. Copper proteins

Cytochrome *c* oxidase is a protein involved in electron transfer.[74] It catalyzes the reduction of dioxygen to water in eukaryotic organisms and some bacteria.[75] Cytochrome *c* oxidase is composed of two subunits which bind four metal centers. Subunit I is

imbedded in the membrane and contains a bimetallic active center formed by iron and copper. Subunit II is outside the membrane bilayer and binds two copper atoms in a "purple copper" Cu_A center. This center is involved in cytochrome *c* binding and may be the primary electron acceptor. Kelly et al. used ESI-MS along with other techniques to probe the structure of the purple copper center.[76] The binding of two copper atoms per protein was verified, and the ligands involved in copper binding were found to be two cysteines, two histidines, and one methionine. Lappalainen et al. examined an engineered Cu_A center built into the *E. coli* cytochrome *bo* quinol oxidase complex.[74] It was necessary to produce the Cu_A binding fragment in a denatured state, and then add copper after the protein was refolded. Mass spectrometry was used to determine the number of copper atoms bound to the engineered center. From the mass difference between the apo-protein and the metal-bound protein, it was determined that two copper atoms bound to the protein fragment, a good indication that the Cu_A binding domain had been expressed and refolded correctly. Slutter et al. expressed the Cu_A domain of the cytochrome ba_3 from *Thermus thermophilus* in *E. coli* in order to examine the metal center in a more stable environment.[75] The expression of a Cu_A domain from a thermostable bacterium yielded a water-soluble fragment amenable to several different electron transfer and electrochemical studies. Mass spectrometry was used in conjunction with other spectroscopic methods to characterize the Cu_A center. ESI-MS was performed on denatured and nondenatured protein fragments. By comparing the mass spectra, it was determined that two copper atoms bound per protein molecule, as expected. A small peak corresponded to the apo-protein plus one copper atom. Azurin is a protein involved in

electron transport found in many microorganisms. It contains a single copper coordinated by one cysteine, two histidines, and a methionine, in addition to a nonbonded carbonyl oxygen. The similarity of the metal coordination to the coordination needed by the Cu_A center prompted Hay et al. to convert the blue copper protein azurin into an azurin containing a purple copper center.[77] ESI-MS was used to confirm that the protein had been engineered correctly and contained two copper atoms under nondenaturing conditions.

C. Zinc proteins

There are several different types of proteases, including different aminopeptidases and metalloproteases. The protease from *Pseudomonas aeruginosa* is a membrane-bound protein with zinc in the active center, weighing approximately 55 kDa.[78] The membrane protease from *Bacillus cereus* is located at the outer side of the cell envelope, and is composed of two subunits, weighing 53 kDa and 65 kDa.[78] It is also thought to contain zinc in the active site. Leopold and Fricke used an on-line coupled HPLC/ICP-MS system for the determination of the metal content of these two metalloproteases, in order to confirm the metal identity and gain knowledge of the metal stoichiometry.[78] Both proteases were purified from the native source, along with an aminopeptidase from *P. aeruginosa* containing no metal center. For both metalloproteases, the zinc concentration increased during the purification procedure, indicating that the metalloproteases did indeed bind zinc. Through the ICP-MS experiments, it was determined that three molecules of zinc were bound per protein molecule in *B. cereus* and one molecule of zinc was bound per protein molecule in *P.*

aeruginosa. Examination of the aminopeptidase using the same procedures revealed no bound metals, as expected.

III. Metals in a Structural Role

A. Calcium proteins

Many calcium-binding proteins undergo a structural change upon binding of the metal. The metal site is often situated within a helix-loop-helix structure known as an EF-hand.[79] Hydrogen/deuterium exchange can be used to monitor the conformation of a protein, since the rate of exchange on a particular area of the protein will be greater if that area is exposed to solvent, i.e. denatured. It has also been shown that the charge state distribution of ESI-MS can be used to monitor the conformation of the protein, as more sites are available for protonation when the protein is unfolded.

Johnson et al. used hydrogen/deuterium exchange to monitor the conformational changes in recoverin.[80] Recoverin is a calcium binding photoreceptor protein with four "EF hands" which is thought to contain a "calcium-myristol switch." The binding of calcium to the protein causes an extension of the N-terminal acyl group away from the protein. In the absence of calcium, this acyl group is more closely associated with the protein. Three forms of the protein were expressed in *E. coli*; one form was unmodified, while the other two forms were N-terminally acylated by different methods. H/D exchange rates were measured for all three forms in the presence and absence of calcium by allowing the proteins to incubate with D_2O, quenching the reaction, and then digesting the protein. The resulting peptides were separated and analyzed with LC/MS. For both

modified and unmodified recoverin, the rate of deuterium exchange was slowed in the presence of calcium for peptides arising from two of the EF hand regions, indicating that in the presence of calcium, these regions are more tightly folded and therefore less accessible to the deuterated solvent. The effect was slightly greater for unmodified recoverin than for modified recoverin, suggesting that the acylated recoverin may possess a more tightly folded structure. The other two EF hand regions showed no difference in exchange rates in the presence or absence of calcium. This indicates that they are not functional, in agreement with their sequences. Four regions of the acylated recoverin exhibited reduced H/D exchange rates in the absence of calcium. Three of these were hydrophobic regions in the N-terminal half the protein, while the fourth was a hydrophobic region near the C-terminus. The reduction in the rate of exchange in the N-terminal regions is presumably due to exclusion of solvent from these regions by the acyl group, which in the absence of calcium is packed against the protein. Another possibility is the stabilization of hydrogen bonds in these regions by interactions with the acyl group, again due to its conformation against the protein. Johnson speculated that the reduction in H/D exchange rate in the C-terminal region may be due to the presence of a binding site for rhodopsin kinase. This site would be inactive in the absence of calcium and possibly hidden by the conformation of the protein. The data presented here validates the theory that recoverin contains a "calcium-myristol switch," extending the acyl group out from the protein in the presence of calcium, and demonstrates the technique of using H/D exchange to obtain conformational information about the protein. Calbindin is a calcium-binding protein thought to be involved in calcium transport for muscle contraction.[52] It is found in

several different mammalian tissues, including the intestine, kidney, and brain. Veenstra et al. examined rat brain calbindin D_{28K} by ESI-MS in order to characterize the calcium binding sites.[79] Native rat brain calbindin contains six EF-hand domains available for calcium binding. In addition, two mutants of calbindin were made, one lacking EF-hand domain 2 (calbindin Δ2) and one lacking EF-hand domains 2 and 6 (calbindin Δ2,6). Veenstra et al. noticed that a shift in the charge state distribution occurred upon addition of a 10-fold excess of calcium acetate to native apo-calbindin. Deconvolution of the spectra revealed four calcium ions bound per mol of protein. The same experiment was repeated using terbium acetate, since terbium has also been shown to bind to calbindin. After an addition of excess terbium acetate, the mass spectra indicated that four terbium ions bound per mol of protein. The same experiments were performed on calbindin Δ2. Peaks corresponding to the apo-protein plus three metal atoms were observed. For calbindin Δ2,6, three calcium atoms were bound per mol of protein. Peaks corresponding to apo-protein plus two or three terbium atoms were observed after treatment of the apo-protein with terbium acetate. These experiments indicated that calbindin is capable of binding four calcium atoms. It also indicates that EF hand 6 is not a calcium or terbium binding site, since its deletion had no effect. Veenstra et al. further examined the charge state distribution shifts of these proteins upon calcium binding, correlating them to known protein conformational shifts detected by fluorescence and circular dichroism spectroscopy.[81] They discovered that for the native protein and both mutants, an increase in fluorescence was noted upon binding of calcium to the apo-protein, suggesting a conformational change. In addition, significant changes in the near-UV circular dichroism

spectra were noted upon binding of calcium to the protein, while few changes to the far-UV circular dichroism spectra were noted, indicated minimal change to the secondary structure of the protein, but substantial change to the tertiary structure of the protein. These changes were mirrored in the mass spectra. For the apo-protein, two charge state distributions were observed, one centered around the -16 charge state and one centered around the -9 charge state. As calcium ions were added by titration, the lower charge state envelope increased in intensity, and deconvolution of this charge state revealed the apo-protein bound to four calcium ions. The shift to lower charge states implies that fewer of the sites are available for deprotonation, indicating a more tightly folded conformation. Calmodulin is found in a number of vertebrate tissues, including muscle, heart, brain and liver, as well as some invertebrates and plants. Calmodulin activates multiple enzymes and cellular functions when bound to calcium atoms.[52] Veenstra et al. used ESI-MS and previous research on the correlation of charge state distribution to conformation to determine the stoichiometry of calcium ions needed to induce a conformational change in calmodulin.[82] For the apo-protein, a charge state distribution centered around the -15 charge state was observed. As calcium was titrated in, a second charge state distribution centered around the -10 charge state began to appear. Little change in the charge state distribution was noticed upon binding of 1-3 calcium atoms. However, the shift in charge state distribution became noticeable upon binding of four calcium ions per mol of protein. As a check, apocalmodulin was titrated with magnesium ions. Deconvolution of the mass spectra revealed up to six magnesium ions bound to the protein; however, no shift in the charge state distribution occurred, indicating no change in

the conformation of the protein. The conformational change induced in calmodulin by calcium binding allows binding of the protein to its target enzymes or small peptides. Nemirovskiy et al. studied the noncovalent association of calmodulin with the peptide melittin.[83] In the absence of calcium, no interaction between melittin and calmodulin was observed. In the presence of insufficient calcium, some of the calmodulin bound to melittin while some did not. Deconvolution of the mass spectra revealed that only two calcium ions were required for calmodulin binding to melittin. Saturation of calmodulin with calcium revealed that up to seven calcium ions could bind to the protein; however, in the saturated solution, the calmodulin bound to melittin contained no less than four calcium ions per mol of protein. Veenstra et al. used ESI-MS to study the noncovalent complexes of calmodulin with the polypeptides protein kinase II (CamK-II) and melittin.[84] When melittin was added to calmodulin in the absence of calcium, no complex was formed. Addition of calcium ions to the protein/peptide mixture gave rise to peaks corresponding to a calmodulin/melittin complex in which four calcium atoms were bound to the calmodulin. When magnesium was used in place of calcium, metal binding to calmodulin was detected, but no complex was formed. When CamK-II was added to apo-calmodulin, again, no complex was detected. Upon addition of calcium to the mixture, peaks corresponding to the CamK-II/calmodulin complex were detected in which four calcium atoms were bound to calmodulin.

Hu et al. used ESI-MS to examine calcium binding stoichiometry to several different calcium-binding proteins; namely calmodulin, α-lactalbumin, parvalbumin, and stromelysin catalytic domain (SCD).[85] Mass spectra were taken of each protein with and

without added calcium. Calmodulin was found to bind a maximum of four calcium atoms per mol of protein, while parvalbumin and α-lactalbumin bound a maximum of two and one calcium atom per mol of protein respectively. The mass spectra of both calmodulin and parvalbumin also contained peaks with fewer bound calcium atoms than the maximum number. SCD has a higher affinity for zinc than for calcium, and several species with varying metal stoichiometry were detected. The protein was found to bind to a maximum of three zinc atoms, while the number of calcium atoms varied from zero to two.

Hu et al. also used ESI to examine the stoichiometry and cooperativity of calcium binding to parvalbumin and calmodulin.[86] Parvalbumin binds calcium in an EF hand domain analogous to that of calmodulin and is found in muscle tissue.[52] For parvalbumin, two different species were detected; apo-parvalbumin and parvalbumin with two calcium ions bound. No peak for apo-parvalbumin plus one calcium ion was detected, indicating cooperative binding of the metals. In addition, two different charge state distributions were observed, one corresponding to apo-parvalbumin and another corresponding to the protein bound to two metals, indicating a change in protein conformation upon metal binding. For calmodulin, peaks corresponding to the apo-protein plus 0-4 calcium ions were observed. As an excess of calcium ions was added, the abundance of the 4-calcium bound species was increased, while the abundance of the 0-calcium bound species decreased. The 3-calcium bound species was never greatly abundant, while the 1-calcium bound species and the 2-calcium bound species were almost equally abundant. This indicated that the first two calcium ions did not bind cooperatively, but that a conformational change took place upon binding of the second calcium which caused the

third and fourth calcium ions to bind cooperatively. Hu et al. examined the calcium binding stoichiometry of frog parvalbumin, comparing the results with the more commonly studied rabbit and rat parvalbumin.[87] They discovered that in the absence of a large excess of calcium, peaks were observed for both the apo-protein plus one calcium ion and the apo-protein plus two calcium ions, with the single-metal species being the more abundant, in contrast to rat parvalbumin. In addition, the calcium binding in frog parvalbumin was not cooperative, as had been noted for rat parvalbumin.

GroEL is a chaperone protein which assists in protein folding.[88] It binds to proteins which are not fully folded, possibly to protect them from unwanted interactions which could lead to inactivation of the protein. Robinson et al. examined the GroEL:α-lactalbumin complex by ESI-MS.[88] α-lactalbumin was modified by removing the calcium ion reducing a disulfide bond, and rearranging the other three disulfide bonds in order to produce a partially folded derivative of the protein [3SS BLA]. ESI-MS was used to determine that the GroEL forms a tetradecamer in solution, and that each oligomer binds one 3SS BLA. H/D exchange rates of this derivative were measured before and after reacting with GroEL. Little change was noticed in the H/D exchange rates of apo- and GroEL bound α-lactalbumin; however, the H/D exchange rate of each subunit of bound GroEL was much lower than that of free GroEL, indicating that a conformation change takes place in this oligomeric protein upon binding to α-lactalbumin.

B. Zinc proteins

Naylor et al. examined charge state distribution to obtain data about the conformation of a metalloprotein.[89] Electrospray ionization produces multiply charged

ions, and the number of charges on the protein is directly related to the number of sites available for protonation (or deprotonation in negative mode). Therefore, a folded protein will have a charge state distribution consisting of lower charge states than that of an unfolded protein. Naylor et al. used the charge state distribution of ESI-MS to obtain information about the conformational changes in the DNA-binding domain of the vitamin D receptor induced by zinc binding. Vitamin D_3 is used in cellular growth and development, and many of its effects are mediated by the vitamin D receptor. The vitamin D receptor contains zinc finger regions which supposedly bind to unique DNA sequences within vitamin D-responsive genes. Although a conformational change in the vitamin D receptor was expected upon binding of zinc, it had not been confirmed. Also, it was not known whether a conformational change takes place upon binding to DNA. Naylor et al. titrated the DNA binding domain of the vitamin D receptor with zinc, and compared the charge state distribution shift to changes in far-ultraviolet circular dichroism spectra of the protein, in order to determine whether the shift in the charge state distribution corresponded with an actual conformation change within the protein. ESI spectra were acquired of the vitamin D receptor DNA binding domain in both the apo and metal bound form. The spectrum of the apo-protein had a distribution centered around the 11+ charge state. Tenfold zinc excess was added to the protein, producing no noticeable change in the charge state distribution. However, the peaks corresponded to the apo form of the protein plus one zinc ion. Two protons were displaced with the addition of one zinc ion. When the concentration of zinc was increased to a twenty-fold excess, the charge state distribution shifted to lower charge states, corresponding to the protein bound to two zinc

atoms. In the presence of a fifty-fold zinc excess, the higher charge state envelope was no longer visible, and a total of four zinc ions were bound to the protein. These results were confirmed by ESI in negative mode, where the charge state distribution shifted from a -10 center for the apo-protein to a -5 center in the presence of a large excess of zinc. Far-UV circular dichroism experiments showed no change in the confirmation of the vitamin D receptor DNA binding domain when the zinc/protein ration was approximately 1. However, when the zinc/protein ratio was increased to approximately 2, a large change in the far-UV circular dichroism spectrum was noted, indicating a structural change in the protein. The data in these experiments suggests that the shift in charge state distribution in the ESI mass spectrum accurately reflects a change in the conformation of the protein upon binding of two zinc ions. Also, since the binding of two additional zinc ions to the protein did not result in a charge state distribution shift, it can be said that ESI-MS is capable of distinguishing between bound metals that cause conformational change and bound metals that do not. This gives ESI mass spectrometry an advantage over many other analytical techniques, in that it is possible to directly measure metal binding stoichiometries, determine the existence of a conformational change, and detect metal binding which does not cause a conformational change. Human interleukin-3 (hIl-3) is a zinc-binding polypeptide released from T-lymphocytes which plays a role in the generation of red blood cells.[90] Van Veelen et al. used a combination of protease treatments and plasma desorption mass spectrometry (PDMS) to characterize the zinc binding domain. After the protein was digested, a solution of zinc-chloride was added to the fragments, which were then analyzed by PDMS. It was found that two different peptide fragments

(11-28 and 80-100) were necessary for zinc binding, proving the ability of mass spectrometry to characterize protein-metal interactions where the metal-binding domain of the protein is nonlinear. The human immunodeficiency virus nucleocapsid protein p7 (HIV-1 Ncp7) is a polypeptide containing two zinc finger domains, where the zinc is coordinated by three cysteines and one histidine. Hathout et al. used ESI-MS to examine intermediates in the oxidation of Ncp7.[91] Samples of the reaction products were taken at intervals during the reaction, and an intermediate was identified by its increase and subsequent decrease in concentration during the course of the reaction. The intermediate was identified as a complex of Ncp7 with the oxidizing agent, with loss of one zinc atom and the formation of disulfide bonds between the six cysteine residues. The final product of the reaction was also characterized by MS, and peaks were observed corresponding to the oxidized apo-Ncp7 with disulfide bonds. Analysis of proteolytic fragments from digestion of the reaction product confirmed the presence and position of disulfide bonds. BRCA1 is a tumor suppressor gene which contains a zinc binding RING finger domain.[92] The RING finger domain consists of eight cysteine and histidine residues which are capable of binding two zinc atoms. Brzovic et al. used a combination of proteolysis and MALDI-TOF to characterize native BRCA-1 and a C61G mutation. A construct was made of BRCA-1 containing the first 76 residues from the N-terminus, including the RING finger region (BC-76). In the absence of zinc, apo-BC-76 showed significant degradation after only three minutes of proteolysis. However, in the presence of zinc only two proteolytic fragments were detected after sixty minutes of digestion, one containing both zinc binding sites and one containing only one binding site. The C61G mutation

altered one of the zinc binding sites, but proteolysis of this mutation in the presence of zinc closely resembled the results from the zinc-bound native protein. The experiments indicated that the metal-bound protein has a conformation more resistant to proteolysis than that of the apo-protein. In addition, further experiments were conducted which placed the RING finger domain within the first 110 residues of BRCA-1. Veenstra et al. used ESI-MS to examine conformational changes within the vitamin D receptor (VDR) upon binding of zinc.[89] Vitamin D receptor contains four zinc binding sites, two of high affinity and two of low affinity. Veenstra correlated the shifts in the charge state distribution of the mass spectra with changes in the CD spectra of the protein. The mass spectrum of the apo-protein had a charge state distribution centered around +11. Binding of one metal to the protein produced no appreciable shift in the charge state distribution. However, the spectrum shifted to lower charge states upon binding of a second zinc ion to the protein. Further addition of zinc did not produce a further shift in the spectrum, although the protein bound four metal atoms. The postulation of a conformational shift in VDR upon binding of the second zinc ion was confirmed by far-UV CD studies.

C. Other metal and mixed metal proteins

Cytochrome *c* is an iron-binding protein found in mitochondria which functions as an electron donor.[52] The iron is not commonly thought to play a structural role. However, Smith used ESI-MS and H/D exchange with proteolysis to characterize local structure change between oxidized and reduced cytochrome *c*.[93] One segment from the interior of the protein showed slower H/D exchange for oxidized cytochrome *c* than for reduced cytochrome *c*, indicating a more folded structure in this segment of the oxidized protein.

Also, H/D exchange was found to be faster in three other segments from oxidized cytochrome *c*, indicating a less tightly folded structure in these segments. Smith demonstrated that the oxidation state of the metal in the active site of the protein can affect the local structure. Jaquinod et al. used H/D exchange and charge state distribution to examine the conformation of native cytochrome c_2 and two of its mutants.[94] For native cytochrome c_2 and for the P35A mutant, a single charge state distribution appeared, with little change upon reduction of pH. For the G34S mutant, however, two different charge state distributions appeared, suggesting two different conformations. H/D exchange experiments confirmed these results, in that the two forms had different reaction kinetics. H/D exchange rates were higher in both of the mutants than the native strain under nondenaturing conditions, indicating a less tightly folded structure for both mutants. Further experiments were conducted on other mutants of cytochrome c_2.[95] The charge state distributions of some of the mutants varied only slightly from that of the wild-type cytochrome c_2. However, the I57N mutant showed a second charge state distribution, analogous to the G34S mutant. Most of the mutants showed either slight or marked increase in H/D exchange rates over the wild-type protein at pD 5.8. Two mutants exhibited lower H/D exchange rates: V11 insert and Y75F, suggesting that these mutants may be more stable than the wild-type protein. The two charge state distributions of the I57N mutant showed different H/D exchange kinetics, as did the G34S mutant, indicating that there are two separate conformations for these mutants. Guy et al. used charge state distribution and H/D exchange to examine the structural role of the tyrosine 64 residue in ferricytochrome c_{553} from *Desulfovibrio vulgaris* Hildenborough.[96, 97] Several mutants

were produced in which this residue was exchanged with another amino acid. Two of the mutants showed little or no increase in H/D exchange rates, while three others showed increased H/D exchange rates, indicating decreased structural stability. These experiments showed the ability of charge state distribution and H/D exchange rates to detect conformational changes produced by site-directed mutagenesis. The toxicity of lead in humans has long been a source of concern. Lead can inhibit the activity of certain enzymes, leading to toxic effects. δ-aminolevulinic acid dehydratase (ALAD) is an enzyme involved in the synthesis of heme in humans, and its activity is inhibited by the binding of lead. Bergdahl et al. used LC/ICP-MS to examine lead bound to human erythrocytes, in order to identify the major protein binding lead.[98] Two proteins were shown to bind lead, one weighing 45 kDa and another weighing 240 kDa. The majority of the bound lead was recovered from the 240 kDa protein, which was tentatively identified as ALAD. ALAD has a theoretical weight of 290 kDa. The 45 kDa protein was not identified. Briand et al. used ESI-MS to characterize complexes of adenylate kinase with P^1,P^5-di(adenosine 5')-pentaphosphate (Ap_5A) and zinc or magnesium ions.[99] Adenylate kinase binds zinc through either four cysteine residues or through three cysteine residues and one asparagine residue. At low pH, the adenylate kinase was detected only in the apo-form, without the characteristic zinc ion. However, allowing adenylate kinase to react with Ap_5A allowed detection of the complex of the two protein including the zinc. Therefore the metal binding was stabilized by complexation of the two proteins. Addition of magnesium rather than zinc to the reaction mixture yielded a complex of adenylate kinase with Ap_5A and two metals. Matrilysin is a metal-binding protein belonging to the

matrix metalloprotein family involved in tissue growth and wound healing.[100] Matrix metalloproteins bind zinc and calcium in order to possess a structure allowing enzyme activity. Feng et al. used ESI-MS to examine the metal binding stoichiometry of matrilysin as well as its complex with two inhibitors.[100] At low pH, only apo-matrilysin was detected, with a charge state distribution centered around 21+. As the pH was increased, a lower charge state distribution appeared, corresponding to the apo-matrilysin plus one or two zinc or calcium atoms. Several species of different metal stoichiometry were detected, ranging from either one zinc or one calcium to two zinc and two calcium. The metal bound matrilysin was allowed to react with two different inhibitors, and in both cases the major complex formed contained the two zinc plus two calcium matrilysin species. The glucocortid receptor DNA binding domain (GRDBD) is capable of binding either zinc or cadmium. Witkowska et al. used ESI-MS to examine the metal binding stoichiometry of the GRDBD.[101] GRDBD was shown to contain either two zinc atoms or two cadmium atoms. The human estrogen receptor contains a highly conserved DNA binding domain (ERDBD) containing two clusters of cysteine residues which bind up to two zinc ions in a zinc-finger construction.[102] Hutchens et al. demonstrated that these zinc-finger regions were able to bind copper. When the apo-protein was exposed to copper, the primary species observed was the apo-protein plus four copper atoms. Two protons were lost per copper atom bound. The saturation of ERDBD with copper suggested the preference of ERDBD for that metal, since saturation of ERDBD with zinc never occurred. Further experiments on this protein examined the apparent conformation change upon binding of ERDBD to copper.[103] Hutchens et al. noticed no change in the

charge state distribution between apo-protein and zinc-bound protein. Both species had a charge state distribution centered around the 10+ charge state. However, the ERDBD-copper species had a charge state envelope centered around the 8+ charge state. Because ERDBD binds four copper atoms preferentially, as opposed to two zinc atoms, Hutchens suggested that a conformational change took place in order to provide cysteine coordination to the extra two copper atoms, reducing the number of available sites for protonation.

IV. Conclusion

Mass spectrometry has been widely used as a tool for the characterization of metalloproteins, from simply determining the identity of the metal center to probing the intermediates in a reaction to monitoring the conformational changes induced by metal binding. The studies have involved a variety of ionization and detection methods, as well as combinations of mass spectrometry with other tools such as circular dichroism and proteolysis. Researchers have discovered in mass spectrometry an analytical technique which is rapid, accurate, requires small amounts of sample, and confirms or complements other techniques. As mass spectrometry improves in accuracy and sensitivity, the uses to which it is put seem only limited by the innovation of the researcher, and the information which it delivers is increasingly useful. The high resolution and high mass accuracy of ESI-FTICR have proven advantageous for the analysis of metalloproteins. It is possible to determine oxidation state as well as stoichiometry of the metal in the active site of a protein. FTICR mass spectrometry of metalloproteins requires special sample handling

and experimental techniques to avoid loss of metal and denaturation of the protein, and future research will focus on careful sample purification to achieve isotopic resolution of increasingly larger metalloproteins and metalloprotein noncovalent complexes.

MASS SPECTRAL ANALYSIS OF NONCOVALENT COMPLEXES

ESI mass spectrometry has been used to examine noncovalent complexes for nearly as long as the technique has been in existence,[48, 67, 73, 83, 84, 100, 104-141] and it has been the subject of a number of review papers.[124, 133, 134, 140, 141] In 1991, Katta et al. used ESI mass spectrometry to detect one of the simplest noncovalent complexes, heme-bound myoglobin.[142] In that same year, Ganem et al. observed hen egg white lysozyme complexes and receptor-ligand complexes with ESI quadrupole mass spectrometry.[110, 111] These experiments opened the field for analysis of noncovalent complexes by mass spectrometry. Smith et al. examined the gentle ESI conditions necessary to observe polypeptide and protein dimers in 1992.[133] Loo et al. used ESI coupled with magnetic sector mass spectrometry to observe primary to quaternary protein structure.[133] Li et al. and He et al. studied stoichiometry and oxidation state of the heme group bound to various proteins.[118, 143] Cao et al. used ESI mass spectrometry in conjunction with capillary electrophoresis to detect the heme-bound alpha and beta subunits of hemoglobin in a single red blood cell.[144] Lei et al. used ESI-TOF mass spectrometry to examine the stoichiometry of multimers of rubrerythrin and hemerythrin, observing that rubrerythrin was tetrameric rather than the expected dimer, and that the mass spectrum of hetero-octameric hemerythrin possibly contained an $\alpha_5\beta_3$ shoulder in addition to the main $\alpha_4\beta_4$

peak.[73] A number of efforts have been made to utilize the high resolution of FTICR mass spectrometry for the examination of noncovalent complexes,[105, 106, 139, 145, 146] with a limited number of examples of isotopic resolution.[105, 138] Isotopic resolution of noncovalent complexes would enable the researcher to accurately determine subunit stoichiometry, as well as identity and oxidation state of metals in the active site of multimeric metalloproteins. However, sample purity presents a barrier to the observation of isotopes. Researchers have explored experimental techniques for decreasing the heterogeneity of species within the analyzer cell,[105, 131, 138, 146, 147] but further research is required to achieve isotopic resolution of high-mass noncovalent complexes. Chapter 5 of this dissertation describes efforts to achieve this for metalloproteins.

References

(1) Karas, M.; Hillenkamp, F. *Anal. Chem.* **1988,** *60*, 2301-2303.

(2) Karas, M.; Bahr, U.; Ingendoh, A.; Nordhoff, E.; Stahl, B.; Strupat, K.; Hillenkamp, F. *Anal. Chim. Acta* **1990,** *241*, 175-185.

(3) Hillenkamp, F.; Karas, M. *Method Enzymol.* **1990,** *193*, 280-295.

(4) Hillenkamp, F.; Karas, M.; Beavis, R. C.; Chait, B. T. *Anal. Chem.* **1991,** *63*, A1193-A1202.

(5) Hillenkamp, F.; Karas, M. *Fresenius J. Anal. Chem.* **1992,** *343*, 27-27.

(6) Cole, R. B. *J. Mass Spectrom.* **2000,** *35*, 763-772.

(7) Fenn, J. B.; Mann, M.; Meng, C. K.; Wong, S. F.; Whitehouse, C. M. *Mass Spectrom. Rev.* **1990,** *9*, 37-70.

(8) Kebarle, P.; Tang, L. *Anal. Chem.* **1993,** *65*, A972-A986.

(9) Edmonds, C. G.; Smith, R. D. *Method Enzymol.* **1990,** *193*, 412-431.

(10) Smith, R. D.; Loo, J. A.; Loo, R. R. O.; Udseth, H. R. *Mass Spectrom. Rev.* **1992,** *11*, 434-443.

(11) Kebarle, P. *J. Mass Spectrom.* **2000,** *35*, 804-817.

(12) Wilm, M.; Mann, M. *Anal. Chem.* **1996,** *68*, 1-8.

(13) Juraschek, R.; Dulcks, T.; Karas, M. *J. Am. Soc. Mass. Spectrom.* **1999,** *10*, 300-308.

(14) Comisarow, M. B.; Marshall, A. G. *J. Mass Spectrom.* **1996,** *31*, 581-585.

(15) Comisarow, M. B.; Marshall, A. G. *J. Mass Spectrom.* **1996,** *31*, 586-587.

(16) Amster, I. J. *J. Mass Spectrom.* **1996,** *31*, 1325-1337.

(17) Marshall, A. G.; Hendrickson, C. L.; Jackson, G. S. *Mass Spectrom. Rev.* **1998,** *17*, 1-35.

(18) Caravatti, P.; Allemann, M. *Org. Mass Spectrom.* **1991,** *26*, 514-518.

(19) Guan, S. H.; Marshall, A. G. *Int. J. Mass Spectrom. Ion Processes* **1996,** *158*, 5-37.

(20) Soni, M. H.; Cooks, R. G. *Anal. Chem.* **1994,** *66*, 2488-2496.

(21) Julian, R. K.; Cooks, R. G. *Anal. Chem.* **1993,** *65*, 1827-1833.

(22) Guan, S. H.; Marshall, A. G. *Anal. Chem.* **1993,** *65*, 1288-1294.

(23) Guan, S. H. *J. Chem. Phys.* **1990,** *93*, 8442-8445.

(24) Easterling, M. L.; Amster, I. J.; van Rooij, G. J.; Heeren, R. M. A. *J. Am. Soc. Mass. Spectrom.* **1999,** *10*, 1074-1082.

(25) Hofstadler, S. A.; Bruce, J. E.; Rockwood, A. L.; Anderson, G. A.; Winger, B. E.; Smith, R. D. *Int. J. Mass Spectrom. Ion Processes* **1994,** *132*, 109-127.

(26) Francl, T. J.; Sherman, M. G.; Hunter, R. L.; Locke, M. J.; Bowers, W. D.; McIver, R. T. *Int. J. Mass Spectrom. Ion Processes* **1983,** *54*, 189-199.

(27) Jeffries, J. B.; Barlow, S. E.; Dunn, G. H. *Int. J. Mass Spectrom. Ion Processes* **1983,** *54*, 169-187.

(28) Easterling, M. L.; Mize, T. H.; Amster, I. J. *Anal. Chem.* **1999,** *71*, 624-632.

(29) Senko, M. W.; Beu, S. C.; McLafferty, F. W. *J. Am. Soc. Mass. Spectrom.* **1995,** *6*, 229-233.

(30) Schweikhard, L.; Guan, S. H.; Marshall, A. G. *Int. J. Mass Spectrom. Ion Processes* **1992,** *120*, 71-83.

(31) Campbell, V. L.; Guan, Z. Q.; Laude, D. A. *J. Am. Soc. Mass. Spectrom.* **1995,** *6*, 564-570.

(32) Pitsenberger, C. C.; Easterling, M. L.; Amster, I. J. *Anal. Chem.* **1996,** *68*, 3732-3739.

(33) Speir, J. P.; Gorman, G. S.; Pitsenberger, C. C.; Turner, C. A.; Wang, P. P.; Amster, I. J. *Anal. Chem.* **1993,** *65*, 1746-1752.

(34) Fujiwara, M.; Naito, Y. *Rapid Commun. Mass Spectrom.* **1999,** *13*, 1633-1638.

(35) Gorshkov, M. V.; Pasa-Tolic, L.; Smith, R. D. *J. Am. Soc. Mass. Spectrom.* **1999,** *10*, 15-18.

(36) Pastor, S. J.; Wilkins, C. L. *Int. J. Mass Spectrom.* **1998,** *175*, 81-92.

(37) Shin, S. K.; Han, S. J. *J. Am. Soc. Mass. Spectrom.* **1997,** *8*, 86-89.

(38) Dale, V. C. M.; Speir, J. P.; Kruppa, G. H.; Stacey, C. C.; Mann, M.; Wilm, M. *Biochem. Soc. Trans.* **1996,** *24*, 943-947.

(39) Senko, M. W.; Speir, J. P.; McLafferty, F. W. *Anal. Chem.* **1994,** *66*, 2801-2808.

(40) Gauthier, J. W.; Trautman, T. R.; Jacobson, D. B. *Anal. Chim. Acta* **1991,** *246*, 211-225.

(41) Shi, S. D. H.; Hendrickson, C. L.; Marshall, A. G.; Siegel, M. M.; Kong, F. M.; Carter, G. T. *J. Am. Soc. Mass. Spectrom.* **1999,** *10*, 1285-1290.

(42) Dufresne, C. P.; Wood, T. D.; Hendrickson, C. L. *J. Am. Soc. Mass. Spectrom.* **1998,** *9*, 1222-1225.

(43) Peiris, D. M.; Yang, Y. J.; Ramanathan, R.; Williams, K. R.; Watson, C. H.; Eyler, J. R. *Int. J. Mass Spectrom. Ion Processes* **1996,** *158*, 365-378.

(44) Little, D. P.; Aaserud, D. J.; Valaskovic, G. A.; McLafferty, F. W. *J. Am. Chem. Soc.* **1996,** *118*, 9352-9359.

(45) Little, D. P.; Speir, J. P.; Senko, M. W.; Oconnor, P. B.; McLafferty, F. W. *Anal. Chem.* **1994,** *66*, 2809-2815.

(46) Jockusch, R. A.; Paech, K.; Williams, E. R. *J. Phys. Chem. A* **2000,** *104*, 3188-3196.

(47) Klassen, J. S.; Schnier, P. D.; Williams, E. R. *J. Am. Soc. Mass. Spectrom.* **1998,** *9*, 1117-1124.

(48) Williams, E. R.; Schnier, P. D.; Jockusch, R. *Abstr. Pap. Am. Chem. Soc.* **1998,** *215*, 115-ANYL.

(49) Jockusch, R. A.; Schnier, P. D.; Price, W. D.; Strittmatter, E. F.; Demirev, P. A.; Williams, E. R. *Anal. Chem.* **1997,** *69*, 1119-1126.

(50) Williams, E. R.; Price, W. D.; Schnier, P. D.; Jockusch, R. A.; Gross, D. S.; Zhao, Y.; Strittmatter, E. *Abstr. Pap. Am. Chem. Soc.* **1996,** *212*, 19-PHYS.

(51) Price, W. D.; Schnier, P. D.; Williams, E. R. *Anal. Chem.* **1996,** *68*, 859-866.

(52) Otsuka, S.; Yamanaka, T.;; Elsevier: Tokyo, 1988; Vol. 8, pp 568.

(53) Yu, X. L.; Wojciechowski, M.; Fenselau, C. *Anal. Chem.* **1993,** *65*, 1355-1359.

(54) Zaia, J.; Jiang, L. C.; Han, M. S.; Tabb, J. R.; Wu, Z. C.; Fabris, D.; Fenselau, C. *Biochemistry* **1996,** *35*, 2830-2835.

(55) Fabris, D.; Zaia, J.; Hathout, Y.; Fenselau, C. *J. Am. Chem. Soc.* **1996,** *118*, 12242-12243.

(56) LeBlanc, J. C. Y. *J. Anal. Atom. Spectrom* **1997,** *12*, 525-530.

(57) Takatera, K.; Watanabe, T. *Anal. Sci.* **1993,** *9*, 19-23.

(58) Takatera, K.; Watanabe, T. *Anal. Sci.* **1993,** *9*, 605-609.

(59) Veenstra, T. D.; Benson, L. M.; Craig, T. A.; Tomlinson, A. J.; Kumar, R.; Naylor, S. *Nat. Biotechnol.* **1998,** *16*, 262-266.

(60) Craig, T. A.; Veenstra, T. D.; Naylor, S.; Tomlinson, A. J.; Johnson, K. L.; Macura, S.; Juranic, N.; Kumar, R. *Biochemistry* **1997,** *36*, 10482-10491.

(61) Moreau, S.; Awade, A. C.; Molle, D.; Legraet, Y.; Brule, G. *J. Agr. Food Chem.* **1995,** *43*, 883-889.

(62) Thorvaldsen, J. L.; Sewell, A. K.; Tanner, A. M.; Peltier, J. M.; Pickering, I. J.; George, G. N.; Winge, D. R. *Biochemistry* **1994,** *33*, 9566-9577.

(63) Griffiths, J. A.; King, J.; Yang, D. F.; Browner, R.; ElSayed, M. A. *J. Phys. Chem.* **1996,** *100*, 929-933.

(64) MichaudSoret, I.; Adrait, A.; Jaquinod, M.; Forest, E.; Touati, D.; Latour, J. M. *Febs Letters* **1997,** *413*, 473-476.

(65) Lafitte, D.; Capony, J. P.; Grassy, G.; Haiech, J.; Calas, B. *J. Mass Spectrom.* **1995**, S192-S196.

(66) Bond, A. M.; Colton, R.; Dagostino, A.; Traeger, J. C.; Downard, A. J.; Canty, A. J. *Inorg. Chim. Acta* **1998,** *267*, 281-291.

(67) Jaquinod, M.; Leize, E.; Potier, N.; Albrecht, A. M.; Shanzer, A.; Vandorsselaer, A. *Tetrahedron Letters* **1993,** *34*, 2771-2774.

(68) Petillot, Y.; Forest, E.; Mathieu, I.; Meyer, J.; Moulis, J. M. *Biochemical Journal* **1993,** *296*, 657-661.

(69) Meyer, J.; Gagnon, J.; Gaillard, J.; Lutz, M.; Achim, C.; Munck, E.; Petillot, Y.; Colangelo, C. M.; Scott, R. A. *Biochemistry* **1997,** *36*, 13374-13380.

(70) Petillot, Y.; Forest, E.; Meyer, J.; Moulis, J. M. *Anal. Biochem.* **1995,** *228*, 56-63.

(71) Armengaud, J.; Gaillard, J.; Forest, E.; Jouanneau, Y. *Eur. J. Biochem.* **1995,** *231*, 396-404.

(72) Remigy, H.; Jaquinod, M.; Petillot, Y.; Gagnon, J.; Cheng, H.; Xia, B.; Markley, J. L.; Hurley, J. K.; Tollin, G.; Forest, E. *Journal of Protein Chemistry* **1997,** *16*, 527-532.

(73) Lei, Q. P.; Cui, X. Y.; Kurtz, D. M.; Amster, I. J.; Chernushevich, I. V.; Standing, K. G. *Anal. Chem.* **1998,** *70*, 1838-1846.

(74) Lappalainen, P.; Aasa, R.; Malmstrom, B. G.; Saraste, M. *J. Biol. Chem.* **1993,** *268*, 26416-26421.

(75) Slutter, C. E.; Sanders, D.; Wittung, P.; Malmstrom, B. G.; Aasa, R.; Richards, J. H.; Gray, H. B.; Fee, J. A. *Biochemistry* **1996,** *35*, 3387-3395.

(76) Kelly, M.; Lappalainen, P.; Talbo, G.; Haltia, T.; Vanderoost, J.; Saraste, M. *J. Biol. Chem.* **1993,** *268*, 16781-16787.

(77) Hay, M. T.; Ang, M. C.; Gamelin, D. R.; Solomon, E. I.; Antholine, W. E.; Ralle, M.; Blackburn, N. J.; Massey, P. D.; Wang, X. T.; Kwon, A. H.; Lu, Y. *Inorganic Chemistry* **1998,** *37*, 191-198.

(78) Leopold, I.; Fricke, B. *Anal. Biochem.* **1997,** *252*, 277-285.

(79) Veenstra, T. D.; Johnson, K. L.; Tomlinson, A. J.; Naylor, S.; Kumar, R. *Biochemistry* **1997,** *36*, 3535-3542.

(80) Neubert, T. A.; Walsh, K. A.; Hurley, J. B.; Johnson, R. S. *Protein Sci.* **1997,** *6*, 843-850.

(81) Veenstra, T. D.; Johnson, K. L.; Tomlinson, A. J.; Kumar, R.; Naylor, S. *Rapid Commun. Mass Spectrom.* **1998,** *12*, 613-619.

(82) Veenstra, T. D.; Johnson, K. L.; Tomlinson, A. J.; Naylor, S.; Kumar, R. *Eur. Mass Spectrom.* **1997,** *3*, 453-459.

(83) Nemirovskiy, O. V.; Ramanathan, R.; Gross, M. L. *J. Am. Soc. Mass. Spectrom.* **1997,** *8*, 809-812.

(84) Veenstra, T. D.; Tomlinson, A. J.; Benson, L.; Kumar, R.; Naylor, S. *J. Am. Soc. Mass. Spectrom.* **1998,** *9*, 580-584.

(85) Hu, P. F.; Ye, Q. Z.; Loo, J. A. *Anal. Chem.* **1994,** *66*, 4190-4194.

(86) Hu, P. F.; Loo, J. A. *J. Mass Spectrom.* **1995,** *30*, 1076-1082.

(87) Hu, P. F.; Buckel, S. D.; Whitton, M. M.; Loo, J. A. *Eur. Mass Spectrom.* **1996,** *2*, 69-76.

(88) Robinson, C. V.; Gross, M.; Eyles, S. J.; Ewbank, J. J.; Mayhew, M.; Hartl, F. U.; Dobson, C. M.; Radford, S. E. *Nature* **1994,** *372*, 646-651.

(89) Veenstra, T. D.; Johnson, K. L.; Tomlinson, A. J.; Craig, T. A.; Kumar, R.; Naylor, S. *J. Am. Soc. Mass. Spectrom.* **1998,** *9*, 8-14.

(90) Vanveelen, P. A.; Smit, V.; Tjaden, U. R.; Vandergreef, J. *Int. J. Mass Spectrom. Ion Processes* **1993,** *126*, 179-185.

(91) Hathout, Y.; Fabris, D.; Han, M. S.; Sowder, R. C.; Henderson, L. E.; Fenselau, C. *Drug Metabolism and Disposition* **1996,** *24*, 1395-1400.

(92) Brzovic, P. S.; Meza, J.; King, M. C.; Klevit, R. E. *J. Biol. Chem.* **1998,** *273*, 7795-7799.

(93) Smith, D. L. *Biochemistry-Moscow* **1998,** *63*, 285-293.

(94) Jaquinod, M.; Halgand, F.; Caffrey, M.; Saintpierre, C.; Gagnon, J.; Fitch, J.; Cusanovich, M.; Forest, E. *Rapid Commun. Mass Spectrom.* **1995,** *9*, 1135-1140.

(95) Jaquinod, M.; Guy, P.; Halgand, F.; Caffrey, M.; Fitch, J.; Cusanovich, M.; Forest, E. *Febs Letters* **1996,** *380*, 44-48.

(96) Guy, P.; Jaquinod, M.; Remigy, H.; Andrieu, J. P.; Gagnon, J.; Bersch, B.; Dolla, A.; Blanchard, L.; Guerlesquin, F.; Forest, E. *Febs Letters* **1996,** *395*, 53-57.

(97) Guy, P.; Remigy, H.; Jaquinod, M.; Bersch, B.; Blanchard, L.; Dolla, A.; Forest, E. *Biochem. Biophys. Res. Commun.* **1996,** *218*, 97-103.

(98) Bergdahl, I. A.; Schutz, A.; Grubb, A. *J. Anal. Atom. Spectrom* **1996,** *11*, 735-738.

(99) Briand, G.; Perrier, V.; Kouach, M.; Takahashi, M.; Gilles, A. M.; Barzu, O. *Arch. Biochem. Biophys.* **1997,** *339*, 291-297.

(100) Feng, R.; Castelhano, A. L.; Billedeau, R.; Yuan, Z. Y. *J. Am. Soc. Mass. Spectrom.* **1995,** *6*, 1105-1111.

(101) Witkowska, H. E.; Shackleton, C. H. L.; Dahlmanwright, K.; Kim, J. Y.; Gustafsson, J. A. *J. Am. Chem. Soc.* **1995,** *117*, 3319- 3324.

(102) Hutchens, T. W.; Allen, M. H.; Li, C. M.; Yip, T. T. *Febs Letters* **1992,** *309*, 170-174.

(103) Hutchens, T. W.; Allen, M. H. *Rapid Commun. Mass Spectrom.* **1992,** *6*, 469-473.

(104) Borchers, C.; Tomer, K. B. *Biochemistry* **1999,** *38*, 11734-11740.

(105) Bruce, J. E.; Vanorden, S. L.; Anderson, G. A.; Hofstadler, S. A.; Sherman, M. G.; Rockwood, A. L.; Smith, R. D. *J. Mass Spectrom.* **1995,** *30*, 124-133.

(106) Bruce, J. E.; Smith, V. F.; Liu, C. L.; Randall, L. L.; Smith, R. D. *Protein Sci.* **1998,** *7*, 1180-1185.

(107) Cheng, X. H.; Morin, P. E.; Harms, A. C.; Bruce, J. E.; BenDavid, Y.; Smith, R. D. *Anal. Biochem.* **1996,** *239*, 35-40.

(108) Fitzgerald, M. C.; Chernushevich, I.; Standing, K. G.; Kent, S. B. H.; Whitman, C. P. *J. Am. Chem. Soc.* **1995,** *117*, 11075- 11080.

(109) Gale, D. C.; Goodlett, D. R.; Lightwahl, K. J.; Smith, R. D. *J. Am. Chem. Soc.* **1994,** *116*, 6027- 6028.

(110) Ganem, B.; Li, Y. T.; Henion, J. D. *J. Am. Chem. Soc.* **1991,** *113*, 7818-7819.

(111) Ganem, B.; Li, Y. T.; Henion, J. D. *J. Am. Chem. Soc.* **1991,** *113*, 6294-6296.

(112) Ganem, B.; Li, Y. T.; Henion, J. D. *Tetrahedron Letters* **1993,** *34*, 1445-1448.

(113) Ganguly, A. K.; Pramanik, B. N.; Tsarbopoulos, A.; Covey, T. R.; Huang, E.; Fuhrman, S. A. *J. Am. Chem. Soc.* **1992,** *114*, 6559- 6560.

(114) Ganguly, A. K.; Pramanik, B. N.; Huang, E. C.; Tsarbopoulos, A.; Girijavallabhan, V. M.; Liberles, S. *Tetrahedron* **1993,** *49*, 7985-7996.

(115) Glocker, M. O.; Bauer, S. H. J.; Kast, J.; Volz, J.; Przybylski, M. *J. Mass Spectrom.* **1996,** *31*, 1221-1227.

(116) Goodlett, D. R.; Loo, R. R. O.; Loo, J. A.; Wahl, J. H.; Udseth, H. R.; Smith, R. D. *J. Am. Soc. Mass. Spectrom.* **1994,** *5*, 614-622.

(117) Kleinekofort, W.; Pfenninger, A.; Plomer, T.; Griesinger, C.; Brutschy, B. *Int. J. Mass Spectrom. Ion Processes* **1996,** *156*, 195-202.

(118) Li, Y. T.; Hsieh, Y. L.; Henion, J. D.; Ganem, B. *J. Am. Soc. Mass. Spectrom.* **1993,** *4*, 631-637.

(119) Li, Y. T.; Hsieh, Y. L.; Henion, J. D.; Senko, M. W.; McLafferty, F. W.; Ganem, B. *J. Am. Chem. Soc.* **1993,** *115*, 8409- 8413.

(120) Li, Y. T.; Hsieh, Y. L.; Henion, J. D.; Ocain, T. D.; Schiehser, G. A.; Ganem, B. *J. Am. Chem. Soc.* **1994,** *116*, 7487- 7493.

(121) Lightwahl, K. J.; Schwartz, B. L.; Smith, R. D. *J. Am. Chem. Soc.* **1994,** *116*, 5271- 5278.

(122) Loo, R. R. O.; Goodlett, D. R.; Smith, R. D.; Loo, J. A. *J. Am. Chem. Soc.* **1993,** *115*, 4391- 4392.

(123) Loo, R. R. O.; Stevenson, T. I.; Mitchell, C.; Loo, J. A.; Andrews, P. C. *Anal. Chem.* **1996,** *68*, 1910-1917.

(124) Loo, J. A. *Mass Spectrom. Rev.* **1997,** *16*, 1-23.

(125) Potier, N.; Donald, L. J.; Chernushevich, I.; Ayed, A.; Ens, W.; Arrowsmith, C. H.; Standing, K. G.; Duckworth, H. W. *Protein Sci.* **1998,** *7*, 1388-1395.

(126) Przybylski, M.; Glocker, M. O. *Angew. Chem.-Int. Edit. Engl.* **1996,** *35*, 807-826.

(127) Raftery, M. J.; Geczy, C. L. *J. Am. Soc. Mass. Spectrom.* **1998,** *9*, 533-539.

(128) Robinson, C. V.; Chung, E. W.; Kragelund, B. B.; Knudsen, J.; Aplin, R. T.; Poulsen, F. M.; Dobson, C. M. *J. Am. Chem. Soc.* **1996,** *118*, 8646- 8653.

(129) Sannes-Lowery, K. A.; Mei, H. Y.; Loo, J. A. *Int. J. Mass Spectrom.* **1999,** *193*, 115-122.

(130) Schwartz, B. L.; Lightwahl, K. J.; Smith, R. D. *J. Am. Soc. Mass. Spectrom.* **1994,** *5*, 201-204.

(131) Schwartz, B. L.; Bruce, J. E.; Anderson, G. A.; Hofstadler, S. A.; Rockwood, A. L.; Smith, R. D.; Chilkoti, A.; Stayton, P. S. *J. Am. Soc. Mass. Spectrom.* **1995,** *6*, 459-465.

(132) She, Y. M.; Ji, Y. P.; He, Y. F.; Liu, S. Y. *Chem. J. Chin. Univ.-Chin.* **1998,** *19*, 1735-1738.

(133) Smith, R. D.; Lightwahl, K. J.; Winger, B. E.; Loo, J. A. *Org. Mass Spectrom.* **1992,** *27,* 811-821.

(134) Smith, R. D.; Bruce, J. E.; Wu, Q. Y.; Lei, Q. P. *Chem. Soc. Rev.* **1997,** *26,* 191-202.

(135) Strupat, K.; Roginaux, H.; Dorsselaer, A. V.; Roth, J.; Vogl, T. *J. Am. Soc. Mass. Spectrom.* **2000,** *11,* 780-788.

(136) Tang, X. J.; Brewer, C. F.; Saha, S.; Chernushevich, I.; Ens, W.; Standing, K. G. *Rapid Commun. Mass Spectrom.* **1994,** *8,* 750-754.

(137) Thiede, B.; von Janta-Lipinski, M. *Rapid Commun. Mass Spectrom.* **1998,** *12,* 1889-1894.

(138) Tolic, L. P.; Bruce, J. E.; Lei, Q. P.; Anderson, G. A.; Smith, R. D. *Anal. Chem.* **1998,** *70,* 405-408.

(139) Tolic, L. P.; Harms, A. C.; Anderson, G. A.; Smith, R. D.; Willie, A.; Jorns, M. S. *J. Am. Soc. Mass. Spectrom.* **1998,** *9,* 510-515.

(140) Veenstra, T. D. *Biophys. Chem.* **1999,** *79,* 63-79.

(141) Veenstra, T. D. *Biochem. Biophys. Res. Commun.* **1999,** *257,* 1-5.

(142) Katta, V.; Chait, B. T. *J. Am. Chem. Soc.* **1991,** *113,* 8534.

(143) He, F.; Hendrickson, C. L.; Marshall, A. G. *J. Am. Soc. Mass. Spectrom.* **2000,** *11,* 120-126.

(144) Cao, P.; Moini, M. *J. Am. Soc. Mass Spectrom.* **1999,** *10,* 184-186.

(145) Chen, R. D.; Cheng, X. H.; Mitchell, D. W.; Hofstadler, S. A.; Wu, Q. Y.; Rockwood, A. L.; Sherman, M. G.; Smith, R. D. *Anal. Chem.* **1995,** *67*, 1159-1163.

(146) Yang, L. Y.; Lee, C. S.; Hofstadler, S. A.; Pasa-Tolic, L.; Smith, R. D. *Anal. Chem.* **1998,** *70*, 3235-3241.

(147) Torto, N.; Hofte, A.; van der Hoeven, R.; Tjaden, U.; Gorton, L.; Marko-Varga, G.; Bruggink, C.; van der Greef, J. *J. Mass Spectrom.* **1998,** *33*, 334-341.

CHAPTER 1

Analysis of Metal Incorporation During Overexpression of *Clostridium Pasteurianum* Rubredoxin by Electrospray FTICR Mass Spectrometry[1]

[1]Taylor, P. K.; D. M. Kurtz, Jr.; I. J. Amster. Submitted to *Journal of Biological Inorganic Chemistry*

Abstract

The rate of production of *Clostridium pasteurianum* rubredoxin overexpressed in *Escherichia coli* was examined by electrospray ionization-Fourier transform ion cyclotron resonance (ESI-FTICR) mass spectrometry. Previous work had shown that this heterologous expression resulted in isolation of both iron-containing (FeRd) and zinc-containing (ZnRd) rubredoxins.[1] In the present work, minimally processed cell lysates of *E. coli* were analyzed in order to monitor the production of FeRd and ZnRd. The sensitivity of the measurement favored FeRd relative to ZnRd, and this differential sensitivity was quantitated using previously separated and purified rubredoxins. A time course study indicated that ZnRd and FeRd are produced simultaneously during overexpression, but at different rates. The ratio of the concentration of ZnRd to FeRd increased in a linear fashion during three hours following induction of overexpression. The data suggest that since only FeRds have been reported from native bacteria and archaea, Zn^{2+} is sequestered from rubredoxins during native biosynthesis. Alternatively, ZnRds may have escaped detection in the native microorganisms. ESI-FTICR mass spectrometry is shown to be a useful tool for monitoring metal insertion during protein biosynthesis.

Key words: mass spectrometry, metal center, rubredoxin, metalloprotein, electrospray ionization

Introduction

The biosynthesis of active metalloproteins requires not only the production of a polypeptide with the correct amino acid sequence, but also the incorporation of a metal or metal-containing complex into the properly folded protein. The metal incorporation may occur either "spontaneously" or with the aid of metallochaperones.[2] Rubredoxin (Rd), a small iron-sulfur metalloprotein, when isolated from the native bacteria, such as *Clostridium pasteurianum*, contains only a single $Fe(SCys)_4$ center.[3] However, when Rd is overexpressed in *E. coli* (which contains no native Rd), both a zinc-containing (ZnRd) and an iron-containing (FeRd) form are obtained.[1] X-ray crystallography has determined that zinc replaces the iron in the metal center of FeRd, with only a slight distortion of the tetrahedral coordination sphere.[4] Because the function of FeRd is believed to be in electron transfer, the ZnRd is presumably an artifact of heterologous overexpression.[1, 5, 6] Recent *in vitro* experiments have shown that the Fe^{2+} in Rd can be readily displaced by Zn^{2+} or Cd^{2+} when the protein is exposed to a modest molar excess of these metal ions under anaerobic conditions. Thus, Fe^{2+} does not have an inherently higher affinity for Rd compared to Zn^{2+} or Cd^{2+}.[7] It is of interest, then, to examine the production of FeRd vs ZnRd during overexpression in order to observe the relative rates of production of these two forms.

Electrospray ionization-Fourier transform ion cyclotron resonance (ESI-FTICR) mass spectrometry is well-suited for the analysis of metalloproteins. The electrospray ionization process is capable of producing protein ions that retain both the metal center and the conformation of the nondenatured protein.[8-12] In addition, the electrospray

process places multiple charges on the protein, allowing the observation of proteins within the mass-to-charge range of conventional instruments.[13] Previous ESI-MS studies were able to detect ZnRd and FeRd as negative ions.[14] Subsequent research by our group has shown that these metalloproteins can be detected either as negative or positive ions, and that the high mass accuracy and high resolution capabilities of FTICR mass spectrometry aid the distinction between iron- and zinc-containing proteins which differ by only 10 Da per metal ion. Here we use ESI-FTICR to monitor the relative rates of production of zinc and iron Rds during overexpression in *E. coli*.

Materials and methods

C. pasteurianum Rd was overexpressed in *E. coli* strain BL 21 (DE3) according to a previously described procedure.[15] For the time course study, three 1-L cell cultures in Luria-Bertani medium were prepared. The metal content of the broth was analyzed prior to inoculation by ICP-AE spectroscopy and both the iron and zinc concentrations were found to be near the limit of detection, ca. 50 ppb. A 25-mL aliquot of each 1-L cell culture was removed prior to induction by addition of isopropyl-β-D-thiogalactopyranoside. Additional 25-mL aliquots were removed at 15-minute intervals beginning thirty minutes after induction and ending 180 minutes after induction. A final 25-mL aliquot of each 1-L cell culture was removed approximately sixteen hours after induction. The cells from each of these aliquots were collected separately by centrifugation, resuspended in 5 mL of Milli-Q purified water (Millipore, Bedford, MA), and lysed by sonication. The supernatant from each culture was retained for metal analysis. After centrifugation of the lysed cell suspension at 15,000g for 30 minutes, the

supernatant, which contained the Rd, was concentrated to a volume of 1.5 mL using a 10 mL Amicon cell with a 3000 Da MW-cutoff membrane (Millipore, Bedford, MA). Further concentration to 0.5 mL was accomplished by centrifugation through a 5000 MW-cutoff filtration membrane (Millipore, Bedford, MA). Removal of nonvolatile salts was accomplished by repeated centrifugation through a Millipore 5000 Da MW-cutoff membrane followed by dilution with 0.4 mL of 10 mM ammonium acetate. Prior to analysis, the protein was resuspended in 0.5 mL of 10 mM ammonium acetate. No further purification steps were performed on the sample.

Purified ZnRd and FeRd were prepared for use as mass spectrometry standards. A separate 1-L culture was grown for three hours after induction of overexpression, and the cells were lysed as described above. The FeRd and ZnRd in the supernatant were separated by anion-exchange chromatography[1] and desalted by repeated ultrafiltration using a Millipore microcentrifuge tube with a 5000 MW-cutoff membrane, followed by resuspension of the protein in 10 mM ammonium acetate. Rd concentrations were determined by UV-visible absorption using ε_{492} = 8850 M^{-1} cm^{-1} for FeRd and ε_{280} = 9530 M^{-1} cm^{-1} for ZnRd.[1, 5, 7]

Mass spectrometry was performed with a Bruker BioApex Fourier transform ion cyclotron resonance mass spectrometer with an unshielded 7 Tesla magnet and an Analytica electrospray ionization source. Samples were ionized by nanospray,[16, 17] using tips fabricated from 100 μm i.d. fused silica. A six-cm length of fused silica was suspended from one end and a 5-gram weight was attached to the other end. A small region of the capillary (ca. 2 mm) was heated with a butane micro-torch (Model 1000,

Microflame), causing the fused silica to separate into two pieces with a fine tip. The resulting fused silica nanospray tip was then glued inside a section of Wiretrol 5 mL glass micropipet (Drummond Scientific Company, Broomall, Pennsylvania) which is mounted inside a Mann style nanospray tip holder. Sample solutions were delivered via a syringe pump at a rate of 100 nL/min. Voltage was applied at the syringe needle, typically 1-1.2 kV, providing a liquid electrical junction. Desolvation was aided by a modification made to the Analytica ion source consisting of the replacement of the glass capillary inlet with a heated metal capillary inlet. The heated metal capillary provides a gentler method of desolvation than high nozzle-skimmer voltages, removing the chance of unwanted dissociation. The capillary temperature was maintained at 150°C for these experiments. Ions were stored in the hexapole ion guide of the Analytica source for 0.5 seconds. After exiting the hexapole, ions were directed to the FTICR analyzer cell through a series of electrostatic lenses. Trap voltages were 1.2 V on both front and back trap plates. Ions were excited for 50 μsec at 200 $V_{p\text{-}p}$, and detected over a range of 800-3200 m/z. No collision gas was used to aid the trapping of the ions, and pressure in the analyzer region was maintained at approximately $8x10^{-10}$ torr. Under these conditions, the Rd signal is due entirely to metal-containing forms.

Isotope compositions in an isotope distribution were assigned by matching the abundances of the observed peaks to theoretically derived data, using a chi-squared statistical fit, as proposed by Senko et al.[18] Molecular weights were calculated from the data by multiplying the mass-to-charge of a peak by its charge value, which was determined from the spacing of the isotope peaks. This procedure is repeated for a

number of isotope peaks in a distribution, and the monoisotopic mass of the ion is extracted by accounting for the number of heavy atoms in each peak. Since the charge on the metal center is not known *a priori*, the initial assumption is made that all excess charge is due to protons. The mass of the protons equal in number to the charge of the ion is subtracted from the mass of the ion to give an estimate of the molecular weight of the protein. This estimate is compared to the expected value, calculated for the known elemental composition of the protein. The difference between the two values is equal to the integer number of charges present on the metal center. This procedure has been described in more detail in an earlier publication.[11]

Results and discussion

ESI-FTICR provides high resolution mass spectral data from which the monoisotopic molecular weight of a protein can be derived. For a protein containing no metal, the monoisotopic mass corresponds to the elemental composition of the protein, which can be calculated by summing the masses of the lowest mass isotope of each atomic species. In calculating the monoisotopic molecular weight of metal-containing Rds, the isotopic distribution of the metals must be taken into account. Only iron- and zinc-containing Rds (FeRd and ZnRd) were examined in this study. The most abundant isotope of iron is ^{56}Fe, but the lowest mass isotope is ^{54}Fe. Theoretically, the lowest mass peak in the mass spectrum should arise from ^{54}Fe and all the other low mass isotopes of the elements (^{12}C, ^{14}N, ^{16}O, ^{32}S, ^{1}H), Figure 1. Experimentally, this peak is difficult to observe, as ^{54}Fe has a natural abundance of only 5.81%. The peak arising from one ^{56}Fe

Figure 1. ESI-FTICR mass spectrum of FeRd, 4+ charge state (bottom) and theoretically derived isotope distribution (top). Arrow indicates the "monoisotopic" peak for this metalloprotein, containing zero ^{13}C's and the most abundant isotope of the metal (^{56}Fe). Comparison of theoretical and experimental deconvoluted mass reveals that the iron is in the Fe(III) oxidation state.

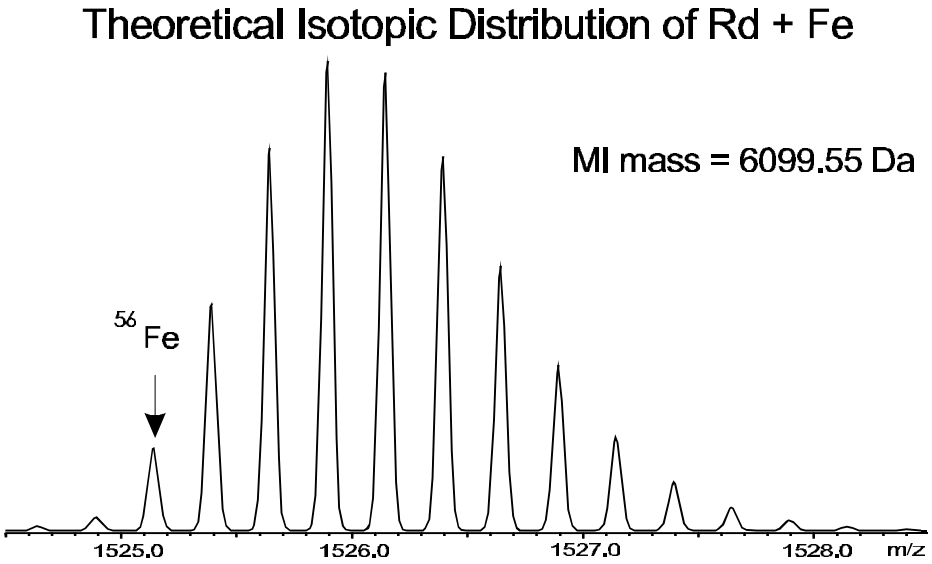
Theoretical Isotopic Distribution of Rd + Fe
MI mass = 6099.55 Da
56 Fe
1525.0
1526.0
1527.0
1528.0
m/z

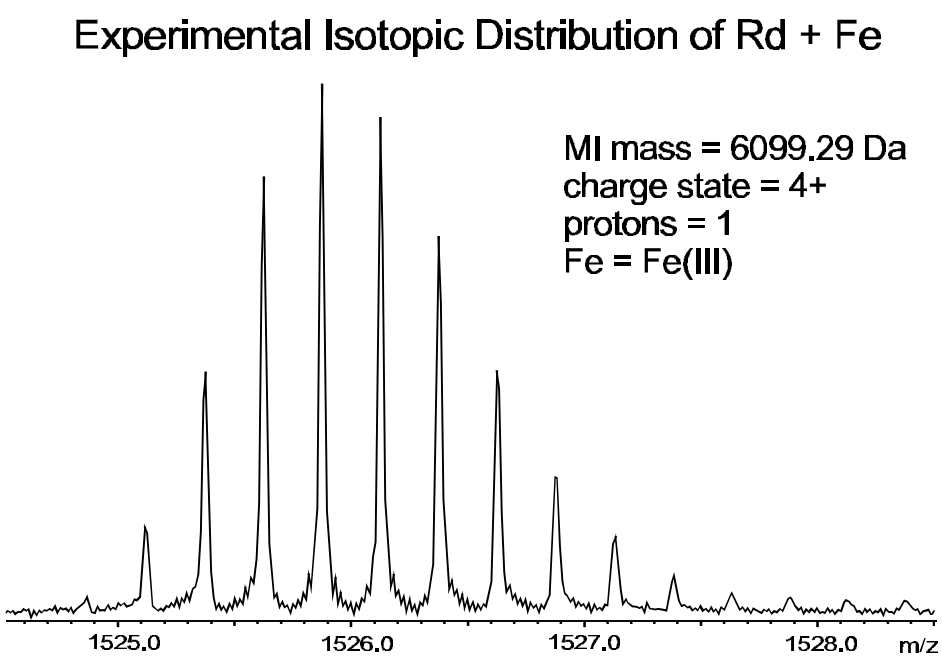
Experimental Isotopic Distribution of Rd + Fe
MI mass = 6099.29 Da
charge state = 4+
protons = 1
Fe = Fe(III)
1525.0
1526.0
1527.0
1528.0
m/z

(91.8% natural isotopic abundance) is much easier to detect. Therefore, in the discussion that follows, "monoisotopic mass" refers to the monoisotopic mass of the apo-Rd plus the mass of ^{56}Fe. ZnRd needs no such clarification, since the lowest mass isotope of zinc (^{65}Zn) is also its most abundant isotope.

Twenty-five milliliter samples were collected from each 1-L culture at 15-minute intervals beginning 30 minutes after induction of overexpression. In order to minimize the possibility of artificially affecting the concentration of either ZnRd or FeRd, the preparation of these 25-mL samples for mass spectrometry consisted only of cell lysis by sonication, concentration, and desalting by buffer exchange. Figure 2 shows representative mass spectra of the cell lysate collected from one 1-L culture at three time points after induction. The FeRd produces an isotopic distribution centered around m/z 1526. The isotopic spacing (0.25 m/z) indicates that these peaks arise from the 4+ charge state of the protein, and the experimentally determined monoisotopic mass is 6096.7 Da. Research has recently been conducted using mass spectrometry to determine the exact oxidation state of the metal in a metalloprotein.[11, 19] The theoretical monoisotopic mass for FeRd calculated from the amino acid sequence plus one iron atom is 6099.55 Da. The three mass-unit difference between experimental and theoretical monoisotopic mass arises because the procedure used to treat the experimental data assumes that all charge arises from excess protons. In the case of a metalloprotein, however, charge resides on the metal, causing this calculation to overestimate the number of protons on the ion, therefore underestimating the mass of the protein. The three mass unit difference indicates that iron is present as Fe(III) in FeRd during the ESI-FTICR experiment. Peaks arising from the

Figure 2. Sample ESI-FTICR mass spectra of cell lysate from the 25-mL aliquots collected at incremental time points after induction. All spectra are expansions of the 4+ charge state. Note the increasing intensity of ZnRd peaks relative to FeRd peaks. a) Mass spectrum of cell lysate collected 30 minutes after induction. b) Mass spectrum of cell lysate collected 90 minutes after induction. c) Mass spectrum of cell lysate collected 180 minutes after induction.

a)

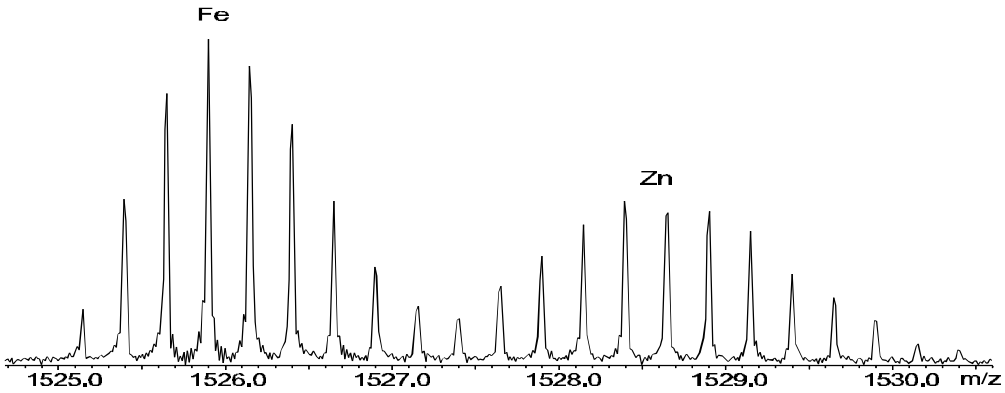
Fe
Zn
1525.0
1526.0
1527.0
1528.0
1529.0
1530.0
m/z

b)

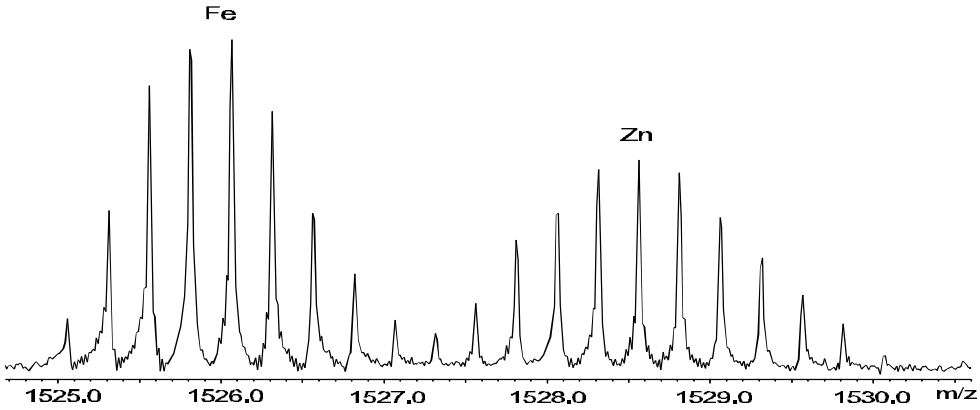
Fe
Zn
1525.0
1526.0
1527.0
1528.0
1529.0
1530.0
m/z

c)

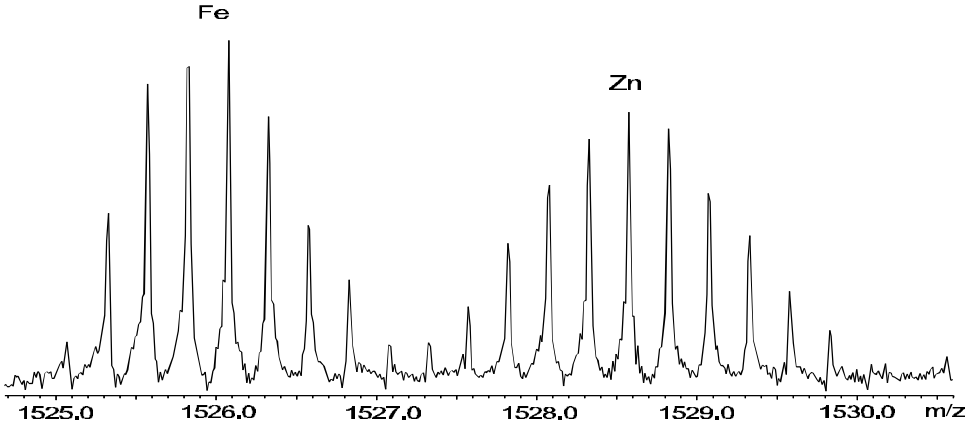
Fe
Zn
1525.0
1526.0
1527.0
1528.0
1529.0
1530.0
m/z

isotopic distribution of the ZnRd appear at m/z 1528.5, and their spacing indicates that the overall charge present on the ion is 4+. Treatment of these data yields a mass of 6105.64 Da. The theoretical monoisotopic mass of ZnRd calculated from the amino acid sequence plus one zinc atom is 6107.55 Da. The two mass unit difference indicates that the zinc is present as Zn(II). Thus, the derived charges on the metal ions agree with those expected for the most stable oxidation states of FeRd and ZnRd under aerobic conditions.

We have noticed a slight difference in the response of the mass spectrometer to ZnRd compared to FeRd. An equimolar mixture of ZnRd and FeRd (as determined by UV-visible absorption spectrophotometry) shows slightly more intense peaks for the FeRd, as can be seen in Figure 3. In order to calibrate the instrument response for the two proteins, we prepared mixtures of purified FeRd and ZnRd standards which had been quantitated by UV-visible spectrophotometry. The relative peak intensities of the Fe- versus ZnRds were determined by summing the intensities of each individual isotope peak, in order to account for the slightly broader isotopic distribution of the ZnRd. The integrated peak intensities for ZnRd versus FeRd in the standard mixtures were plotted versus relative concentration, Figure 4. The slope of this plot is 0.688, which shows that the ZnRd produces a weaker signal, perhaps due to a lower ionization efficiency. The equation derived from this plot was then used to determine the molar ratios of ZnRd to FeRd from the ratio of the experimentally determined isotope peak intensities derived from the 25-mL samples taken after induction. The ratio of ZnRd/FeRd peak intensity in the thirty-minute sample averaged between all three runs was found to be 0.71, yielding a concentration ratio of 1.03. Thus, the concentration of ZnRd was equal to that of FeRd in

Figure 3. ESI-FTICR mass spectrum of equimolar (10 μM each FeRd and ZnRd) mixture of previously purified and separated Fe- and ZnRd. The ZnRd signal appears to be approximately half that of the FeRd. This is an expansion of the 4+ charge state.

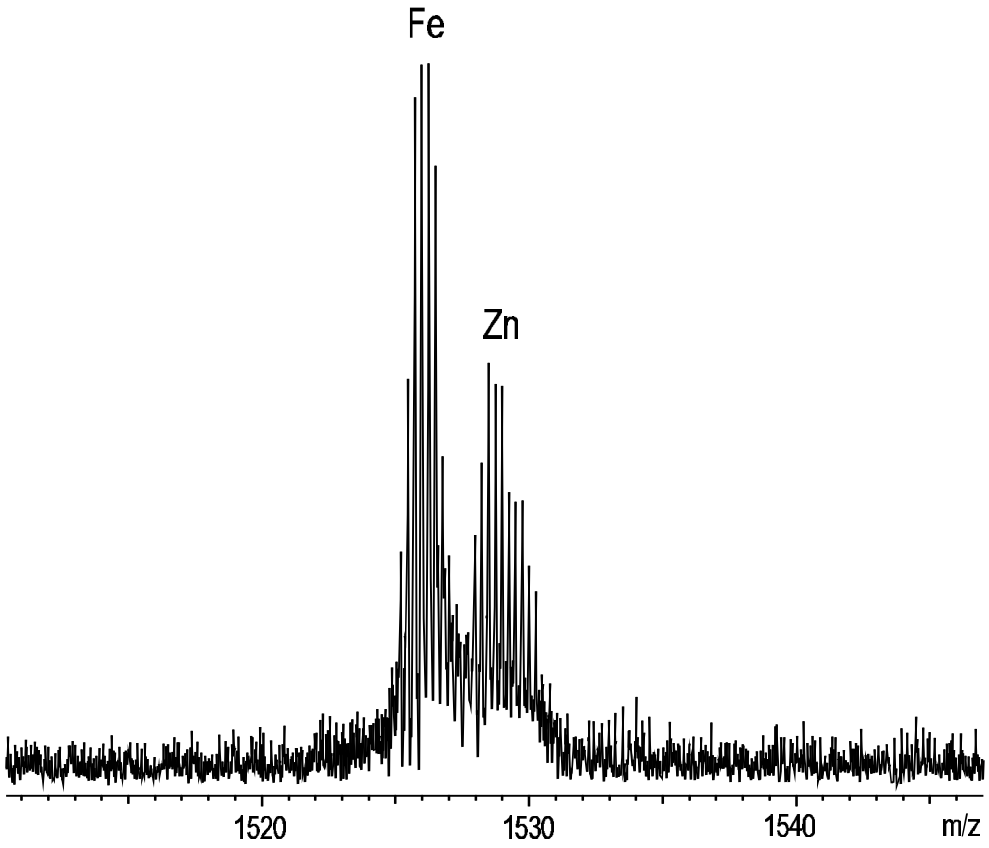
Fe
Zn
1520
1530
1540
m/z

Figure 4. Plot of the ratio of Zn- to FeRd summed signal intensity measured by ESI-FTICR versus the ratio of Zn- to FeRd sample concentration determined by UV-visible spectrophotometry. Total protein concentration was maintained at 10 mM, and the ZnRd/FeRd concentration ratio was prepared through calculated dilutions of stock solution. The error bars correspond to ±1 standard deviation.

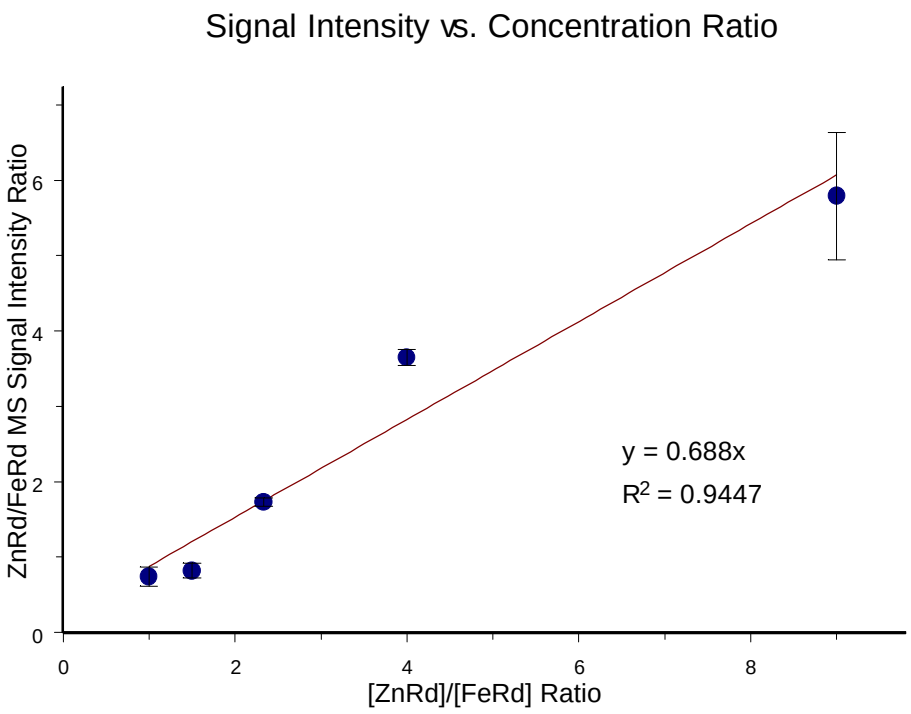
Signal Intensity vs. Concentration Ratio
ZnRd/FeRd MS Signal Intensity Ratio
0
2
4
6
0
2
4
6
8
[ZnRd]/[FeRd] Ratio
y = 0.688x
R2 = 0.9447

this sample. The remainder of the samples, collected at 15-minute increments, were analyzed, and the ratios of ZnRd/FeRd concentration were extracted from the mass spectra in the same fashion. Figure 5 shows the plot of ZnRd/FeRd concentration ratio vs. time up to 16 hours after induction, averaged over three runs. The plot indicates a linear increase in the amount of ZnRd produced during overexpression relative to FeRd through the first 180 minutes after induction. The final sample, taken 16 hours after induction, shows an increase in the ratio of [ZnRd]/[FeRd] (2.1). This value is less than the ratio that extrapolates from the data from the first 180 minutes. The total amount of Rd produced over the time course was also determined. The concentration of FeRd in the mass spectrometry samples was determined by UV-visible absorption spectrophotometry, using $\varepsilon_{492} = 8850\ M^{-1}cm^{-1}$ for $Fe^{3+}Rd$.[5] The concentration of ZnRd was then calculated using the spectrophotometrically determined FeRd concentration and the ZnRd/FeRd concentration ratio determined by mass spectrometry. The concentrations of Fe- and ZnRds were then summed to obtain the total Rd concentrations. All three of the aforementioned parameters are plotted in Figure 6 as a function of time after induction of overexpression. The data indicate that *de novo* biosynthesis of Rd is occurring throughout the first three hours of the time course following induction. The final time point, taken 16 hours after induction, shows a significant decrease in the total Rd concentration, suggesting the onset of cell death and lysis.

Figure 5. Plot of ZnRd/FeRd concentration vs. time after induction. The slope indicates that the concentration of ZnRd increases relative to FeRd throughout overexpression. Error bars correspond to ±1 standard deviation, calculated from three runs over each time point.

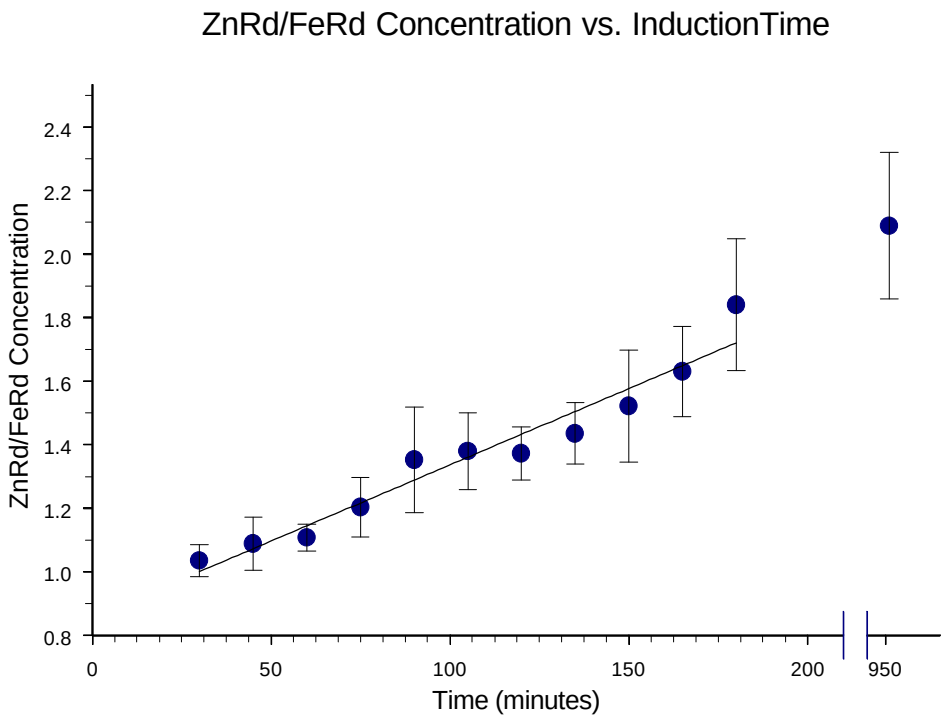
ZnRd/FeRd Concentration vs. InductionTime
ZnRd/FeRd Concentration
2.4
2.2
2.0
1.8
1.6
1.4
1.2
1.0
0.8
0
50
100
150
200
950
Time (minutes)

Figure 6. Plot of total Rd concentration vs. time after induction. FeRd concentration was determined by UV-visible spectrophotometry, while ZnRd concentration was calculated using the ZnRd/FeRd concentration ratio determined by mass spectrometry. The plot indicates that Rd is being made throughout 180 minutes of overexpression. However, the protein concentration at the 16 hour time point has greatly decreased. Error bars correspond to ±1 standard deviation, calculated from three runs over each time point.

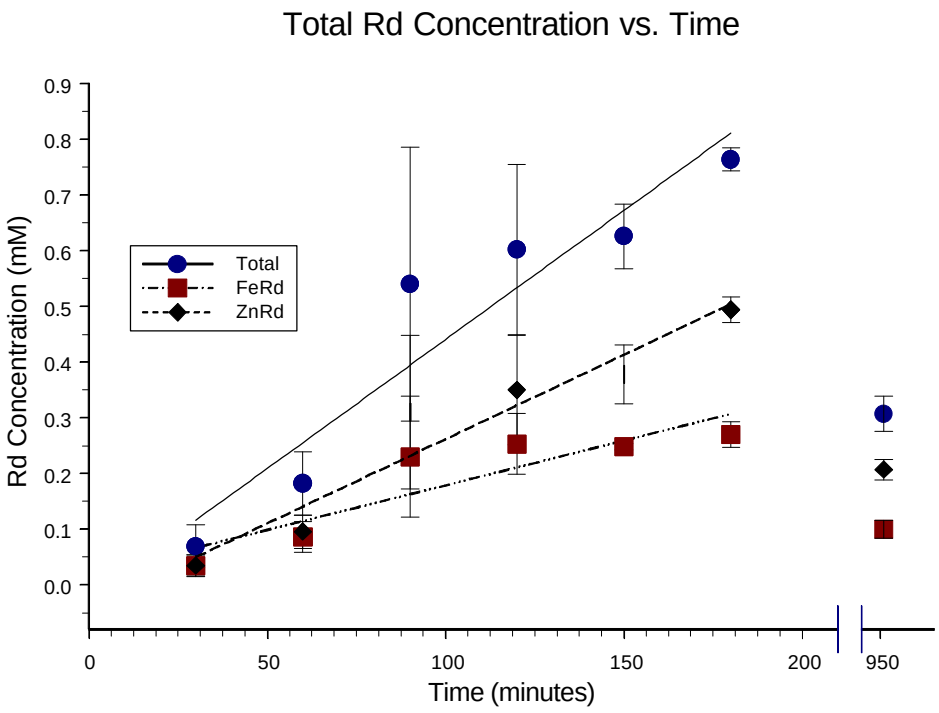
Total Rd Concentration vs. Time
Rd Concentration (mM)
0.9
0.8
0.7
0.6
0.5
0.4
0.3
0.2
0.1
0.0
Total
FeRd
ZnRd
0
50
100
150
200
950
Time (minutes)

Conclusion

Zinc and iron are normally the two most abundant transition metal ions present in *E. coli*, and their uptake reflects the relative affinities of the overexpressed metalloprotein.[20] Therefore, relative uptake of these two metals are unlikely to affect the ratios of the corresponding Rds. On the other hand, previous *in vitro* studies have shown that excess Zn^{2+} will substantially displace Fe^{2+} from native reduced *C. pasteurianum* FeRd over several hours, i.e., in a time scale similar to that monitored in the present study.[7] Therefore, the present *in vivo* results are consistent with either a higher rate of Zn^{2+} vs Fe^{2+} uptake by apo-Rd during its biosynthesis or displacement of Fe^{2+} by Zn^{2+} from FeRd following its biosynthesis. The fact that substantial amounts of ZnRd are detected even at the earliest time point (30 min) following induction of overexpression would suggest that ZnRd is not produced from FeRd at least at the early stages of overexpression. The 16-hour time point in Figure 6 is more difficult to interpret, since the total Rd concentration decreased. However, the data for this time point indicates that zinc has not completely displaced iron in Rd at 16 hours after induction. We also cannot rule out a contribution from differential sequestration of Zn^{2+} vs Fe^{2+} within *E. coli* cells. The redox chemistry of iron is unlikely to be a factor, since the laboratory growth conditions used for *E. coli* result in a fairly reducing environment within the cells, and most of the detectable "free" iron is present as Fe^{2+}, even in an aerobic atmosphere.[21] We have in fact noted previously that the vast majority of FeRd overexpressed in *E. coli* is in the reduced form prior to cell lysis (D. M. Kurtz, K. A. Richie, M. K. Eidsness, unpublished results).

The distribution of both iron and zinc within *E. coli* cells is tightly regulated,[22, 23] and this statement is generally true for other microorganisms, including *C. pasteurianum*. Thus, the question arises as to the distribution of Fe- vs ZnRd in *C. pasteurianum* and other Rd-containing microbes, of which at least 14 are known.[24] In all cases, only iron-containing forms of Rd have been reported from the native organisms. Therefore, given our results, these microorganisms may completely sequester Zn^{2+} from Rd during and even after its biosynthesis. Alternatively, it is possible that ZnRd is produced by these microorganisms, but has remained undetected up to now. This latter possibility could be due to a relative lack of sensitive spectroscopic methods for detection of zinc in proteins, and to a lack of any known activity for a ZnRd. Future mass spectrometric analyses of *C. pasteurianum* cell extracts are planned in order to determine the presence or absence of ZnRd in the native microorganism.

Acknowledgments

The authors would like to thank Kim Richie, Marly Eidsness, and Amy Burden for experimental assistance and helpful discussions. We would also like to acknowledge financial support from the Center for Metalloenzyme Studies at the University of Georgia (NSF Research Training Group Award DBE-9413236). IJA acknowledges the support of the National Science Foundation (CHE-9974579).

REFERENCES

(1) Richie, K. A.; Teng, Q.; Elkin, C. J.; Kurtz, D. M. *Protein Sci.* **1996,** *5*, 883-894.

(2) Hausinger, R. P. In *Mechanisms of Metallocenter Assembly*; Hausinger, R. P., Eichhorn, G. L., Marzilli, L. G., Eds.: NY, 1996, pp 1-18.

(3) Watenpaugh, K. D.; Sieker, L. C.; Jensen, L. H. *J. Mol. Biol.* **1980,** *138*, 615-633.

(4) Dauter, Z.; Wilson, K. S.; Sieker, L. C.; Moulis, J. M.; Meyer, J. *Proc. Natl. Acad. Sci. U.S.A.* **1996,** *93*, 8836-8840.

(5) Eidsness, M. K.; Odell, S. E.; Kurtz, D. M.; Robson, R. L.; Scott, R. A. *Protein Eng.* **1992,** *5*, 367-371.

(6) Mathieu, I.; Meyer, J.; Moulis, J. M. *Biochem. J.* **1992,** *285*, 255-262.

(7) Bonomi, F.; Iametti, S.; Kurtz, D. M.; Ragg, E. M.; Richie, K. A. *J. Biol. Inorg. Chem.* **1998,** *3*, 595-605.

(8) Brown, C.; Camilleri, P.; Haskins, N. J.; Saunders, M. *J. Chem. Soc. Chem. Commun.* **1992**, 761-764.

(9) Jaquinod, M.; Guy, P.; Remigy, H.; Halgand, F.; SaintPierre, C.; Forest, E. *Analusis* **1996,** *24*, 152-154.

(10) Wang, F.; Freitas, M. A.; Marshall, A. G.; Sykes, B. D. *Int. J. Mass Spectrom.* **1999,** *192*, 319-325.

(11) Johnson, K.; Verhagen, M.; Brereton, P.; Adams, M.; Amster, I. *Anal. Chem.* **2000,** *72*, 1410-1418.

(12) Lei, Q. P.; Cui, X. Y.; Kurtz, D. M.; Amster, I. J.; Chernushevich, I. V.; Standing, K. G. *Anal. Chem.* **1998,** *70*, 1838-1846.

(13) Fenn, J. B.; Mann, M.; Meng, C. K.; Wong, S. F.; Whitehouse, C. M. *Mass Spectrom. Rev.* **1990,** *9*, 37-70.

(14) Petillot, Y.; Forest, E.; Mathieu, I.; Meyer, J.; Moulis, J. M. *Biochem. J.* **1993,** *296*, 657-661.

(15) Eidsness, M. K.; Richie, K. A.; Burden, A. E.; Kurtz, D. M.; Scott, R. A. *Biochemistry* **1997,** *36*, 10406-10413.

(16) Valaskovic, G. A.; Kelleher, N. L.; Little, D. P.; Aaserud, D. J.; McLafferty, F. W. *Anal. Chem.* **1995,** *67*, 3802-3805.

(17) Wilm, M.; Mann, M. *Anal. Chem.* **1996,** *68*, 1-8.

(18) Senko, M. W.; Beu, S. C.; McLafferty, F. W. *J. Am. Soc. Mass Spectrom.* **1995,** *6*, 229-233.

(19) He, F.; Hendrickson, C. L.; Marshall, A. G. *J. Am. Soc. Mass Spectrom.* **2000,** *11*, 120-126.

(20) D'Souza, V. M.; Holz, R. C. *Biochemistry* **1999,** *38*, 11079-11085.

(21) Keyer, K.; Imlay, J. A. *Proc. Natl. Acad. Sci. U.S.A.* **1996,** *93*, 13635-13640.

(22) Patzer, S. I.; Hantke, K. *Mol. Microbiol.* **1998,** *28*, 1199-1210.

(23) Touati, D. *Arch. Biochem. Biophys.* **2000,** *373*, 1-6.

(24) Eidsness, M. K.; Burden, A. E.; Richie, K. A.; Kurtz, D. M.; Scott, R. A.; Smith, E. T.; Ichiye, T.; Beard, B.; Min, T. P.; Kang, C. H. *Biochemistry* **1999,** *38*, 14803-14809.

CHAPTER 2

Space Charge Effects on Mass Accuracy for Multiply Charged Ions in ESI-FTICR[1]

[1]Taylor, P. K.; I. J. Amster. Submitted to *Journal of the American Society for Mass Spectrometry*

ABSTRACT

Ion space charge causes systematic shifts in the observed cyclotron frequencies of ions, limiting accurate mass measurements in FTICR. Previous studies of space charge effects on mass accuracy have focused on singly charged ions. Presented here are studies of space charge effects on mass accuracy for multiply charged ions produced by electrospray ionization. Axialization of the ion cloud by quadrupolar excitation increases space charge-induced shifts in observed frequency but reduces the random errors in measurements by distributing ions in the analyzer cell in a reproducible manner. Space charge-induced shifts in observed frequency are observed to be independent of charge state. Because all ions experience the same space charge-induced frequency shift, internal calibration is accurate without regard to differences between the charge states of the calibrant and analyte peaks. Space charge-induced frequency shifts in externally calibrated mass spectra can be corrected to provide significant improvement in mass accuracy for such measurements.

INTRODUCTION

Fourier transform ion cyclotron resonance (FTICR) mass spectrometry is a technique known for its high mass resolution and mass accuracy. These features enhance a wide variety of mass spectrometric studies, including polymer analysis,[1-6] oxidation state studies of metalloproteins,[7, 8] high throughput proteomics and database searching,[9-20] and protein sequencing.[21-24] Space charge effects have long been known to limit mass accuracy measurements in FTICR mass spectrometry.[25, 26] Space charge arises from the influence of the electric field of ions in the trapped analyzer cell upon each other, and it has been quantified in the equation for the observed frequency of motion of ions in a magnetic field developed by Jeffries, Barlow, and Dunn, and refined by McIver and coworkers, Equation 1.[27, 28] The first term in the right side of the equation is the unperturbed cyclotron frequency, where q is the coulombic charge on the ion, B is the strength of the magnetic field, and m is the mass of the ion. The second term is equal to the magnetron frequency of the ions, produced by the influence of the voltage used to trap the ions within the cell, where a is the diameter of the cell, α is a constant determined by the cell geometry, and V is the voltage applied to the trap plates. The third term quantifies the space charge effect on observed frequency, where ρ is the ion density, G_i is a constant that is related to the geometry of the ion cloud, and ε_0 is the permittivity of free space. The greatest variation in the magnitude of the space charge effect arises from differences in ion density, caused by changes in the number of ions within the cell from one ionization event to the next. Unless space charge is either taken into account or eliminated, high mass accuracy measurements cannot be reliably achieved. This is particularly true for

MALDI experiments due to the large shot-to-shot variation in ion yield. A recent study of MALDI-FTICR showed space charge-induced variations in measured mass of 50-100 ppm in a 4.7 Tesla instrument.[2]

$$\omega_{obs} = \frac{qB}{m} - \frac{2\alpha V}{a^2 B} - \frac{q\rho G_i}{\varepsilon_o B} \quad \textbf{(1)}$$

A number of valuable efforts have been made to study and quantitate space charge effects on mass accuracy for singly charged ions.[2, 25, 27-36] Jeffries et al. presented a mathematical treatment of space charge in the scanning ICR experiment.[27] McIver and coworkers based their equation for space charge (Equation 1) on Jeffries' work.[28] Chen and Comisarow have examined space charge by representing rotating ions as a pair of points, line charges, or cylinders.[29, 30] Recently, Easterling et al. have examined space charge-induced shifts in observed frequency for high mass ions formed by matrix-assisted laser desorption/ionization (MALDI).[2] Smith and coworkers have developed a deconvolution routine known as DeCAL which systematically removes the space charge-induced frequency shifts in mass spectra of multiply-charged ions.[37] Further efforts have been made to reduce or negate the effects of space charge through physical means.[38-43] Increasing the magnetic field strength decreases the magnitude of space charge effects, among other benefits.[44, 45] A more general approach involves the manipulation of the ion population within the cell, typically through variation of the ICR pulse sequence. The trap plates may be momentarily grounded, suspended trapping,[41] or an asymmetric trap plate voltage can be applied to reduce the number of ions in the cell. The smaller number of ions trapped in this manner greatly reduces the effects of space charge. A third method

for reducing the effect of space charge on mass accuracy is to use an internal calibrant,[43, 44, 46, 47] as the calibrant is subjected to the same frequency shift as the species of interest. Equation 1 suggests that space charge-induced frequency shifts are proportional to the charge on an ion, and that multiply-charged ions should exhibit proportionally larger shifts than their singly-charged counterparts. If this is true, then one would need to take charge state into account even when performing internal calibration. Furthermore, it is often impractical to use an internal standard with electrospray ionization, as mixtures are susceptible to suppression effects that can favor the production of one ionic species over others. In such a case, external calibration must be used. For external calibration in ESI-FTICR, it is necessary to have a quantitative understanding of space charge effects on mass accuracy in order to compensate for differences in ion population between the analyte and the calibrant mass spectra. The recently published DECAL method for compensating for space charge effects relies on knowing the relationship between charge state and frequency shift.[37] For all these reasons, it is important to characterize the effect of ion population and charge state on observed frequency, in order to achieve high mass accuracy. Here we use electrospray ionization FTICR to examine space charge induced frequency shifts for multiply charged ions and discern the effect of charge state on mass accuracy.

EXPERIMENTAL

Melittin, insulin, ubiquitin, hemoglobin, insulin chain B, and myoglobin were purchased from Sigma (St. Louis, MO) and used without further purification. All samples were dissolved in a solution of 49:49:2 water:methanol:acetic acid (v/v) to a concentration

of 10 μM. Internal calibration was performed by mixing 30 μL of hemoglobin with 30 μL of insulin chain B. Ions were produced via nanospray through tips fabricated in-house from 100 μm i.d. fused silica (Supelco, Bellefonte, PA).[48] Sample solutions were introduced to the spray tips with by a syringe pump operated at a flow rate of 6 μL/hr. Approximately 1.2 kV was applied to the needle of the syringe, which forms a liquid junction with the emitter tip.

Mass spectrometry was performed with a Bruker BioApex 7 T FTICR mass spectrometer equipped with an Analytica source which has been modified by replacing the glass capillary with a heated metal capillary interface.[8] The heated metal capillary was maintained at a temperature of 150°C. Quadrupolar excitation (QE)[49, 50] was performed with nitrogen as the collision gas for all samples except ubiquitin, for which helium was used. The gas pulse was applied for four seconds, raising the pressure in the analyzer between 6 x 10^{-5} torr and 2 x 10^{-4} torr, and the QE pulse was initiated simultaneously. QE was continued at 35.7 V_{p-p} for six seconds after closing the pulse valve, until the pressure in the analyzer reached 1 x 10^{-7} torr. A subsequent thirty second pumpdown delay allowed pressure in the analyzer to reach 1-2 x 10^{-8} torr, at which time the ions were excited and detected. These QE conditions were optimized to produce remeasurement efficiencies over 99%.[49, 51] For the space charge experiments utilizing QE, a packet of ions was produced and guided into the cell through a series of electrostatic lenses. QE was used to center the ions, and a single scan was acquired. The ionization pulse was turned off, and two more single scans were obtained using QE to remeasure the original ion packet. In this manner, three separate measurements were made for the same population of ions. A

50 μs cell quench pulse was then applied to the trap plates to remove approximately 10% of the ions from the cell. QE and remeasurement were then used to acquire three more mass spectra of the remaining ion population. The sequence of partial cell quench followed by three acquisitions was repeated until the signal had either decreased by an order of magnitude or was undetectable.

The experiments done without QE and without collision gas were performed by optimizing the signal intensity and then acquiring three mass spectra, each with a separate ionization pulse. The length of the ionization pulse was then decreased slightly (500 μs) to reduce the signal intensity, and three more mass spectra were acquired. This procedure was repeated until the signal was undetectable. The experiments done without QE but with a gas pulse were performed in the same fashion, except that a 4 second gas pulse and a 30 second pump down delay were included prior to excitation/detection. The ubiquitin and insulin spectra used to demonstrate space charge correction were obtained using identical pulse sequences. Four ionization pulses were interspersed with two 1.5 second gas pulses. A 90 second delay to pump away the gas was followed by excitation/detection. The front and rear trap plates were held at 0.5 and 0.65 volts, respectively.

RESULTS AND DISCUSSION

Ions produced by electrospray ionization exhibit systematic shifts in their observed frequency that correlate with the number of ions in the cell. Figure 1 shows mass spectra for the 3+ charge state of insulin exhibiting a frequency shift that correlates with signal intensity. For these experiments, the ions were axialized by QE prior to detection. Figure

Figure 1. ESI-FTICR mass spectra of insulin, using quadrupolar excitation to isolate the 3+ charge state and short cell quenches to systematically reduce ion density, exhibiting a frequency shift. (a) The 3+ charge state of insulin at full intensity. (b) The same ion packet after repeated quadrupolar excitation and short cell quenches, at 60% of the full intensity. (c) The same ion packet at 25% of the full intensity. The dashed line bisecting the base peak in (a) is meant to guide the eye in observing the space charge-induced frequency shift.

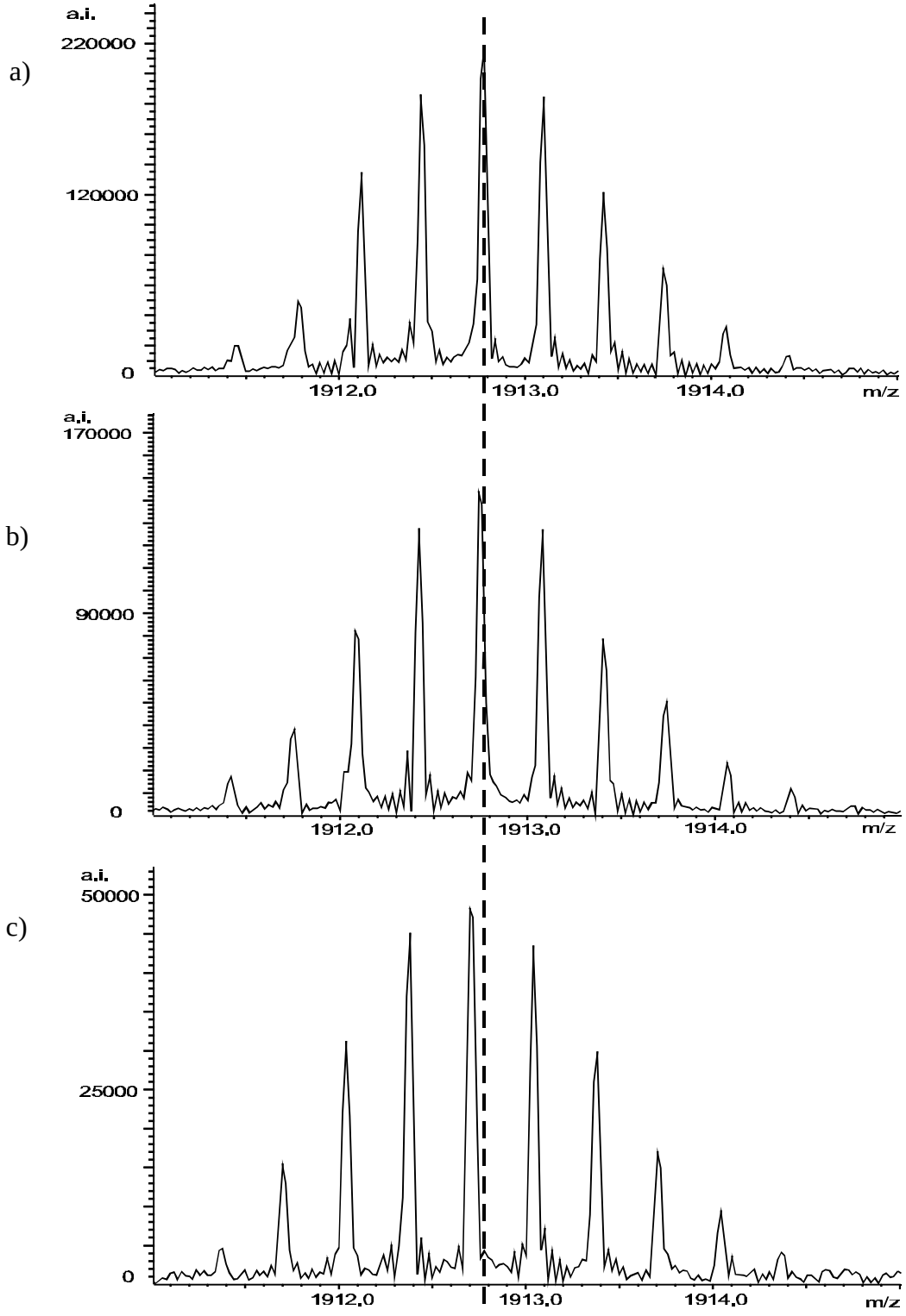
a)
a.i.
220000
120000
0
1912.0
1913.0
1914.0
m/z
b)
a.i.
170000
90000
0
1912.0
1913.0
1914.0
m/z
c)
a.i.
50000
25000
0
1912.0
1913.0
1914.0
m/z

1a shows insulin at full intensity; Figure 1b shows the same ion packet, after a series of remeasurements and short cell quenches, at 60% of its original intensity; and Figure 1c shows the same ion packet at 25% of its original intensity. The mass-to-charge ratio of the peaks are observed to systematically shift to lower values (higher frequency) as the total ion intensity decreases, in qualitative agreement with Equation 1. The frequency shift between the peaks in Figure 1a and 1c is 2.5 Hz, or 43 ppm. Clearly, calibration with the top mass spectrum would lead to unacceptably large errors if applied to a mass spectrum with a total ion intensity as in the bottom mass spectrum.

Previous research using MALDI-FTICR has shown that the magnitude of random errors in frequency measurement depend on the manner in which the ion cloud is treated prior to excitation and detection.[2] The largest errors were observed when the ions experienced no collisional damping of their axial motion, and the least when the ions were subjected to quadrupolar excitation prior to detection. This result is also observed in these experiments, as shown in Figure 2. Figure 2a shows a plot of the observed frequency shift versus total signal intensity for the 3+ charge state of insulin, with no collisional quenching of the ions prior to detection. The measured property of signal intensity correlates to the ion density term of Equation 1, as image current is directly proportional to the amount of charge being detected. The scatter observed in the plot (R^2 = 0.92) indicates fluctuations in the ion density, as ions assume different distributions along the central axis of the cell prior to the excite pulse. Figure 2b shows a plot of observed frequency versus signal intensity for the 3+ charge state of insulin when a short nitrogen gas pulse was introduced just after ions were injected into the cell. This gas pulse

Figure 2. Plots of signal intensity vs. frequency for the monoisotopic peak of the 3+ charge state of insulin under various conditions of axial cooling. (a) Insulin with no gas pulse, exhibiting the largest observed scatter. (b) Insulin with a short gas pulse to damp axial motion through collisions. Less scatter is observed in the plot, as evidenced by the higher R^2 correlation constant. The slope of this plot is almost three times as steep as that of (a), indicating an increase in space charge. (c) Insulin with QE applied to axialize the ions. This plot shows the smallest amount of scatter and the largest space charge effects.

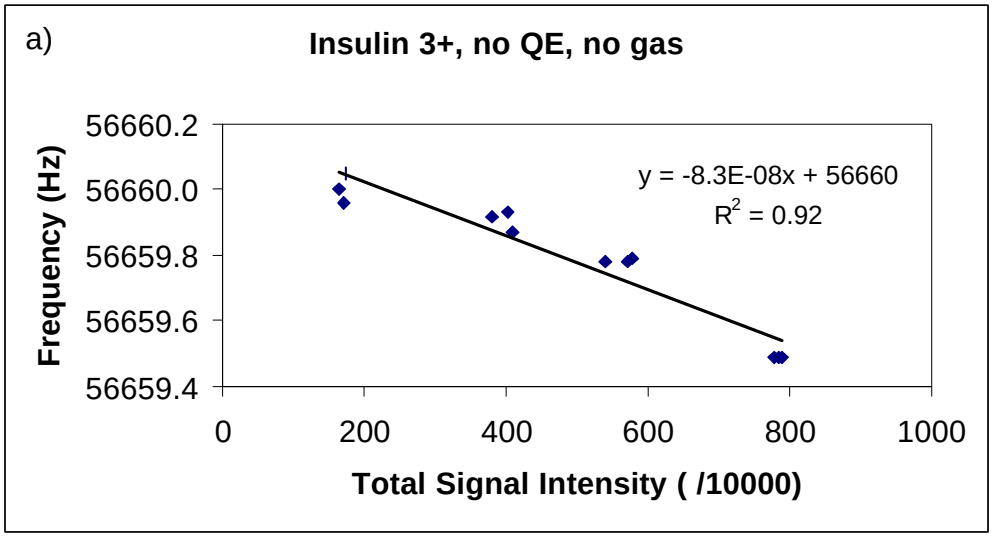
a)
Insulin 3+, no QE, no gas
Frequency (Hz)
56660.2
56660.0
56659.8
56659.6
56659.4
y = -8.3E-08x + 56660
R2 = 0.92
0
200
400
600
800
1000
Total Signal Intensity (/10000)

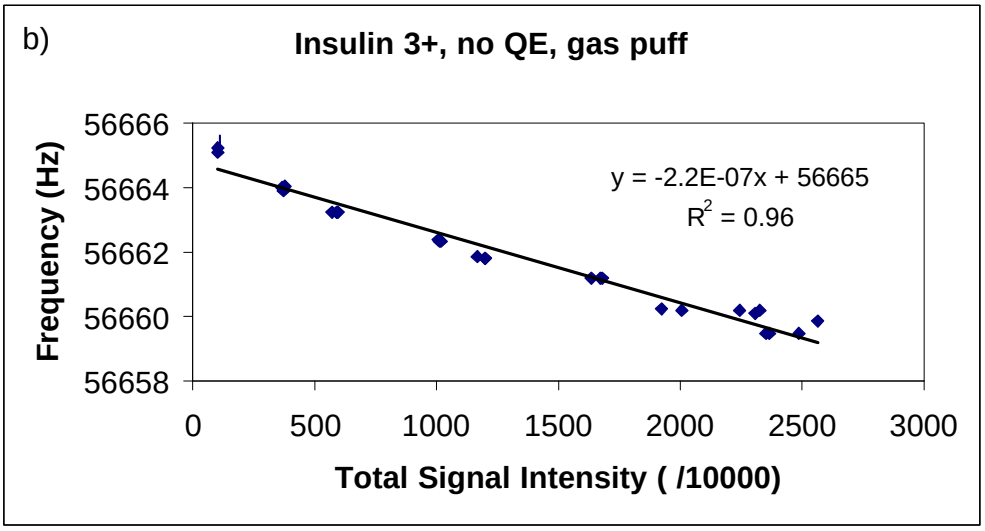
b)
Insulin 3+, no QE, gas puff
Frequency (Hz)
56666
56664
56662
56660
56658
y = -2.2E-07x + 56665
R2 = 0.96
0
500
1000
1500
2000
2500
3000
Total Signal Intensity (/10000)

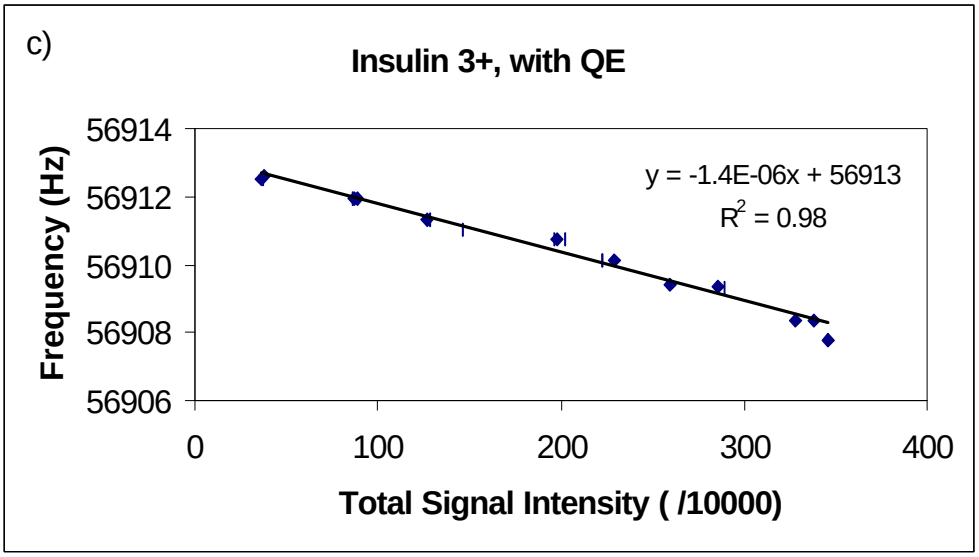
c)
Insulin 3+, with QE
Frequency (Hz)
56914
56912
56910
56908
56906
y = -1.4E-06x + 56913
R2 = 0.98
0
100
200
300
400
Total Signal Intensity (/10000)

provides collisional damping of the axial ion motion, reducing the distribution of the ions along the magnetic field axis within the cell. This creates a more reproducible ion distribution, leading to a reduction in the amount of scatter in the plot ($R^2 = 0.96$). Figure 2c shows a plot of frequency versus signal intensity for the 3+ charge state of insulin with a QE pulse applied. The QE pulse was used to center (axialize) the ions within the cell and reduce their magnetron motion, creating the most reproducible ion distribution between experiments, yielding a plot with the least amount of scatter ($R^2 = 0.98$).

The magnitude of the space charge effect is also influenced by the compression of the ion cloud from collisional damping and quadrupolar excitation, as can be seen from the change in slopes of Figures 2a-c. The slopes of these plots are a measure of the space charge-induced frequency shifts. The smallest slope, denoting the least change in frequency and the smallest space charge effect, is found when the ions experience no collisional damping, Figure 2a. The greatest effect is seen when quadrupolar excitation is applied, Figure 2c, as a result of the high ion density created when the ions are squeezed into the center of the FTICR analyzer cell. In order to reduce random errors in mass measurement, we choose to utilize QE, despite the more pronounced space charge effect and its concomitant larger systematic error.

According to the space charge term in the observed frequency equation developed by Jeffries et al.,[27] and McIver and coworkers,[28] the decrease in observed frequency attributed to the space charge effect should scale with the number of charges on the ion, Equation 1. For example, a doubly-charged ion should experience twice the space charge induced frequency shift of a singly-charged ion, a triply-charged ion should experience

three times the shift, etc. The slopes of the plots of observed frequency versus signal intensity for ions of charge states from 1+ to 8+ is shown in Table 1. As mentioned above, the signal intensity is a proportional to both of the number of charges on an ion and the number of ions measured. A given number of doubly-charged ions will produce a peak with twice the intensity than that from the same number of singly charged ions. For these experiments, total signal intensity was calculated by summing the individual peak intensities. This value correlates to *charge* density rather than *ion* density. The frequency of a selected peak was monitored as the total signal intensity was varied systematically. As can be seen in Table 1, there is no systematic increase in space charge effect with increasing charge state, in contradiction to the term for space charge effect in Equation 1. There are variations in the slopes of the plots ($\pm$ 18%), but these variations do not appear to correlate with the charge state of the ion. Two possible explanations for these variations can be postulated. First, there may be a higher-order term for space charge in the equation for observed frequency, Equation 1. A more likely possibility is that the variations may be caused by experimental parameters that are difficult to control. For example, the pulsed introduction of gas for collisional damping is unlikely to produce an identical pressure each time, leading to slightly different ion spatial distributions from experiment to experiment. To reduce the experimental errors in the slopes of the space charge plots, a series of measurements was performed on ions of differing charge states present in the cell at the same time. In this manner, all ions experience identical experiment-to-experiment variations in the parameters that are difficult to control. A short gas pulse was applied to dampen the axial motion of the ions and reduce the amount

Table 1. Measured slopes and intercepts for plots of observed frequency versus total ion intensity for ions with charge states from 1+ to 8+.

Protein	Charge State	Slope	Intercept (Hz)
Melittin	1	-9.9×10^{-7}	38217
Melittin	2	-1.1×10^{-6}	76423
Insulin	3	-1.4×10^{-6}	56913
Ubiquitin	6	-1.1×10^{-6}	76180
Myoglobin	8	-1.2×10^{-6}	49310

of scatter in the plots rather than using QE to axialize ions. Plots of frequency vs. signal intensity for ubiquitin and cytochrome *c* are shown in Figure 3a-d. Figure 3a shows the 8+ charge state of ubiquitin at m/z 1071, Figure 3b shows the 7+ charge state at m/z 1224, Figure 3c shows the 6+ charge state at m/z 1428, and Figure 3d shows the 8+ charge state of a cytochrome *c* component at m/z 1545. A close examination of the data shows that the residual errors, that is the deviation of individual measurements from the least squares fitted line, is the same for all the different ions at each intensity measurement. This shows that there is some variability due to random error between measurements, but that in a given measurement, all ions are experiencing the same conditions. The slopes of the plots for the ions at m/z 1071, 1428, and 1545 lie within the range of $-2.8 \times 10^{-7} \pm 7\%$. The relative standard deviation in the slopes of these line is 8%, and so we conclude that the slopes of the plots in Figure 3a, 3c, and 3d are the same within experimental error. The slope of the plot for the ion of m/z 1224 is -2.3×10^{-7}, Figure 3b, and is smaller than the other measurements by 18%, an amount roughly equal to two standard deviations. Thus a small but statistically significant difference is observed in the slope of the space charge plot for this ion. We can only speculate on the nature of this small difference. One possibility is that the space charge induced shift may have a weak dependence on the relative abundance of the ions. Figure 4 shows a representative mass spectrum from the series of measurements. As can be seen, the m/z 1224 ion, which had the lowest slope in its space charge plot, is by far the most abundant ion in the mass spectrum. In a previous study of space charge effects on mass accuracy for singly-charged ions, it was found that the frequency shifts of all ions were the same, and independent of their relative abundance,

Figure 3. Plots of frequency vs. signal intensity for a range of charge states monitored simultaneously as a function of ion intensity, using a gas pulse to damp the axial motion of the ions. The ion density was varied by detuning the skimmer potential. (a) Ubiquitin 8+ charge state, at m/z 1071. (b) Ubiquitin 7+ charge state, at m/z 1224. (c) Ubiquitin 6+ charge state, at m/z 1428. (d) Cytochrome *c* (contaminant), 8+ charge state, at m/z 1545.

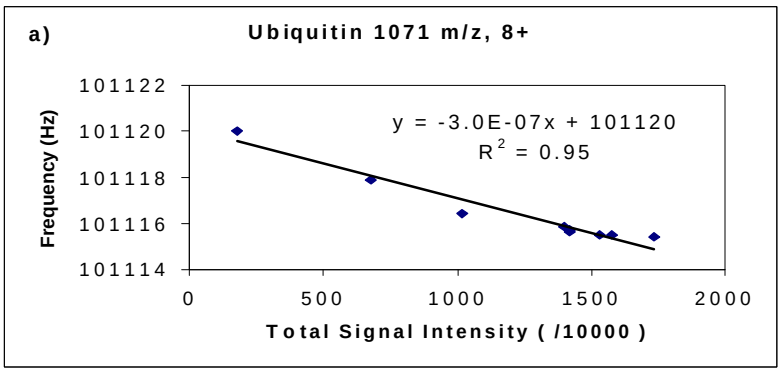
a)
Ubiquitin 1071 m/z, 8+
Frequency (Hz)
101122
101120
101118
101116
101114
y = -3.0E-07x + 101120
R2 = 0.95
0
500
1000
1500
2000
Total Signal Intensity (/10000)

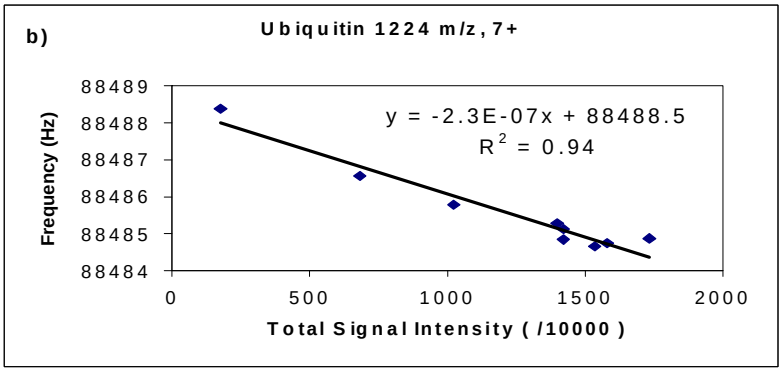
b)
Ubiquitin 1224 m/z, 7+
Frequency (Hz)
88489
88488
88487
88486
88485
88484
y = -2.3E-07x + 88488.5
R2 = 0.94
0
500
1000
1500
2000
Total Signal Intensity (/10000)

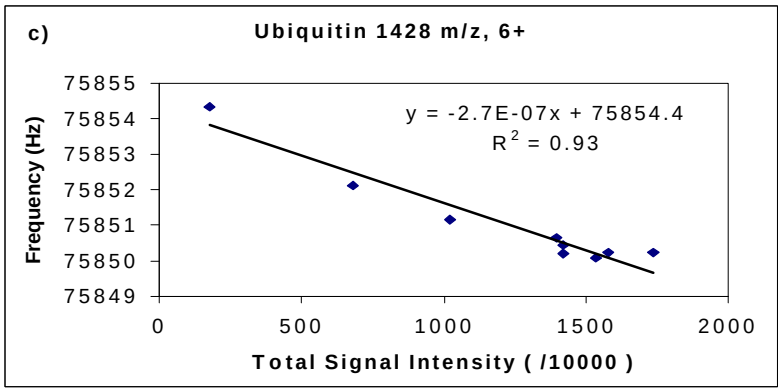
c)
Ubiquitin 1428 m/z, 6+
Frequency (Hz)
75855
75854
75853
75852
75851
75850
75849
y = -2.7E-07x + 75854.4
R2 = 0.93
0
500
1000
1500
2000
Total Signal Intensity (/10000)

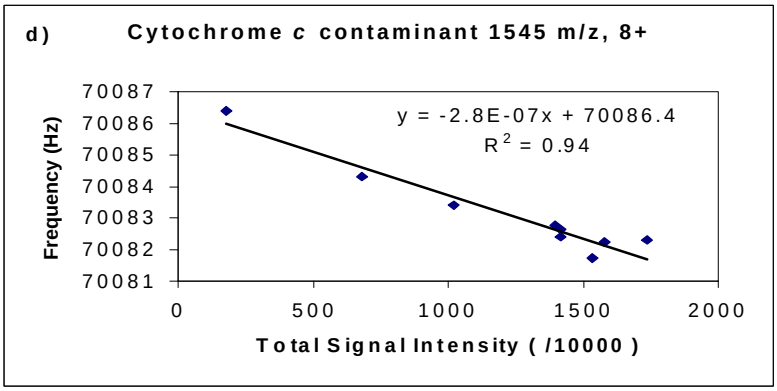
d)
Cytochrome c contaminant 1545 m/z, 8+
Frequency (Hz)
70087
70086
70085
70084
70083
70082
70081
y = -2.8E-07x + 70086.4
R2 = 0.94
0
500
1000
1500
2000
Total Signal Intensity (/10000)

Figure 4. Sample mass spectrum of a range of charge states monitored simultaneously as a function of ion intensity, showing the relative abundance of each species in the cell.

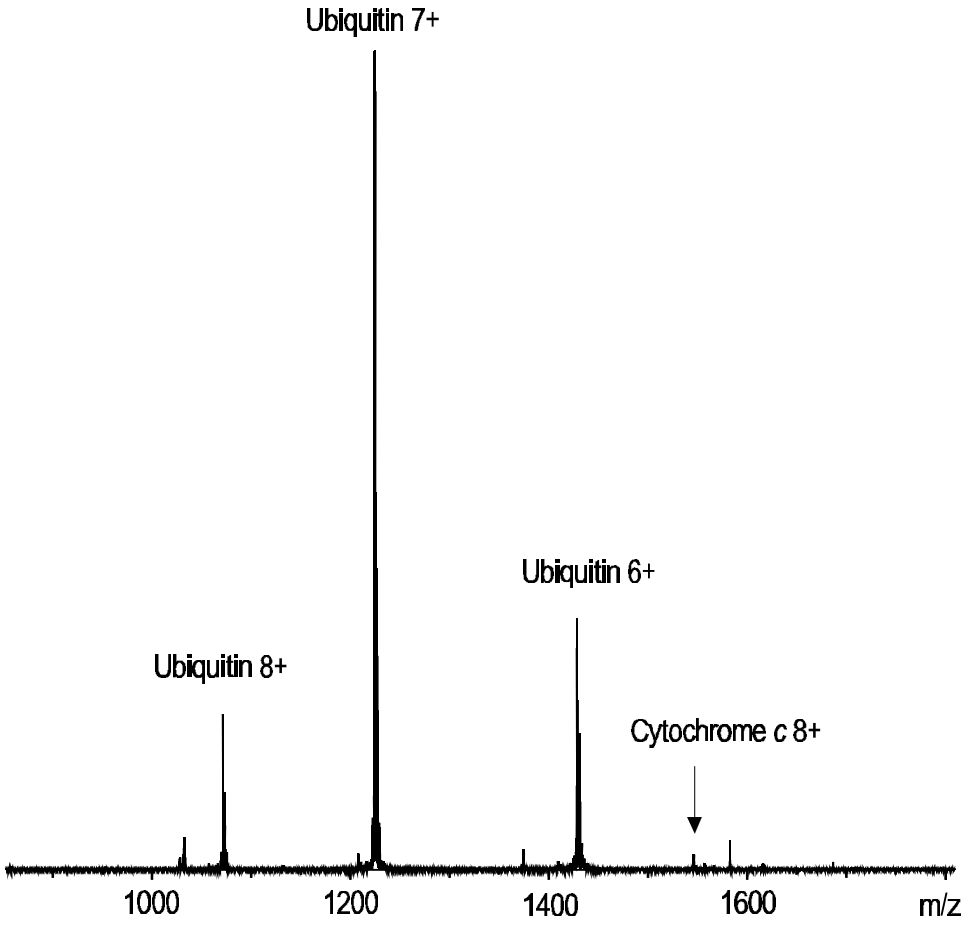
Ubiquitin 7+
Ubiquitin 6+
Ubiquitin 8+
Cytochrome c 8+
1000
1200
1400
1600
m/z

and so such an effect, if present for multiply-charged ions, would be surprising. It should be noted that the difference in the slope is small (a factor of two larger than the standard deviation in the measurement), and that this effect is a small perturbation to the general observation that all slopes are the same. The very low abundance cytochrome *c* ion at m/z 1545 (<3% relative abundance) exhibits the same slope as the ions of 20%-30% relative abundance, and only the most abundant peak exhibits a smaller slope. Some space charge behaviors have been reported that are sensitive to relative abundance. For example, the loss of coherence of an orbiting ion cloud through coulombic interactions with other ion clouds, dubbed ion cloud shearing, is known to effect low abundance ions more profoundly than higher abundance ions.[52] Further studies will be required to determine if the small but perceptible difference in the slope of the space charge plots is related to the abundance of the ions.

Since there appears to be no effect on the magnitude of the space charge-induced frequency shifts with variation in charge state, it is possible to calibrate using two peaks which bracket the peak of interest without regard for their charge state. Table 2 shows the data for the 8+ through 13+ charge states of hemoglobin chain A, calibrated internally with the 2+ (m/z 1748) and 3+ (m/z 1166) charge states of insulin chain B. The mass errors are small, approximately 1 ppm for interpolated values, 6 ppm for an extrapolated value. Internal calibration is successful because the space charge-induced frequency shift is not dependent on charge state, and because the calibrant and analyte peaks experience the same total ion density and therefore the same space charge-induced frequency shift.

Table 2. Experimentally determined monoisotopic mass and error for internally calibrated ions with charge states from 8+ to 13+.

m/z	Charge State	Experimental MI mass	Theoretical MI mass	Error (ppm)
1158	13+	15043.99	15043.90	6.0
1255	12+	15043.92	15043.90	1.3
1369	11+	15043.92	15043.90	1.3
1506	10+	15043.88	15043.90	1.3
1673	9+	15043.90	15043.90	< 1.0
1882	8+	15043.90	15043.90	< 1.0

Internal calibration is sometimes difficult to implement. For example, an online LC/ESI-MS experiment would require a second, concurrent method of sample introduction for the calibrant. External calibration introduces a systematic error due to differences in ion population between calibrant and analyte, but these effects can be accounted for using Equation 2, developed by Easterling et al,[2] where $f_{estimated}$ is the frequency after adjustment for space charge, $f_{measured}$ is the frequency obtained with external calibration, c is the slope of the frequency vs. ion intensity plot, $I_{calibrant}$ is the total ion intensity of the calibrant, and $I_{analyte}$ is the total ion intensity of the analyte. Table 3 shows externally calibrated monoisotopic masses and errors for four charge states of insulin calibrated with ubiquitin, as well as monoisotopic masses and errors after correction for space charge. The ubiquitin calibrant spectrum and insulin analyte spectrum were obtained using the same conditions, and the intensities were obtained by summing the intensities of the individual isotope peaks. The slope used for space charge correction was -2.7×10^{-7}, obtained from the frequency vs. intensity plot of ubiquitin m/z 1428, without QE. The errors prior to adjustment for space charge range from 13 ppm to 18 ppm. These errors are relatively small, even without correcting for space charge, because QE was not used in this experiment, reducing the density of the ion distribution. Nevertheless, correcting for space charge-induced frequency shifts using Equation 2 reduces the error by an order of magnitude, from an average of 16 ppm to 1.6 ppm. Clearly accounting for space charge in this manner increases the level of mass accuracy. We have attempted to apply the procedure of external calibration followed by correction for space charge to larger biological molecules, but it has proven less successful. As the

Table 3. Monoisotopic mass values derived from the 3+ to 5+ charge states of insulin, before and after correction for space charge. Errors are calculated from the theoretical monoisotopic mass of 5729.600.

m/z	Charge State	Calculated MI mass (Da)	Ext. Calib MI mass (Da)	Error (ppm)	Adjusted MI mass (Da)	Error (ppm)
956	6	5729.600	5729.672	12.5	5729.607	1.1
1146	5	5729.600	5729.687	15.1	5729.608	1.3
1433	4	5729.600	5729.698	17.1	5729.600	-0.1
1910	3	5729.600	5729.702	17.7	5729.577	-4.0

size of the molecule and number of charge states in the spectrum increases, the pattern of constructive/destructive interference in the transient becomes more complex.[53, 54] This complexity affects the magnitude of the spectral peaks, so that the total signal intensity obtained by summing the intensities of the individual isotope peaks is not truly representative of the total ion density within the cell.[53] The procedure of internal calibration works well for these larger molecules. As shown in Table 2, ions with 13+ charges can be calibrated using ions with 2+ to 3+ charges, while still achieving low ppm mass accuracy.

$$f_{estimated} = f_{measured} + c(I_{calibrant} - I_{analyte}) \qquad (2)$$

CONCLUSIONS

Space charge produces a shift in observed frequency with variations in ion density, limiting mass accuracy. Prior research on singly charged ions produced by MALDI has shown a reduction in random error in measurements of cyclotron frequency when ion motion is collisionally damped.[2] This finding has proven to be equally valid for multiply charged ions produced by ESI. On the other hand, the space charge effect is more significant when the ion cloud is more compressed, e.g. by collisional damping of axial motion or by quadrupolar excitation. Therefore, the same techniques commonly used to produce better signal can reduce mass accuracy by increasing the space charge. However, the space charge-induced frequency shift is a systematic error, and can be treated through proper calibration. Space charge-induced frequency shifts do not change with increasing

charge on the ion, in contrast to expectations based on Equation 1. Significantly, the space charge-induced frequency shifts are the same for a distribution of ions with various charge states when they are monitored simultaneously. Thus, it is possible to achieve high mass accuracy of one ion species through internal calibration without regard for the charge state of either the calibrant or the analyte peaks. External calibration can be improved by the use of a correction factor for space charge. If the total ion intensities of the analyte and calibrant peaks can be accurately determined, a frequency correction factor based on the slope of a frequency versus total ion intensity plot for the calibrant can greatly improve mass accuracy. As the mass of the analyte and range of charge states increases, the determination of the total ion intensity by summation of the individual peak intensities becomes problematic, reducing the accuracy of external calibration. The best mass accuracy for high mass species is achieved when the mass of the calibrant and analyte are comparable.

ACKNOWLEDGMENTS

The authors are grateful for generous financial support from NSF (CHE-9974579).

REFERENCES

(1) Maziarz, E. P.; Baker, G. A.; Wood, T. D. *Macromolecules* **1999,** *32*, 4411-4418.

(2) Easterling, M. L.; Mize, T. H.; Amster, I. J. *Anal. Chem.* **1999,** *71*, 624-632.

(3) Easterling, M. L.; Mize, T. H.; Amster, I. J. *Int. J. Mass Spectrom. Ion Processes* **1997,** *169*, 387-400.

(4) Heeren, R. M. A.; Dekoster, C. G.; Boon, J. J. *Anal. Chem.* **1995,** *67*, 3965-3970.

(5) Dekoster, C. G.; Duursma, M. C.; Vanrooij, G. J.; Heeren, R. M. A.; Boon, J. J. *Rapid Commun. Mass Spectrom.* **1995,** *9*, 957-962.

(6) Dey, M.; Castoro, J. A.; Wilkins, C. L. *Anal. Chem.* **1995,** *67*, 1575-1579.

(7) He, F.; Hendrickson, C. L.; Marshall, A. G. *J. Am. Soc. Mass Spectrom.* **2000,** *11*, 120-126.

(8) Johnson, K.; Verhagen, M.; Brereton, P.; Adams, M.; Amster, I. *Anal. Chem.* **2000,** *72*, 1410-1418.

(9) Li, J. J.; Kelly, J. F.; Chemushevich, I.; Harrison, D. J.; Thibault, P. *Anal. Chem.* **2000,** *72*, 599-609.

(10) Borchers, C.; Peter, J. F.; Hall, M. C.; Kunkel, T. A.; Tomer, K. B. *Anal. Chem.* **2000,** *72*, 1163-1168.

(11) Davis, M. T.; Lee, T. D. *J. Am. Soc. Mass Spectrom.* **1998,** *9*, 194-201.

(12) Kosaka, T.; Takazawa, T.; Nakamura, T. *Anal. Chem.* **2000,** *72*, 1179-1185.

(13) Eriksson, J.; Chait, B. T.; Fenyo, D. *Anal. Chem.* **2000,** *72*, 999-1005.

(14) Green, M. K.; Johnston, M. V.; Larsen, B. S. *Anal. Biochem.* **1999,** *275*, 39-46.

(15) Clauser, K. R.; Baker, P.; Burlingame, A. L. *Anal. Chem.* **1999,** *71*, 2871-2882.

(16) Fenyo, D.; Qin, J.; Chait, B. T. *Electrophoresis* **1998,** *19*, 998-1005.

(17) Takach, E. J.; Hines, W. M.; Patterson, D. H.; Juhasz, P.; Falick, A. M.; Vestal, M. L.; Martin, S. A. *J. Protein Chem.* **1997,** *16*, 363-369.

(18) Oconnell, K. L.; Stults, J. T. *Electrophoresis* **1997,** *18*, 349-359.

(19) Mann, M.; Hojrup, P.; Roepstorff, P. *Biol. Mass Spectrom.* **1993,** *22*, 338-345.

(20) Goodlett, D. R.; Bruce, J. E.; Anderson, G. A.; Rist, B.; Pasa-Tolic, L.; Fiehn, O.; Smith, R. D.; Aebersold, R. *Anal. Chem.* **2000,** *72*, 1112-1118.

(21) Shevchenko, A.; Wilm, M.; Mann, M. *J. Protein Chem.* **1997,** *16*, 481-490.

(22) Shevchenko, A.; Loboda, A.; Shevchenko, A.; Ens, W.; Standing, K. *Anal. Chem.* **2000**.

(23) Shevchenko, A.; Chernushevich, I.; Ens, W.; Standing, K. G.; Thomson, B.; Wilm, M.; Mann, M. *Rapid Commun. Mass Spectrom.* **1997,** *11*, 1015-1024.

(24) Stevenson, T. I.; Loo, J. A.; Greis, K. D. *Anal. Biochem.* **1998,** *262*, 99-109.

(25) Sommer, H.; Thomas, H.; Hipple, J. *Physics Reviews* **1949,** *76*, 1877.

(26) Beauchamp, J.; Armstrong, J. *Rev. Sci. Instrum.* **1969,** *40*, 123.

(27) Jeffries, J. B.; Barlow, S. E.; Dunn, G. H. *Int. J. Mass Spectrom. Ion Processes* **1983,** *54*, 169-187.

(28) Francl, T. J.; Sherman, M. G.; Hunter, R. L.; Locke, M. J.; Bowers, W. D.; McIver, R. T. *Int. J. Mass Spectrom. Ion Processes* **1983,** *54*, 189-199.

(29) Chen, S. P.; Comisarow, M. B. *Rapid Commun. Mass Spectrom.* **1991,** *5*, 450-455.

(30) Chen, R.; Marshall, A. G. *Int. J. Mass Spectrom. Ion Processes* **1994,** *133*, 29-38.

(31) Han, S. J.; Shin, S. K. *J. Am. Soc. Mass Spectrom.* **1997,** *8*, 319-326.

(32) Ledford, E. B.; Rempel, D. L.; Gross, M. L. *Anal. Chem.* **1984,** *56*, 2744-2748.

(33) Ledford, E. B.; Rempel, D. L.; Gross, M. L. *Int. J. Mass Spectrom. Ion Processes* **1984,** *55*, 143-154.

(34) Mitchell, D. W.; Smith, R. D. *Phys. Rev. E* **1995,** *52*, 4366-4386.

(35) Peurrung, A. J.; Kouzes, R. T. *Int. J. Mass Spectrom. Ion Processes* **1995,** *145*, 139-153.

(36) Uechi, G. T.; Dunbar, R. C. *J. Am. Soc. Mass Spectrom.* **1992,** *3*, 734-741.

(37) Bruce, J. E.; Anderson, G. A.; Brands, M. D.; Tolic, L. P.; Smith, R. D. *J. Am. Soc. Mass Spectrom.* **2000,** *11*, 416-421.

(38) Anderson, J. S.; Laude, D. A. *Int. J. Mass Spectrom. Ion Processes* **1996,** *158*, 163-174.

(39) Hofstadler, S. A.; Laude, D. A. *J. Am. Soc. Mass Spectrom.* **1992,** *3*, 615-623.

(40) Hogan, J. D.; Laude, D. A. *Anal. Chem.* **1990,** *62*, 530-535.

(41) Laude, D. A.; Beu, S. C. *Anal. Chem.* **1989,** *61*, 2422-2427.

(42) Stults, J. T. *Anal. Chem.* **1997,** *69*, 1815-1819.

(43) Burton, R. D.; Matuszak, K. P.; Watson, C. H.; Eyler, J. R. *J. Am. Soc. Mass Spectrom.* **1999,** *10*, 1291-1297.

(44) Senko, M. W.; Hendrickson, C. L.; PasaTolic, L.; Marto, J. A.; White, F. M.; Guan, S. H.; Marshall, A. G. *Rapid Commun. Mass Spectrom.* **1996,** *10*, 1824-1828.

(45) Gorshkov, M. V.; Tolic, L. P.; Udseth, H. R.; Anderson, G. A.; Huang, B. M.; Bruce, J. E.; Prior, D. C.; Hofstadler, S. A.; Tang, L. A.; Chen, L. Z.; Willett, J. A.; Rockwood, A. L.; Sherman, M. S.; Smith, R. D. *J. Am. Soc. Mass Spectrom.* **1998,** *9,* 692-700.

(46) Hofstadler, S. A.; Griffey, R. H.; Pasa-Tolic, L.; Smith, R. D. *Rapid Commun. Mass Spectrom.* **1998,** *12,* 1400-1404.

(47) Lorenz, S. A.; Moy, M. A.; Dolan, A. R.; Wood, T. D. *Rapid Commun. Mass Spectrom.* **1999,** *13,* 2098-2102.

(48) Wilm, M.; Mann, M. *Anal. Chem.* **1996,** *68,* 1-8.

(49) Speir, J. P.; Gorman, G. S.; Pitsenberger, C. C.; Turner, C. A.; Wang, P. P.; Amster, I. J. *Anal. Chem.* **1993,** *65,* 1746-1752.

(50) Schweikhard, L.; Guan, S. H.; Marshall, A. G. *Int. J. Mass Spectrom. Ion Processes* **1992,** *120,* 71-83.

(51) Campbell, V. L.; Guan, Z. Q.; Laude, D. A. *J. Am. Soc. Mass Spectrom.* **1995,** *6,* 564-570.

(52) Mitchell, D. W.; Smith, R. D. *Int. J. Mass Spectrom. Ion Processes* **1997,** *165,* 271-297.

(53) Easterling, M. L.; Amster, I. J.; van Rooij, G. J.; Heeren, R. M. A. *J. Am. Soc. Mass Spectrom.* **1999,** *10,* 1074-1082.

(54) Hofstadler, S. A.; Bruce, J. E.; Rockwood, A. L.; Anderson, G. A.; Winger, B. E.; Smith, R. D. *Int. J. Mass Spectrom. Ion Processes* **1994,** *132,* 109-127.

CHAPTER 3

Study of the Binding of the Substrate Oxygen to Multimeric Hemoglobin by ESI-FTICR[1]

[1]Taylor, P. K.; I. J. Amster. Submitted to *Journal of the American Society for Mass Spectrometry*

Abstract

Electrospray ionization Fourier transform mass spectrometry provides the first reported isotopically resolved mass spectrum of heterotetrameric bovine hemoglobin, as well as binding of the substrate oxygen to the noncovalent complex. Accurate monoisotopic masses are obtained for denatured and heme-bound alpha and beta subunits. Spraying the protein from a nondenaturing solvent reveals dimer and tetramer complexes. Rigorous sample desalting and careful manipulation of the ion population to reduce space charge effects are required to achieve isotopic resolution for the multimers. A peak corresponding to the tetramer complex plus dioxygen is observed in the mass spectrum. Four molecules of dioxygen are observed to bind to the tetramer and two to the dimer when their solutions are saturated with oxygen prior to analysis.

Introduction

Mass spectrometry has become a common tool for the examination of proteins, particularly since the advent of electrospray ionization (ESI). ESI is a technique that is well-suited for protein analysis, because it produces multiply charged ions of relatively low mass-to-charge ratio that lie within the operating capabilities of standard mass spectrometers.[1] The combination of ESI with Fourier transform ion cyclotron resonance (FTICR) mass spectrometry has proven to be a powerful method for the study of proteins, because of its high mass accuracy and high mass resolution.[2, 3] A theoretical isotopic distribution can be obtained either from the amino acid sequence or through the averagine method, and statistical matching of the experimental isotopic abundances with the theoretical distribution can determine the isotopic composition of each peak.[4] Each isotope peak can then be deconvoluted to obtain a value for the monoisotopic mass, and these values can then be averaged together to obtain a highly accurate monoisotopic mass value.

ESI has been widely applied to the study of noncovalent complexes.[5] It is a technique capable of gentle desolvation of ions without disruption of the weak forces that are present in a holoprotein. Multiply charged protein complexes typically have mass-to-charge ratios in the range of 2000-5000, even though their molecular weights may exceed 100,000 Da, allowing the observation of these high-mass species with mass spectrometers having relatively modest mass ranges.[6-13] Isotopic resolution for noncovalent complexes by ESI-FTICR has also been demonstrated for a small number of proteins, although it is far from a simple matter.[14] As the mass of the ion increases, its cyclotron frequency

decreases, and the isotopes and their corresponding cyclotron frequencies become more closely spaced. As these frequency differences become small, destructive interference causes the detected signal to appear as a short beat (10-100 ms) with a long period (several seconds). The beat period is inversely proportional to the square of the mass of the ion.[15] Thus it becomes increasingly difficult to obtain good signal-to-noise for high mass ions. Recording the second beat in the transient is necessary to obtain isotopic resolution,[16] therefore the rotating ion packet must maintain coherence for increasingly longer periods of time as the mass of the ion increases. An additional concern is the preservation of noncovalent interactions, which requires that the samples be maintained under nondenaturing conditions, typically a pure aqueous solution of neutral pH. These conditions are not optimal for ESI, causing the reduction of signal-to-noise ratio. Nanospray is useful for nebulizing solutions with no organic component, since its lower flow rate and lower droplet size are more conducive to rapid desolvation.[17]

In this report, we use ESI-FTICR to examine bovine hemoglobin at several levels of structure, ranging from accurate mass measurement of the alpha and beta subunits, to measurement of the tetrameric quaternary complex, to measurements of the oxygen binding by the tetramer complex. Hemoglobin has been the subject of a number of mass spectrometry studies.[12, 13, 18-29] Hemoglobin is found extensively in both vertebrate and invertebrate organisms, and is involved in oxygen transport.[30] Under nondenaturing conditions, hemoglobin forms a heterotetramer of four heme-containing subunits bound by noncovalent interactions in the stoichiometry $\alpha_2\beta_2$, much like a dimer of dimers. The heme-bound alpha subunit has a mass of approximately 15,660 Da while the heme-bound

beta subunit has a mass of approximately 16,560 Da. Each heme group is capable of binding one O_2 molecule, and the heterotetramer is capable of binding up to four oxygen molecules. The observation of O_2 binding by the hemoglobin heterotetramer using mass spectrometry has not previously been reported. Here we show that the stoichiometry of substrate to protein can be accurately determined by mass spectrometry.

Experimental

Sample purity, primarily removal of most or all salt adducts, has proven to be essential in experiments seeking high resolution mass spectra of noncovalent complexes. Bovine hemoglobin was obtained from Sigma (St. Louis, MO) and desalted by concentrating using a 30 kDa cutoff ultrafiltration membrane (Millipore, Bedford, MA). Samples were resuspended in 10 mM ammonium acetate and this process was repeated five times. Samples were suspended in a mixture of 49:49:2 water:methanol:acetic acid (v/v) with a final concentration of 10 μM for observation of the denatured alpha and beta subunits. A 90:10 water:methanol solvent mixture was used to observe the emergence of heme binding. Samples were suspended in 10 mM ammonium acetate with a final tetramer concentration of 20 μM for the observation of dimer and tetramer. For the studies of oxygen binding, 300 μL of a 20 μM tetramer concentration hemoglobin sample were placed in a Slide-A-Lyzer dialysis cassette (Pierce, Rockford, IL). The cassette was placed in a 250 mL bath of 10 mM ammonium acetate through which oxygen was bubbled at an approximate rate of 2 L per hour. The sample was allowed to dialyze overnight in the oxygenated buffer, and was then withdrawn and used without further purification.

Mass spectra were collected on a Bruker BioApex FTICR mass spectrometer (Billerica, MA) with a 7 Tesla magnet. The mass spectrometer has been modified to include a heated metal capillary interface, which provides gentle desolvation for biological samples dissolved in non-denaturing solvents such as ammonium acetate. The capillary temperature was held at 150°C for all experiments. This temperature appeared to have no adverse effects on the observation of the noncovalent dimer and tetramer complexes. Samples were introduced using nanospray,[17] with tips fabricated in-house from 100 μm i.d. fused silica (Polymicro Technologies, Phoenix, AZ). Fabrication of the nanospray tips has been described previously.[31] A syringe pump was used to infuse the hemoglobin at a rate of 7 μL/hr. The spectrum collected in 49:49:2 water:methanol:acetic acid and the one collected in 10% methanol were obtained with the same instrumental parameters. The ionization pulse was 15 milliseconds in length, at 200 V_{p-p}. Front and back trap plates were held at 1.0 and 1.2 volts, respectively. The mass spectrum of the hemoglobin dimer was examined using a shorter ionization time and storage within the hexapole, 10 milliseconds and 0.5 seconds. The excite pulse was not changed, while the trap voltages were lowered to 0.6 and 0.75 volts prior to detection. The lower trap voltages were required to achieve enough mass resolution to observe the isotopic structure in the dimer peaks. This technique was extended in the observation of tetramer peaks, for which storage time in the hexapole was reduced to 0.3 seconds. The excite pulse was shortened to 30 microseconds, and the excite voltage was increased to 283 V_{p-p}. Cell trap voltages were reduced to 0.3 and 0.4 volts during detection.

Results and Discussion

The mass spectrum of bovine hemoglobin in denaturing solvent (50% methanol) shows two sets of peaks, corresponding to the alpha and beta subunits, as shown in Figure 1a. The mass spectrum of the alpha subunit yields a monoisotopic mass of 15044.2 Da, in good agreement with the calculated mass of 15043.9 Da. The beta subunit produces a monoisotopic mass of 15944.4 Da, which agrees well with the calculated mass of 15944.3 Da. There is no evidence of protein-bound heme, as expected under these denaturing conditions. The heme is not covalently bound to the protein, but rather resides in a hydrophobic packet of the folded subunit. Under these denaturing conditions, the protein unfolds, and the heme is readily lost. The mass spectrum of bovine hemoglobin sprayed under less denaturing conditions, 10% methanol, also contains peaks corresponding to the alpha and beta subunits of the protein, but in addition contains some low-intensity peaks, shown in Figure 1b, corresponding to the monomeric alpha and beta subunits of hemoglobin plus an iron-containing heme group. The alpha plus heme peaks have an apparent monoisotopic mass of 15658.99 Da, one mass unit below the calculated mass of 15660.08 Da. The beta plus heme peaks have an apparent monoisotopic mass of 16559.53 Da, one mass unit below the calculated mass of 16560.49 Da. Calculated masses were generated from the elemental composition of the subunits plus the elemental composition of neutral protoporphyrin IX containing one iron atom. The apparent masses are calculated assuming that all the charge on the ion is provided by extra protons. However, earlier research by Henion and coworkers indicated that the heme group is always found with a +1 charge, and suggested that the iron was in the Fe(III) oxidation

Figure 1. Mass spectrum of hemoglobin monomer. (a) Monomer in 49:49:2 water:methanol:acetic acid. Alpha and beta subunits are clearly distinguishable. No heme binding is visible. Asterisk denotes noise peak. (b) Monomer in 10% methanol. Non-heme bound alpha and beta subunits are still visible, but heme bound alpha and beta subunits are also apparent.

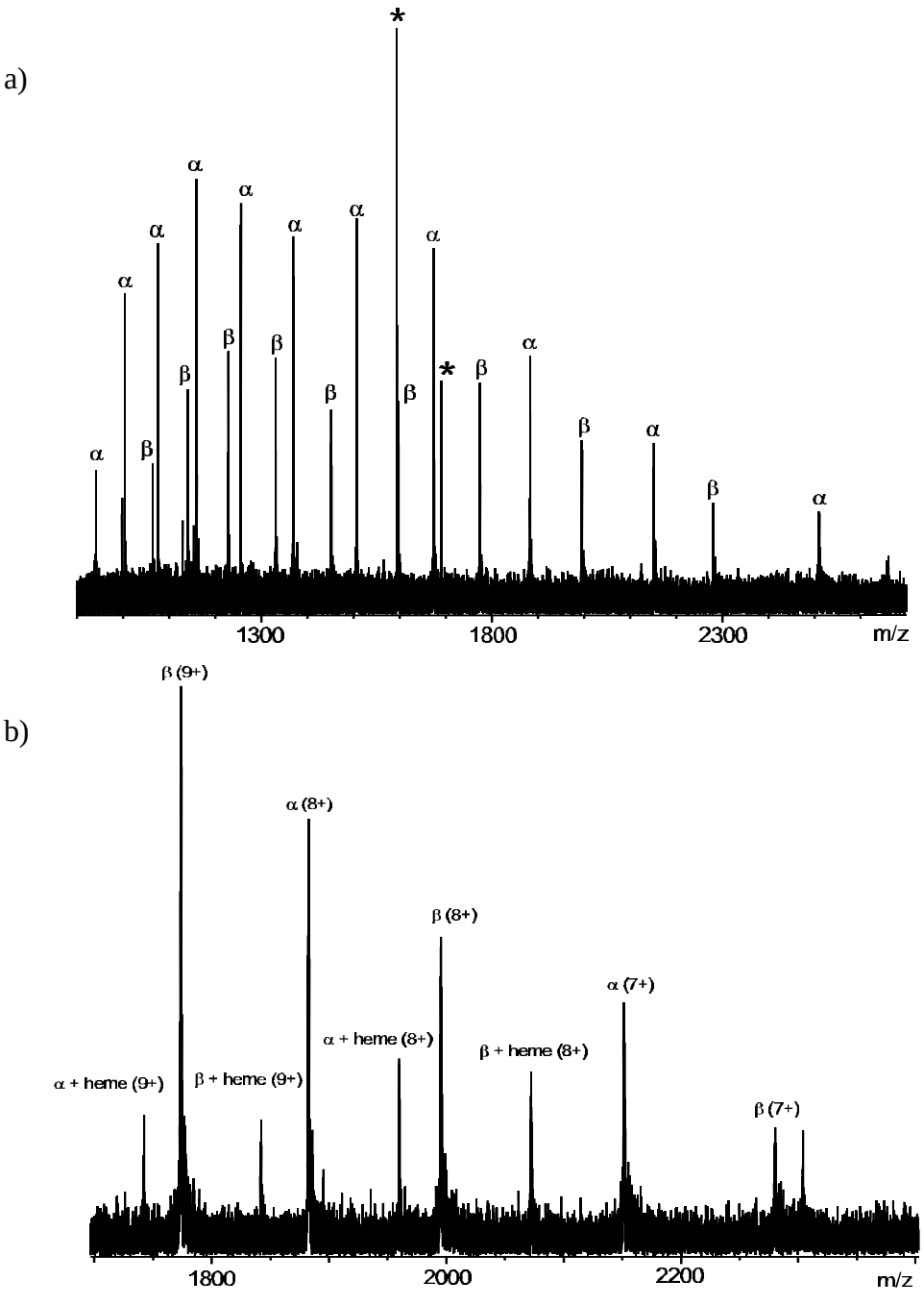
a)
α
β
*
1300
1800
2300
m/z
b)
β (9+)
α (8+)
β (8+)
α (7+)
α + heme (8+)
β + heme (8+)
α + heme (9+)
β + heme (9+)
β (7+)
1800
2000
2200
m/z

state,[18] a finding confirmed for other heme proteins by Marshall and coworkers.[32] Deprotonation of the carboxyl groups in the heme combined with iron in the Fe(III) oxidation state causes the heme group to have a total charge of +1. When the charge on the heme is taken into account, the measured monoisotopic masses for both the alpha and beta heme-bound subunits agree with the calculated masses within 5 ppm.

When the protein is electrosprayed from 10 mM ammonium acetate solution, peaks arising from a dimeric form of hemoglobin are observed, Figure 2. The dimer peaks have a monoisotopic mass of 32221.09 Da, in good agreement with the theoretical mass both as calculated from the amino acid sequence and as calculated from generated monomer data. The dimer is composed of alpha subunit plus beta subunit plus two heme groups. The dimer peaks also exhibit an additional peak at higher mass. Using the averagine method to determine the monoisotopic peak,[4] the monoisotopic mass was calculated to be 32253.13 Da, 32 Da greater than the mass of the base dimer peak, suggesting that the dimer is binding one molecule of O_2. A second, less intense series of peaks is also observed in the dimer portion of the mass spectrum. These peaks have an average mass of 31646 Da and correspond to the mass of one alpha subunit plus one beta subunit plus a single heme group.

In order to verify that the high mass peak in the dimer mass spectrum is due to the binding of molecular oxygen, a sample of hemoglobin was placed in a dialysis cassette which was submerged in a bath of ammonium acetate. Oxygen was bubbled through the bath, providing a source of oxygen-saturated buffer for exchange. The sample was allowed to undergo buffer exchange overnight. Figure 3 shows an expansion of the

Figure 2. Mass spectrum of hemoglobin dimer in 10 mM ammonium acetate, showing several different species. One distribution arises due to dimer composed of alpha plus beta subunits plus a single heme group. A second distribution arises from dimer composed of alpha plus beta subunits plus two heme groups. Adduct peaks are composed of alpha plus beta subunits plus two heme groups plus a single O_2 molecule. Asterisk denotes noise peak.

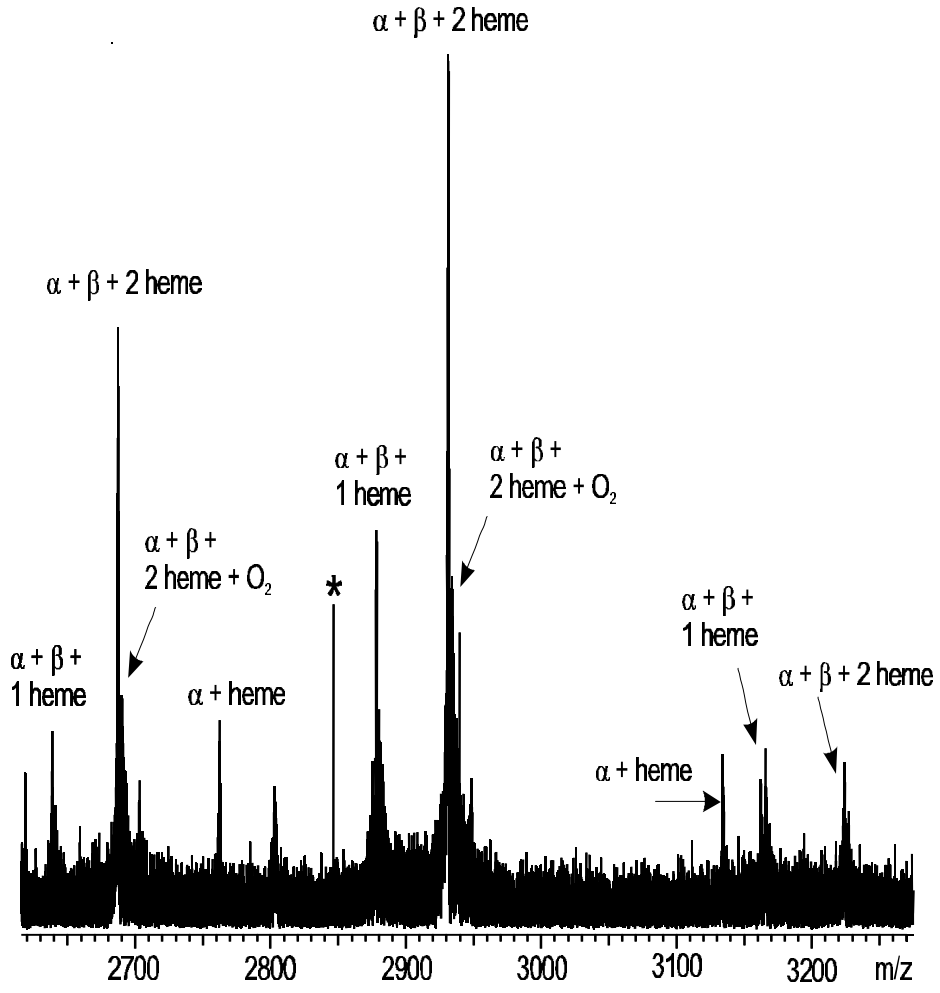
α + β + 2 heme
α + β + 2 heme
α + β +
1 heme
α + β +
2 heme + O2
α + β +
2 heme + O2
*
α + β +
1 heme
α + β +
1 heme
α + heme
α + heme
α + β + 2 heme
2700
2800
2900
3000
3100
3200
m/z

Figure 3. Dimer of hemoglobin, before and after oxygenation. (a) Dimer prior to oxygenation. Adduct peaks arise from sodium and potassium. (b) Dimer after overnight buffer exchange with oxygen-saturated buffer. Shows a mass shift of 65 Da, corresponding to the binding of two oxygen molecules, one per heme group.

a)

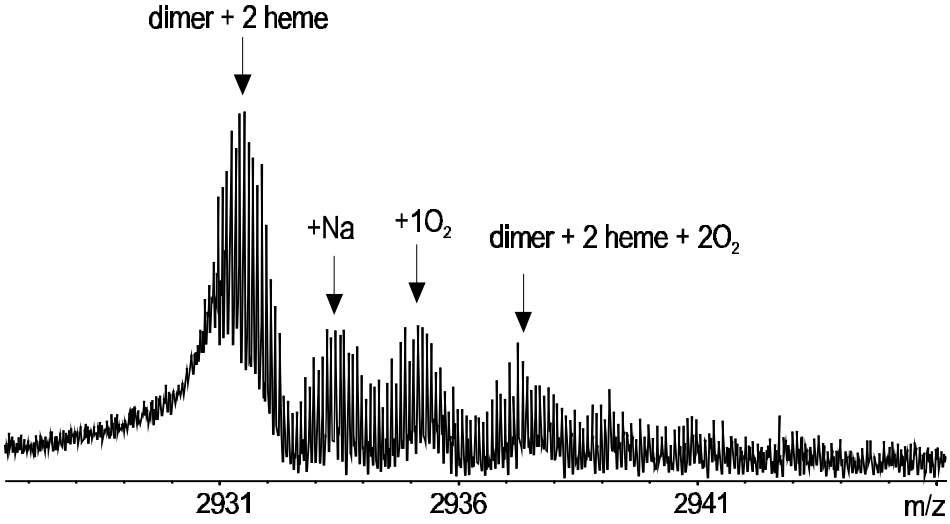
dimer + 2 heme
+Na
+1O2
dimer + 2 heme + 2O2
2931
2936
2941
m/z

b)

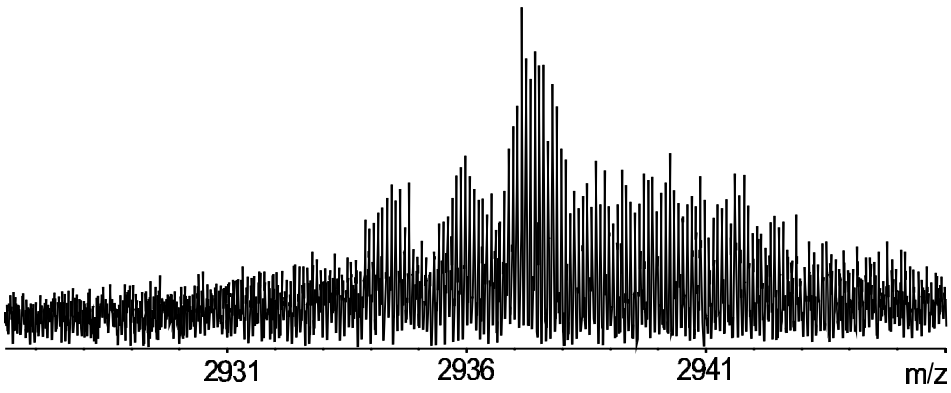
2931
2936
2941
m/z

hemoglobin dimer peak in the mass spectrum before and after oxygenation. Figure 3a shows the non-oxygenated dimer. Figure 3b shows the oxygenated dimer. The primary peak in Figure 3b has a mass of 32286.18 Da, a 65 Da mass increase over the non-oxygenated dimer, indicating the binding of two dioxygen molecules. No peaks due to non-oxygenated dimer were seen in this sample. The additional peaks at higher m/z are most likely due to Na^+ - H^+ exchange.

Peaks arising from the tetrameric form of hemoglobin are also visible under nondenaturing solvent conditions. Narrowband excitation of the tetramer peaks combined with carefully chosen excitation and trapping parameters allows observation of a second beat in the transient, Figure 4a, at approximately 2.3 seconds. Fourier transformation of the transient reveals that the tetramer peaks are isotopically resolved, Figure 4b. Unfortunately, the isotope statistics do not permit confident assignment of the monoisotopic peak. Nevertheless, charge state deconvolution reveals an average tetramer mass of 64441.6 Da, in good agreement with the theoretical mass of two alpha subunits plus two beta subunits plus four heme groups. As with the dimer peaks, the tetramer peaks also exhibit an additional peak at higher mass. Charge state deconvolution of the adduct yields a mass of 64475.7 Da, a 34 Da difference. Based on the known binding of hemoglobin to oxygen and the evidence of the dimer, it is reasonable to assign the adduct peaks as oxygen-bound tetramer. A mass spectrum of the oxygen saturated tetramer was measured, Figure 5. Charge state deconvolution yields an average mass of 64568.12 Da, an increase of 127 Da over the mass of the non-oxygenated tetramer, consistent with the binding of four oxygen molecules.

Figure 4. Tetramer of hemoglobin and corresponding FID. (a) FID of narrowband excitation of hemerythrin dimer. Note that the second beat arises after approximately 2.45 seconds. (b) Isotopically resolved mass spectrum of hemoglobin tetramer. First section arises from tetramer of $\alpha_2 b_2$ stoichiometry plus four heme groups. Second section is 34 mass units higher, arising from a single O_2 molecule bound to the tetramer.

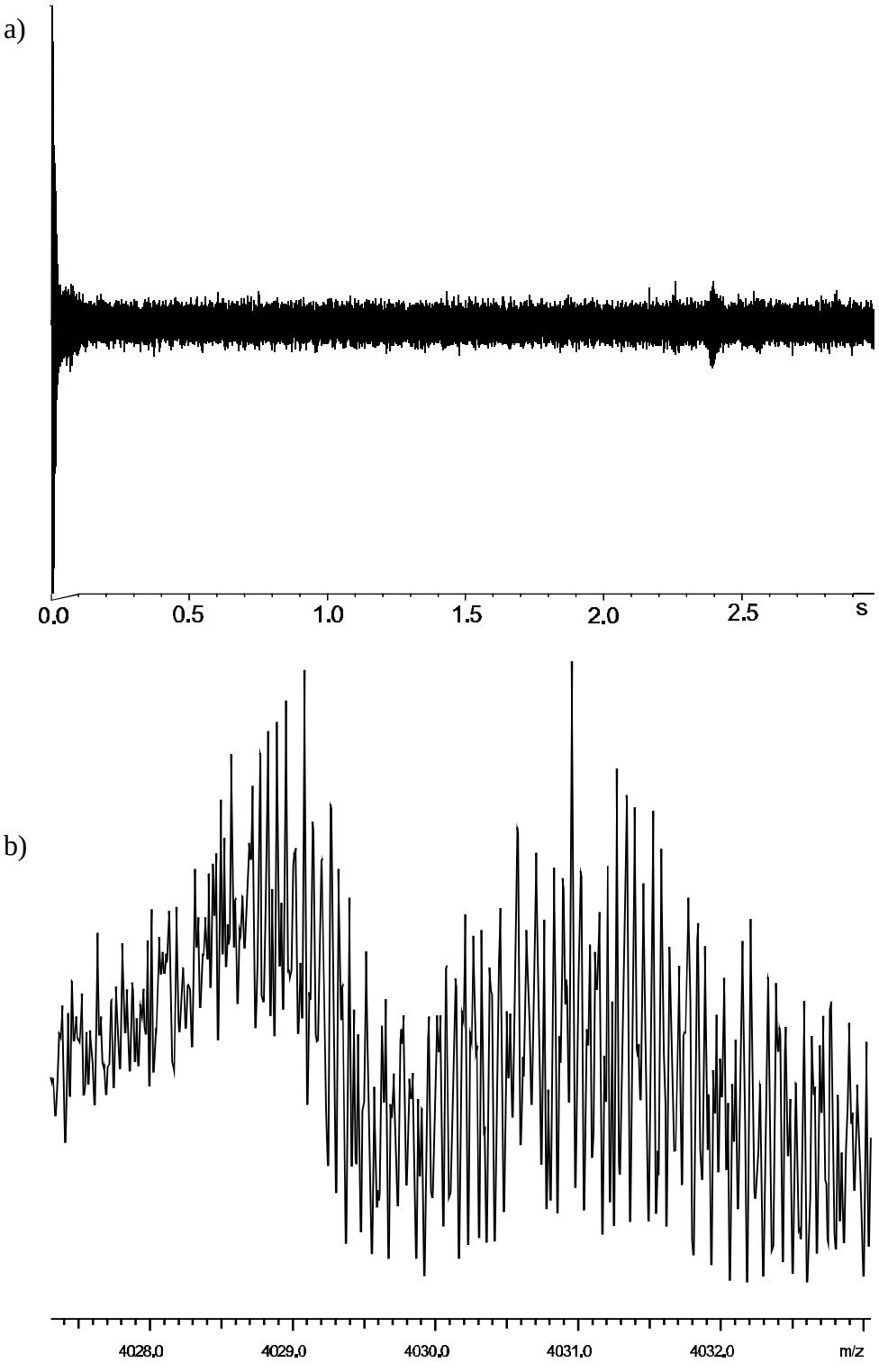
a)
0.0
0.5
1.0
1.5
2.0
2.5
s
b)
4028.0
4029.0
4030.0
4031.0
4032.0
m/z

Figure 5. Mass spectrum of hemoglobin tetramer after oxygenation. Arrows mark peaks corresponding to a mass of 127 Da higher than non-oxygenated tetramer, indicating one oxygen molecule binding onto each heme group. Lower mass peaks correspond to a loss of 526 Da from the non-oxygenated tetramer mass, indicating degradation.

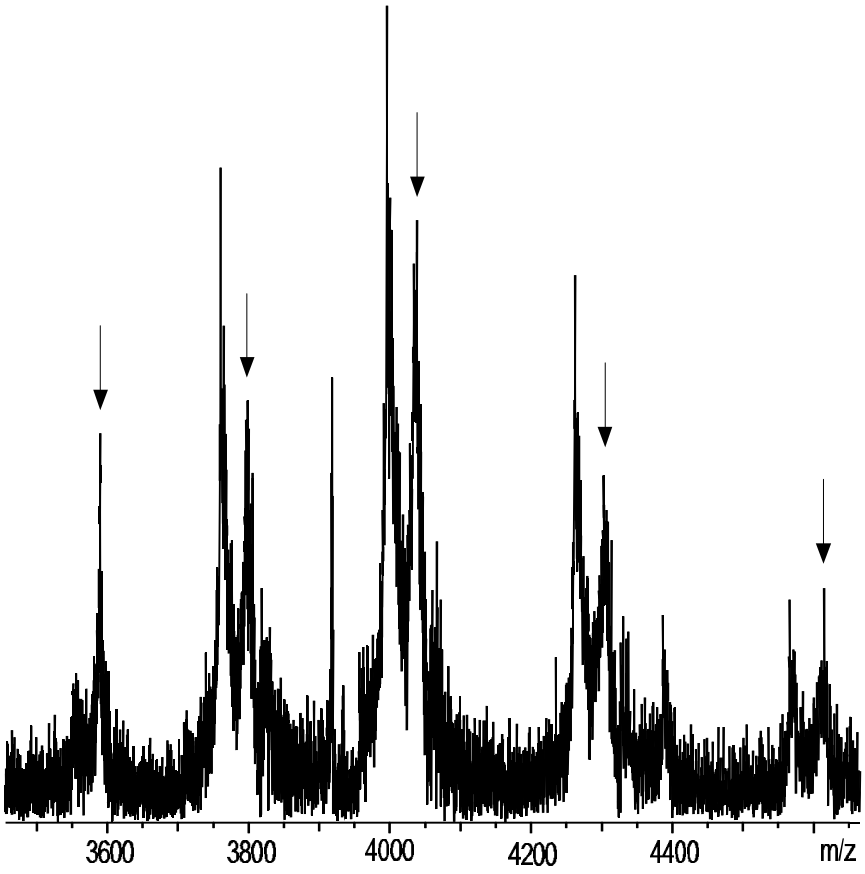
3600
3800
4000
4200
4400
m/z

Conclusion

These studies demonstrate the utility of ESI-FTICR for characterizing the stoichiometry of multimeric metalloproteins as well as the stoichiometry of substrate-complex binding. In denaturing solvents, accurate monoisotopic masses for the two subunits have been obtained. Under non-denaturing conditions, an $\alpha\beta$ dimer and $\alpha_2\beta_2$ tetramer were observed, as well as peaks from oxygen-bound multimers. It is interesting to note that although two heme groups are present per dimer, only one molecule of oxygen was bound per dimer unless the solution was saturated with oxygen. This is consistent with the known reversible oxygen binding properties of this protein. Once the sample solution was saturated with oxygen, two molecules of oxygen were found to bind to the dimer and four to the tetramer. No trimer peaks have been observed, indicating that the multimers seen here are specific noncovalent complexes rather than examples of nonspecific aggregation. In order to produce a transient long enough to observe isotopic resolution of the high molecular-mass tetramer, it is essential to reduce space charge effects as much as possible. Shorter ionization pulses, which cause fewer ions to be transported to the cell, and lower trapping voltages are the principle means used to reduce space charge effects in these experiments. Sample purity and high signal to noise ratio are also key factors in the observation of high resolution peaks at high mass to charge.

Acknowledgments

The authors would like to thank Brian Shira for helpful discussions. We would also like to acknowledge support from the National Science Foundation (CHE-9974579).

REFERENCES

(1) Fenn, J. B.; Mann, M.; Meng, C. K.; Wong, S. F.; Whitehouse, C. M. *Mass Spectrom. Rev.* **1990,** *9,* 37-70.

(2) Amster, I. J. *J. Mass Spectrom.* **1996,** *31,* 1325-1337.

(3) Marshall, A. G.; Hendrickson, C. L.; Jackson, G. S. *Mass Spectrom. Rev.* **1998,** *17,* 1-35.

(4) Senko, M. W.; Beu, S. C.; McLafferty, F. W. *J. Am. Soc. Mass Spectrom.* **1995,** *6,* 229-233.

(5) Loo, J. A. *Mass Spectrom. Rev.* **1997,** *16,* 1-23.

(6) Fitzgerald, M. C.; Chernushevich, I.; Standing, K. G.; Kent, S. B. H.; Whitman, C. P. *J. Am. Chem. Soc.* **1995,** *117,* 11075- 11080.

(7) Ganem, B.; Li, Y.; Henion, J. *J. Am. Chem. Soc.* **1991,** *113,* 6294.

(8) Ganem, B.; Li, Y.; Henion, J. *J. Am. Chem. Soc.* **1991,** *113,* 7818.

(9) Lei, Q. P.; Cui, X. Y.; Kurtz, D. M.; Amster, I. J.; Chernushevich, I. V.; Standing, K. G. *Anal. Chem.* **1998,** *70,* 1838-1846.

(10) Lightwahl, K. J.; Springer, D. L.; Winger, B. E.; Edmonds, C. G.; Camp, D. G.; Thrall, B. D.; Smith, R. D. *J. Am. Chem. Soc.* **1993,** *115,* 803- 804.

(11) Tang, X. J.; Brewer, C. F.; Saha, S.; Chernushevich, I.; Ens, W.; Standing, K. G. *Rapid Commun. Mass Spectrom.* **1994,** *8,* 750-754.

(12) Lightwahl, K. J.; Schwartz, B. L.; Smith, R. D. *J. Am. Chem. Soc.* **1994,** *116,* 5271- 5278.

(13) Loo, J. A.; Loo, R. R. O.; Andrews, P. C. *Org. Mass Spectrom.* **1993,** *28*, 1640-1649.

(14) Tolic, L. P.; Bruce, J. E.; Lei, Q. P.; Anderson, G. A.; Smith, R. D. *Anal. Chem.* **1998,** *70*, 405-408.

(15) Easterling, M. L.; Amster, I. J.; van Rooij, G. J.; Heeren, R. M. A. *J. Am. Soc. Mass Spectrom.* **1999,** *10*, 1074-1082.

(16) Hofstadler, S. A.; Bruce, J. E.; Rockwood, A. L.; Anderson, G. A.; Winger, B. E.; Smith, R. D. *Int. J. Mass Spectrom. Ion Process.* **1994,** *132*, 109-127.

(17) Wilm, M.; Mann, M. *Anal. Chem.* **1996,** *68*, 1-8.

(18) Li, Y. T.; Hsieh, Y. L.; Henion, J. D.; Ganem, B. *J. Am. Soc. Mass Spectrom.* **1993,** *4*, 631-637.

(19) Cao, P.; Moini, M. *J. Am. Soc. Mass Spectrom.* **1999,** *10*, 184-186.

(20) Scaloni, A.; Pieragostini, E.; Malorni, A.; Ferrara, L.; Di Luccia, A. *Biochimie* **1998,** *80*, 333-338.

(21) Houston, C. T.; Reilly, J. P. *Rapid Commun. Mass Spectrom.* **1997,** *11*, 1435-1439.

(22) Tang, Q.; Harrata, A. K.; Lee, C. S. *Anal. Chem.* **1996,** *68*, 2482-2487.

(23) Witkowska, H. E.; Green, B. N.; Morris, M.; Shackleton, C. H. L. *J. Mass Spectrom.* **1995**, S111-S115.

(24) Ferranti, P.; Malorni, A.; Pucci, P. *Methods Enzymol.* **1994,** *231*, 45-65.

(25) Sakairi, M. *Rapid Commun. Mass Spectrom.* **1993,** *7*, 1108-1112.

(26) Manca, L.; Ferranti, P.; Barone, F.; Nitti, G.; Malorni, A.; Pucci, P.; Naitana, S.; Masala, B. *Int. J. Biochem.* **1993,** *25*, 1935-1938.

(27) Lightwahl, K. J.; Loo, J. A.; Edmonds, C. G.; Smith, R. D.; Witkowska, H. E.; Shackleton, C. H. L.; Wu, C. S. C. *Biol. Mass Spectrom.* **1993,** *22*, 112-120.

(28) Wada, Y.; Hayashi, A.; Fujita, T.; Matsuo, T.; Katakuse, I.; Matsuda, H. *Int. J. Mass Spectrom. Ion Process.* **1983,** *48*, 209-212.

(29) McComb, M. E.; Oleschuk, R. D.; Chow, A.; Ens, W.; Standing, K. G.; Perreault, H.; Smith, M. *Anal. Chem.* **1998,** *70*, 5142-5149.

(30) Otsuka, S.; Yamanaka, T.;; Elsevier: Tokyo, 1988; Vol. 8, pp 568.

(31) Taylor, P.; Kurtz, D. J.; Amster, I. *Journal of Biological Inorganic Chemistry* **2000,** *submitted*.

(32) He, F.; Hendrickson, C. L.; Marshall, A. G. *J. Am. Soc. Mass Spectrom.* **2000,** *11*, 120-126.

CHAPTER 4

Achieving Isotopic Resolution of Noncovalent Complexes of Metalloproteins by ESI-FTICR[1]

[1]Taylor, P. K.; D. M. Kurtz, Jr; I. J. Amster. To be submitted to *Journal of the American Society for Mass Spectrometry*

ABSTRACT

Five multimeric metalloprotein species are examined by electrospray ionization Fourier transform ion cyclotron resonance (ESI-FTICR) mass spectrometry. Isotopically resolved mass spectra are obtained for noncovalent complexes with masses ranging from 25 kDa to 86 kDa. Metalloproteins are a particularly difficult class of molecules for holoprotein analysis, as the methods generally used for purification and desalting often remove the metal from the protein. In order to achieve isotopic resolution, the sample must be rigorously desalted, as these large molecules offer more sites for proton-sodium exchange, and the heterogeneity of multiply sodiated species causes a decrease in the duration of the beats in the transient signal and thus a decrease in signal-to-noise. Gentle desolvation of the ions formed by electrospray is required to avoid disruption of the noncovalent interactions that bind the subunits to each other. A heated metal capillary interface was found to be useful for this purpose. In order to achieve isotopic resolution, space charge effects must be minimized in the FTICR analyzer cell by controlling the duration of the ionization event and the amplitude of the trapping voltage.

INTRODUCTION

Noncovalent interactions between protein and peptides play an important role in the chemistry of biomolecules for processes such as molecular recognition, as well as enzyme-substrate, protein-ligand, and antibody-antigen interactions.[1] These interactions are structurally specific in nature. Many physiologically active proteins are multimeric and possess active sites at the interface of the subunits.[1] Noncovalent interactions between the subunits of the folded protein lead to aggregation into a specific quaternary structure. These interactions are relatively weak and can be disrupted in protein solutions by altering the pH, the percentage of organic solvent, or by using a denaturing agent.[2-4] The detection of specific noncovalent interactions by electrospray ionization (ESI) mass spectrometry has been demonstrated by a number of researchers.[4-38] Until recently, mass spectrometry was not suitable for examining noncovalent complexes because these interactions were disrupted during the ionization process prior to mass measurement. With the appropriate experimental conditions, ESI can be used to examine a solution in or near its physiological state, thereby maintaining the oligomeric stoichiometry of multimeric proteins during ionization.[5, 12-14, 18, 21, 28, 31, 39-42] For example, the tetrameric protein soy bean agglutinin (MW ~ 116 kDa), one of the first examples of the measurement of a multimeric protein complex by mass spectrometry, was observed by ESI-time-of-flight (ESI-TOF) mass spectrometry to produce ions between m/z 4000 and 5000 that correspond to the tetrameric holoprotein.[31] Octamers and dodecamers were also detected at lower abundance and higher mass-to-charge. The oligomeric structure of 4-oxalocrotonate tautomerase has been observed by ESI-TOF,[12, 13] and by ESI Fourier transform ion

cyclotron resonance (ESI-FTICR) mass spectrometry using in-trap cleanup methods to remove adduction.[43] ESI measurements of a sequence specific protein-DNA complex have been reported.[9] Noncovalent dimers of leucine zipper peptides have been detected by ESI, ionspray, liquid beam desorption, and laser desorption mass spectrometry.[44-47] ESI quadrupole mass spectrometry has been used to examine the avidin-biotin complex.[27] These and other results support the claim that higher order structures are retained in the gas phase by using the appropriate sample handling procedures.

ESI-TOF mass spectrometry is useful for examining noncovalent interactions because of the wide mass range of this instrument. However, the ESI-TOF mass spectrometer has limited mass resolution. ESI-quadrupole mass spectrometry has also been used to examine noncovalent interactions under physiological conditions, but the mass resolution and mass-to-charge range is limited with this instrument. The mass-to-charge of multimeric protein ions produced by ESI under nondenaturing conditions often exceeds the mass range of standard quadrupole mass spectrometers, and only those instruments with an extended mass range can be used for such studies.[10, 18, 19, 27, 48] ESI-FTICR mass spectrometry combines high resolution with a wide mass range, and therefore offers additional capabilities for the study of noncovalent interactions.[6, 8, 17, 28, 32, 43]

Although FTICR mass spectrometry seems well suited for the analysis of protein multimers, a few issues are worth consideration. First is the time scale of the ESI-FTICR experiment. A high resolution ESI-FTICR experiment requires that the noncovalent complex is stable for 1-10 s, five orders of magnitude longer than the 100 μs required for ESI-TOF measurements. While several examples of FTICR analysis of noncovalent

protein multimers have been published,[6, 8, 9, 17, 28, 32, 43, 44, 49-51] only a few show isotopic resolution.[43, 50] These examples have served to establish that the lifetime of multiply-charged noncovalent complexes is suitable for FTICR analysis. Another consideration is that in the FTICR experiment, all species in the cell are detected at the same time. The constructive and destructive interferences of the observed frequencies of the closely spaced isotope species in the cell produce a beat pattern in the transient that is recorded.[52, 53] As the mass of the molecule increases, the beats in the transient become shorter in duration and more widely spaced in time.[54] In order to achieve isotopic resolution, it is necessary to sample at least two beats in the transient.[54, 55] For high mass molecules such as noncovalent complexes, the challenge is maintaining the coherence of the ion packet for the long time necessary (several seconds) to observe the second beat in the transient, a requirement for obtaining isotopic resolution.[55]

Here we present a study of five metalloprotein noncovalent complexes with molecular weights from 25 kDa to 86 kDa that illustrate the capabilities and challenges of using ESI-FTICR for such measurements. Metalloproteins are more difficult to analyze as holoproteins than standard proteins. The purification and desalting methods that have been successful for other proteins often result in loss of the metal in the metalloprotein active site, thus limiting the types of procedures that can be used.[43, 56, 57] Also, the metal centers of some metalloproteins are unstable toward ionization, leading to heterogeneity in the detected species. These and other issues are illustrated in the present work.

EXPERIMENTAL

Clostridium pasteurianum [2Fe-2S] ferredoxin was isolated as the native protein from bacterial culture.[58] *Desulfovibrio vulgaris* nigerythrin and *Desulfovibrio vulgaris* rubrerythrin were obtained by overexpression in *Escherichia coli*.[59] Bovine hemoglobin was obtained from Sigma (St. Louis, MO). Ferredoxin was desalted by repeated ultrafiltration with a 10 kDa MWCO membrane (Millipore, Bedford, MA) followed by resuspension in 10 mM ammonium acetate. Final ferredoxin dimer concentration was approximately 10 μM. Nigerythrin and rubrerythrin were desalted by 16 hours of dialysis in a bath of 10 mM ammonium acetate in a 10 kDa Slide-A-Lyzer dialysis cassette (Pierce, Rockford, IL). Final concentration was 20 μM for nigerythrin dimer, hemoglobin heterodimer and rubrerythrin tetramer. Concentration for bacterial proteins was determined by UV-visible spectrophotometry. Hemoglobin heterotetramer was desalted by repeated centrifugation through a 30 kDa MWCO ultrafiltration tube (Millipore, Bedford, MA) followed by resuspension in 10 mM ammonium acetate. Final tetramer concentration was 20 μM. All proteins except the hemoglobin heterodimer were sprayed out of 10 mM ammonium acetate. The hemoglobin heterodimer was sprayed out of 10% methanol.

Mass spectrometry was performed with a 7 Tesla FTICR mass spectrometer (Bruker BioApex, Billerica, MA) equipped with an electrospray ion source (Analytica, Branford, CT). We were unable to observe any multimers with the standard glass capillary, and so it was replaced by a heated metal capillary inlet.[60] The heated metal capillary provides gentler desolvation and allows the noncovalent complex to be more

easily observed. A capillary temperature of 150◦C to 200°C was used for these experiments. Samples were ionized via nanospray, through tips fabricated in-house from 100 μm i.d fused silica (Polymicro Technologies, Phoenix, AZ; Supelco, Bellefonte, PA). Pumping was provided through a syringe pump at 6 μL/hr, and the nanospray voltage was applied at the needle of the syringe. Space charge proved to be a major concern in the observation of multiple beats in the transient. The ion density within the cell was carefully controlled in order to minimize space charge effects. This was achieved by accumulating ions in the external hexapole for times no greater than 7 msec. Trap voltages were 0.5 and 0.65 volts for the front and back traps for ferredoxin and nigerythrin, and 0.4 and 0.55 volts for hemoglobin dimer and tetramer and rubrerythrin. These relatively low trap voltages reduced space charge, enabling the observation of isotopic structure for the high mass species presented here.

RESULTS AND DISCUSSION

A relatively low molecular-weight protein dimer was used to identify the experimental conditions necessary to observe a holoprotein noncovalent complex with isotopic resolution. Ferredoxin from *Clostridium pasteurianum* (CpFd) forms a dimer containing one [2Fe-2S] cluster per subunit, with a dimer mass of approximately 23 kDa. Previous ESI-quadrupole mass spectrometric research on CpFd had shown a multiplicity of peaks within each charge state of the dimer, but the peaks were not well resolved.[61] The ESI-FTICR mass spectrum of CpFd dimer is shown in Figure 1. At this relatively low molecular weight (for a protein multimer), isotopic resolution is readily achieved. The

sample requires more extensive desalting than ordinary samples. Ferredoxin required moderate capillary temperatures (150°C) in order to accomplish adequate desolvation. Figure 1a shows the mass spectrum, and the inset is an expansion of the 11+ charge state, demonstrating isotopic resolution. Three different isotopic distributions are evident within the 11+ charge state. The most abundant of these corresponds to a MW of 23222.2 Da, which is 30 Da higher than the theoretical dimer MW of 23192.5 Da, calculated from the amino acid sequence containing one [2Fe-2S] cluster per subunit.[62] Previous research with iron-sulfur proteins has demonstrated that sulfur adducts arise in the presence of free cysteines by formation of a dithiol.[60] CpFd contains five cysteines, of which four are ligands to the iron-sulfur cluster. The fifth cysteine is free and capable of forming a bond to inorganic sulfur. The 30 Da mass difference between the theoretical dimer mass and the mass of the most abundant peak is too great for a sodium adduct, but too small for a sulfur adduct. Figure 2 shows a comparison between the experimental isotopic distribution and theoretical isotopic distributions generated for the dimer plus a sodium adduct and the dimer plus a sulfur adduct. Careful examination of the width and shape of the experimental peak reveals that it is composed of a mixture of a dimer plus sodium with a dimer plus sulfur, an assignment only discernable through the high resolution of ESI-FTICR. This assignment is confirmed by the peaks centered around m/z 2116 in Figure 1, which appear approximately 32 Da above the most abundant peak and are assigned as the addition of both a sulfur and a sodium to the dimer. Petillot and coworkers also observed three sets of peaks in the dimer mass spectrum of CpFd, which were assigned as the dimer plus multiple sodium and potassium adducts. The high resolution and high mass accuracy

Figure 1. ESI-FTICR mass spectrum of [2Fe-2S] ferredoxin from *Clostridium pasteurianum*, a 23 kDa dimer. a) Mass spectrum of the 12+ through 10+ charge states, with an expansion of the 11+ charge state showing isotopic resolution, binding of sodium and addition of sulfur to the dimer. b) Transient for this mass spectrum, showing a second beat at 0.45 s.

a)

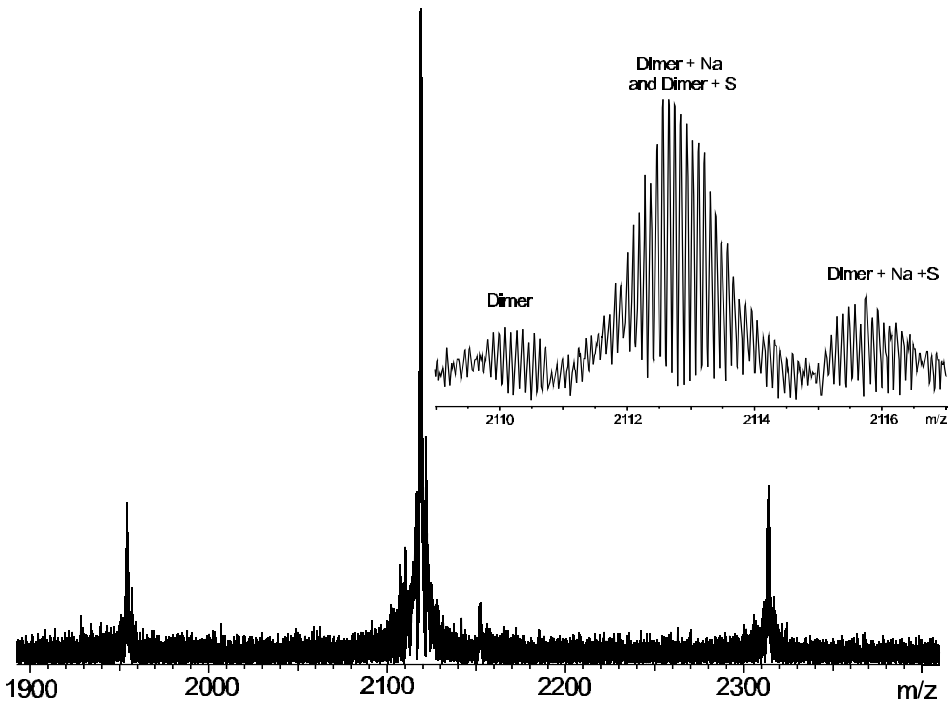
Dimer + Na
and Dimer + S
Dimer
Dimer + Na +S
2110
2112
2114
2116
m/z
1900
2000
2100
2200
2300
m/z

b)

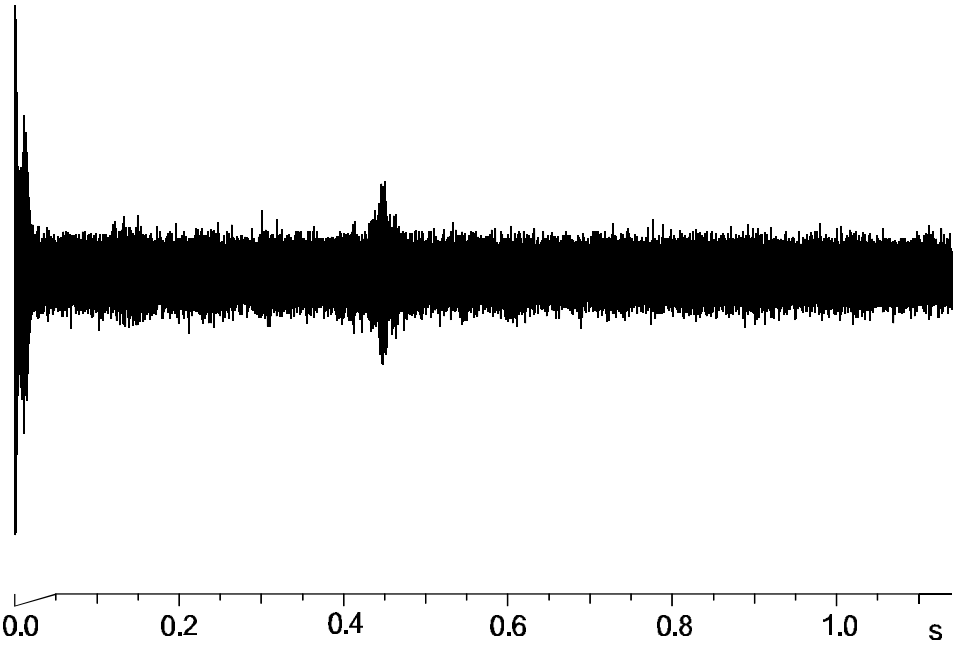
0.0
0.2
0.4
0.6
0.8
1.0
s

Figure 2. Comparison of the isotopic distribution of the most abundant peak in the 11+ charge state for CpFd with theoretical isotopic distributions generated for the dimer plus sodium and for the dimer plus sulfur. a) Theoretical isotopic distribution of CpFd dimer plus sulfur. b) Experimental isotopic distribution of the most abundant peak in the 11+ charge state of CpFd. c) Theoretical isotopic distribution of CpFd dimer with a single sodium-proton exchange.

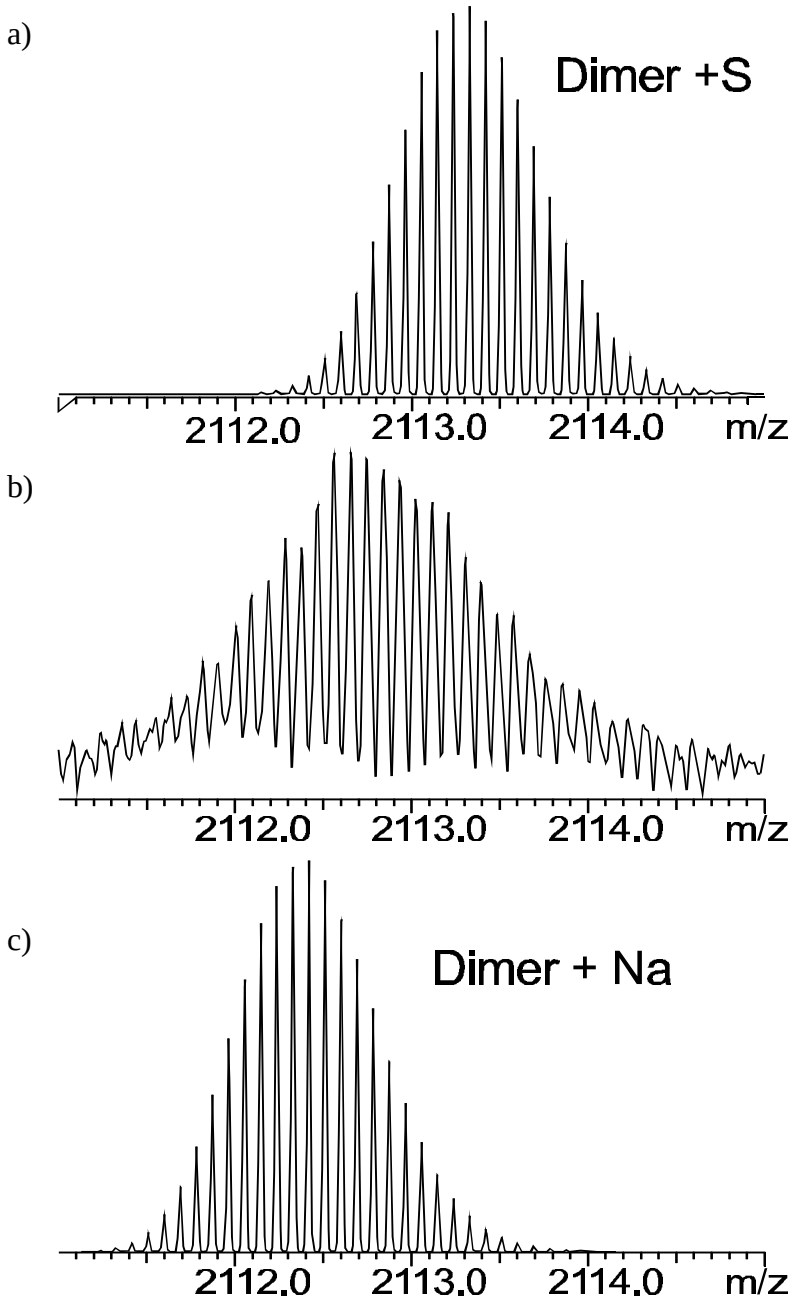
a)
Dimer +S
2112.0
2113.0
2114.0
m/z
b)
2112.0
2113.0
2114.0
m/z
c)
Dimer + Na
2112.0
2113.0
2114.0
m/z

of the FTICR instrument shows that these higher mass species are a result of sodium binding and sulfur adduction.

The peak centered around m/z 2110 appears in the correct range for the dimer, although poor isotope statistics do not allow this assignment to be made with high accuracy. To verify the mass of the dimer, the protein was placed in 25% MeOH, causing partial disruption of the noncovalent interactions. The aposubunit of the monomer gave a monoisotopic mass of 11417.3 Da, in good agreement with the mass calculated from the amino acid sequence, 11418.6 Da, assuming the formation of two internal disulfide bonds between the cysteines that normally bind the [2Fe-2S] cluster. Accurate assignment of monoisotopic mass requires that the oxidation state of the metal cluster be taken into account.[60] For the CpFd dimer, each [2Fe-2S] cluster carries a 2+ oxidation state, so that four charges are attributed to the metal clusters. For example, assigning the molecular weight from the mass-to-charge value of the 11+ charge state in the mass spectrum required the subtraction of only 7 protons from the mass of the ion.

Identification of the peaks in the dimer mass spectrum arising from sodium binding and sulfur adduction requires high-resolution. Figure 1b shows the transient obtained for the dimer, exhibiting a second beat at 0.45 s. The beats in the transient are due to destructive interference of the cyclotron frequencies associated with the isotopes of the most abundant charge state. The duration between beats is given by Equation 1, where Δt is the beat period, m is the molecular mass of the complex (in Da), B is magnetic field strength in Tesla, and z is the charge state of the principal peak.[54] For the 11+ charge state of this 23 kDa complex, the calculated beat period is 0.4 s, as observed for the

experimental data. The charge state distribution falls within the range m/z 1900-2400. This narrow distribution of relatively low charge states is consistent with the expected mass spectrum of a folded protein, as many of the potential sites for protonation are not accessible with a compact protein structure. The dimer is the only type of multimer observed, indicating specific aggregation consistent with the known biologically relevant multimer stoichiometry of this protein.

$$\Delta t \cong \frac{2\pi m^2}{zB} x10^{-8} \qquad (1)$$

Most biologically interesting noncovalent complexes have higher molecular weights than ferredoxin, and so we have worked to increase the mass range of the protein complexes that can be examined with isotopic resolution. Figure 3 shows the ESI-FTICR mass spectrum of the heterodimer of bovine hemoglobin, obtained at a capillary temperature of 200°C. The dimer has a monoisotopic mass of 32221.1 Da, in good agreement with the calculated mass of 32220.6 Da for a complex of one alpha subunit, one beta subunit, and two iron-containing heme groups. Hemoglobin exists predominantly in solution as a heterotetramer with $\alpha_2\beta_2$ stoichiometry. No evidence is found in the mass spectrum of a trimer form of hemoglobin, or of a homodimer of either α_2 or β_2 stoichiometry, indicating the species observed results from specific aggregation. Although some heterodimer was in evidence in a pure aqueous solution, the strongest signal for dimer was obtained with a 10% MeOH solution. To avoid space charge-induced peak broadening, it was necessary to use low trapping voltages, 0.5 V and 0.65 V for the front and back trap plates, respectively. Figure 3a shows a narrowband mass spectrum of the

Figure 3. ESI-FTICR mass spectrum of the dimer of bovine hemoglobin, with a mass of 32 kDa, corresponding to the alpha and beta subunits with their iron-containing heme groups. a) Narrowband mass spectrum of hemoglobin dimer in 10% MeOH, with an expansion of the 11+ charge state showing isotopic resolution. b) Transient for this mass spectrum, showing seven beats in 5.2 seconds.

a)

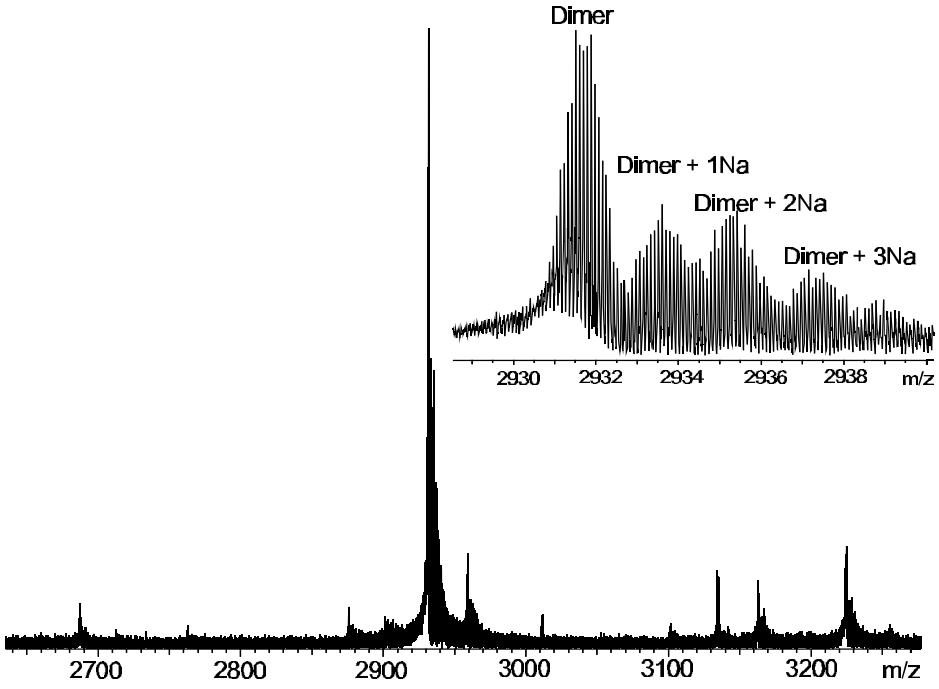
Dimer
Dimer + 1Na
Dimer + 2Na
Dimer + 3Na
2930
2932
2934
2936
2938
m/z
2700
2800
2900
3000
3100
3200
m/z

b)

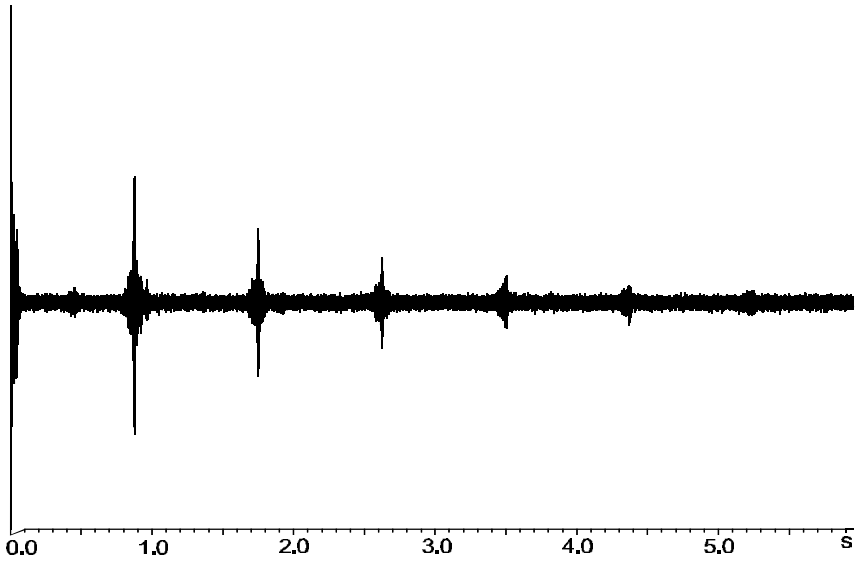
0.0
1.0
2.0
3.0
4.0
5.0
s

11+ charge state, with the inset expansion showing the resulting isotopic structure. In addition to the dimer, higher mass peaks are observed corresponding to the substitution of up to three sodium cations for protons. In between the peaks corresponding to the substitution by one and two sodium cations, there is some signal in the region corresponding to the addition of dioxygen. We have been able to increase the abundance of this second oxygen molecule by saturating the protein solution with oxygen has prior to analysis. These results are the subject of a separate paper.[63] Figure 3b shows the transient for this spectrum, which persists for over five seconds, with seven beats, ensuring isotopic resolution. At higher mass, beats in the transient are expected to become more widely spaced, as can be seen by comparison with Figure 1b. From Equation 1, the beat period is predicted to be 0.85 s, in close agreement with the observation.

As an example of a higher mass dimeric protein, the mass spectrum of nigerythrin from *Desulfovibrio vulgaris* is shown in Figure 4. Under native conditions, nigerythrin forms a dimer weighing approximately 40 kDa in which each subunit contains an FeS_4 rubredoxin-like site as well as an oxo-bridged diiron site.[59] Figure 4a shows the mass spectrum of the nigerythrin dimer obtained at a capillary temperature of 200 °C, with the expansion showing the isotope peaks. Figure 4b shows the transient for the nigerythrin mass spectrum, with four beats appearing in five seconds, exhibiting the expected increased spacing of the transient beats with increasing mass. The wide mass range of the isotope distribution can be attributed to the presence of sodium adducts. The opportunity for sodium-proton exchange appears to increase as the protein complexes become larger. Removing sodium requires increasingly rigorous desalting techniques. In this case, we

Figure 4. ESI-FTICR mass spectrum of nigerythrin from *Desulfovibrio vulgaris*. Nigerythrin forms a 44 kDa dimer with two metal-containing active sites per subunit; one is an FeS_4 cluster, while the other is an oxo-bridged diiron site. a) Mass spectrum of the 12+ through 10+ charge states, with an expansion of the 11+ charge state showing isotopic resolution. The broad isotopic distribution is likely caused by sodium adduction. b) Transient for this mass spectrum, with an expansion showing the third and fourth beats at approximately 3.2 and 4.8 seconds, respectively.

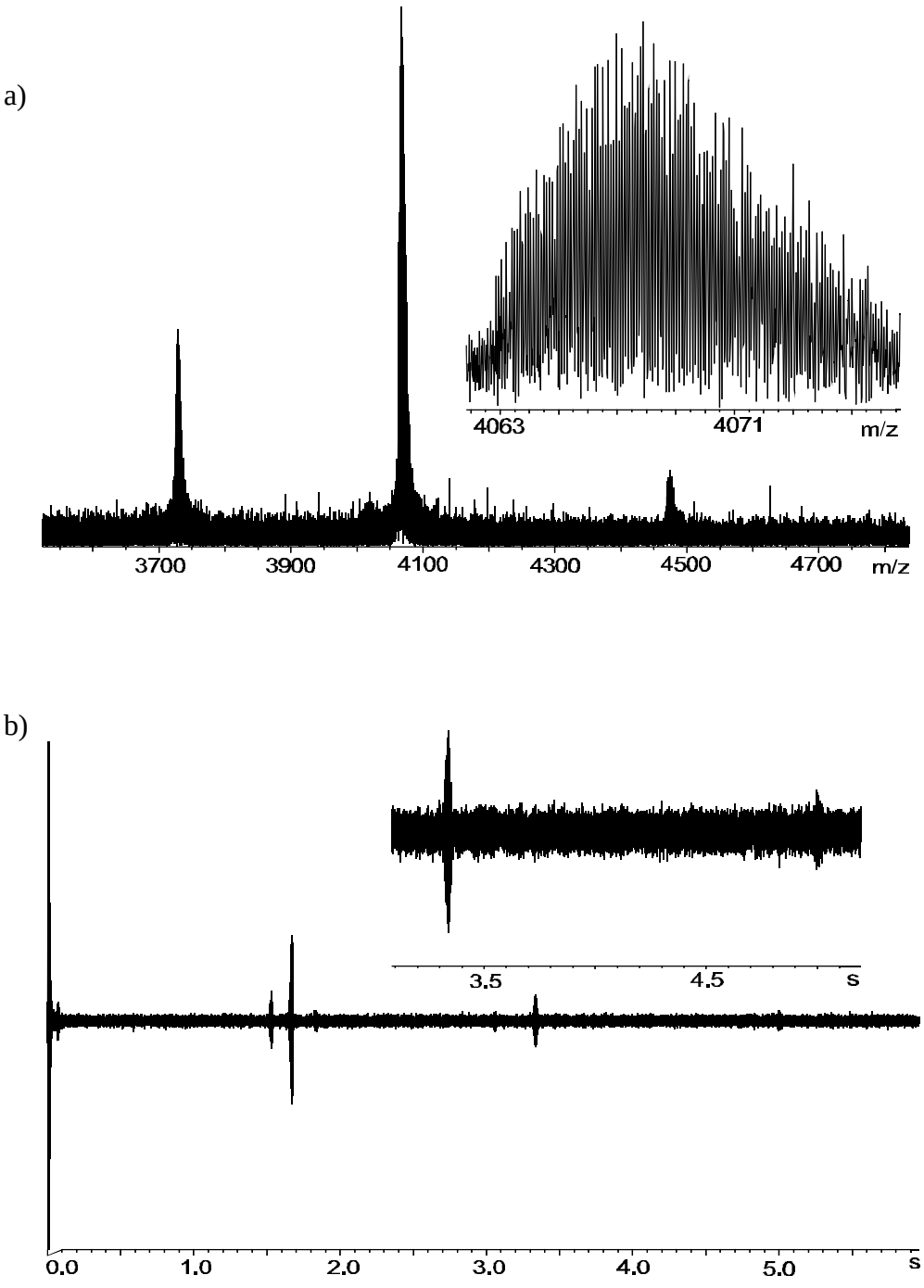
a)
4063
4071
m/z
3700
3900
4100
4300
4500
4700
m/z
b)
3.5
4.5
s
0.0
1.0
2.0
3.0
4.0
5.0
s

were unable to remove all traces of sodium even after 16 hours of dialysis. Attempts to remove sodium using compounds such as citrate[43] resulted in loss of the metal from the protein. Although isotopic resolution is achieved, a reliable monoisotopic MW cannot be extracted from these data, as the isotopic composition of the data cannot be assigned reliably. Nevertheless, an average mass of 44712.2 Da can be extracted from the data, which was 180 Da higher than the average mass of 44532.1 Da calculated from the amino acid sequence plus six iron atoms. Preliminary sequence data on the *D. vulgaris* genome was obtained from The Institute for Genomic Research website at http://www.tigr.org. To determine whether this 180 Da mass difference could be attributed to other factors besides the presence of multiple adducts, the protein was run under denaturing conditions (49:49:2 H_20:MeOH:HOAc v:v) to determine the monoisotopic mass of the monomer aposubunit. The experimentally determined monoisotopic mass of the monomer was found to be 22180.5 Da, a difference of 97 mass units from the calculated mass of 22083.9 Da, most likely due to disparity in the actual amino acid sequence from the published sequence. The average mass of the subunit obtained from this measurement is 22192 Da. Using the measured value, we calculate a molecular weight for the dimer of 44,720 Da (22192 x 2 + 56 (Fe) x 6), in close agreement to the measured value (180 ppm error).

Figure 5 shows the mass spectrum of the heterotetrameric form of hemoglobin, obtained by maintaining the analyte under nondenaturing conditions and analyzing at a capillary temperature of 200 °C. The inset is an expansion of the 17+ charge state,showing isotopic resolution. Figure 6 shows a comparison of expected versus

Figure 5. ESI-FTICR mass spectrum of tetrameric bovine hemoglobin, under nondenaturing conditions. The 64 kDa tetramer has $\alpha_2\beta_2$ stoichiometry, with each subunit binding an iron-containing heme group. a) Mass spectrum of the 18+ through 16+ charge states, with expansion of the 17+ charge state showing isotopic resolution. b) Transient for this mass spectrum, showing a second beat at approximately 2.4 seconds.

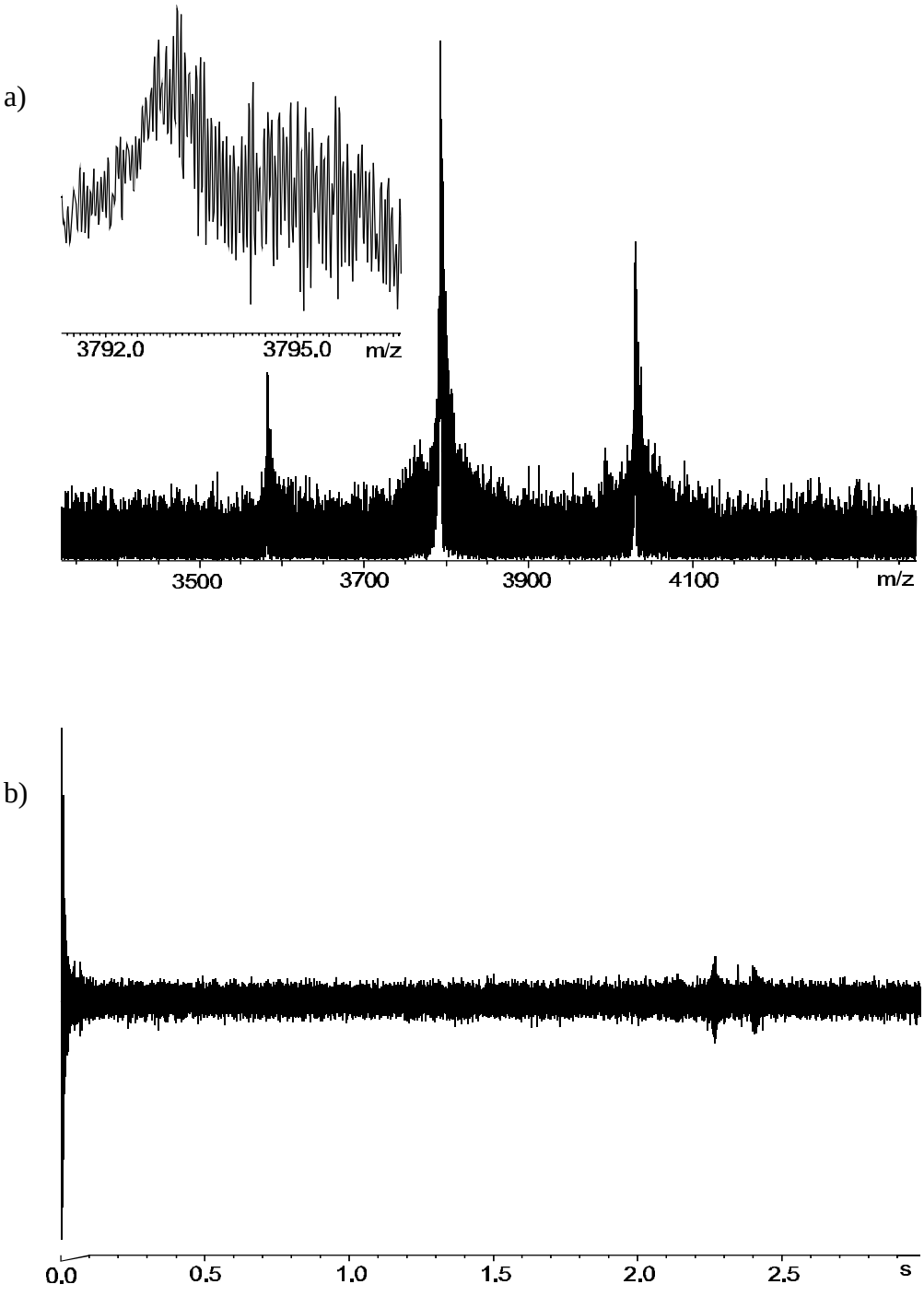
a)
3792.0
3795.0
m/z
3500
3700
3900
4100
m/z
b)
0.0
0.5
1.0
1.5
2.0
2.5
s

Figure 6. Comparison of expected versus measured isotopic envelope for the 17+ charge state of heterotetrameric hemoglobin. a) Expected isotopic distribution, calculated for the heterotetramer with $\alpha_2\beta_2$ stoichiometry. b) Measured isotopic distribution, broader due to sodium adduction.

a)

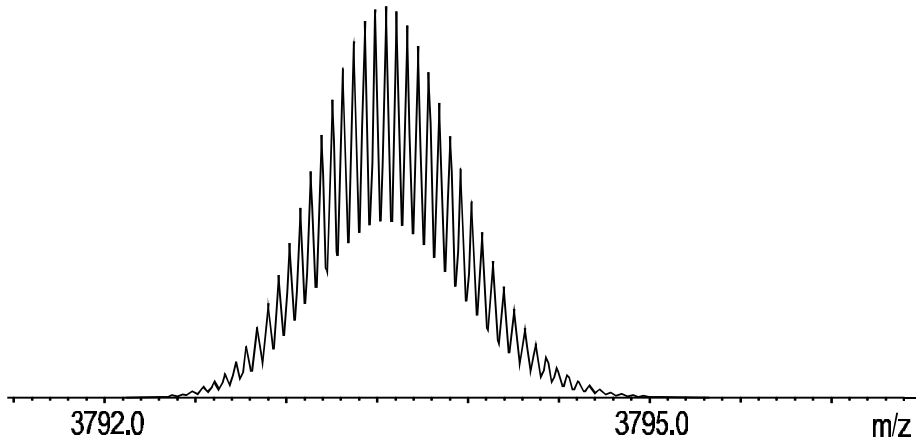

b)

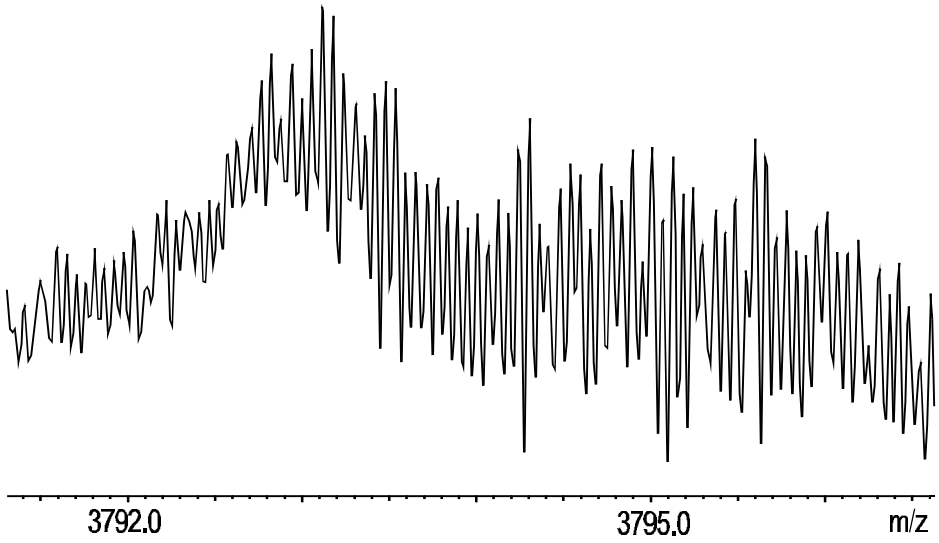

measured isotopic envelope. The wide distribution of isotope peaks is consistent with sodium contamination. The most rigorous desalting techniques have not been able to remove all of the sodium adduction, but minimizing the adduction allows observation of the second beat in the transient at approximately 2.3 seconds, Figure 5b. Smith and coworkers have used ammonium citrate to remove sodium adducts from holoproteins that contain no metal, followed by sustained off-resonance irradiation in order to remove the resulting citric acid adducts.[43] Attempts to utilize this method for these experiments resulted in loss of the metal from the proteins and degradation of the multimer. The breadth of the isotope distribution may also be due to binding of dioxygen. Saturation of the protein solution allows us to observe the binding of up to four molecules of dioxygen to this substrate.[63] In addition to the problem of adduction, space charge has also proven to be a consideration. In order to achieve the second beat in the transient, it was necessary to further reduce the voltage on the front and back trap plates to 0.4 and 0.55 volts, respectively. A shorter hexapole storage time (0.1 seconds) also seemed to aid the observation of isotopic resolution, by reducing the number of high-energy collisions in the hexapole which could disrupt the noncovalent interactions. Because of the poor isotope statistics, the monoisotopic mass cannot be reliably assigned. Nevertheless, this is the highest mass isotopically resolved mass spectrum yet reported for metalloprotein. An average mass of 64463 Da can be derived from these data, which compares favorably to the calculated value of 64473 Da.

Figure 7 shows a mass spectrum of *Desulfovibrio vulgaris* rubrerythrin, a tetrameric protein with a MW of 86 kDa. Rubrerythrin contains an FeS_4 site and an oxo-

Figure 7. ESI-FTICR mass spectrum of rubrerythrin from *Desulfovibrio vulgaris*. Rubrerythrin has an FeS_4 active site as well as an oxo-bridged diiron site, and has a high sequence homology to nigerythrin. However, only an 86 kDa tetrameric form of rubrerythrin has been seen by mass spectrometry. a) Mass spectrum of the 20+ through 17+ charge states. b) Transient for this mass spectrum, with expansion showing a second beat at approximately 4.0 seconds. Although the second beat in the mass spectrum is discernable, the isotope peaks are indistinguishable from the noise in the mass spectrum.

a)

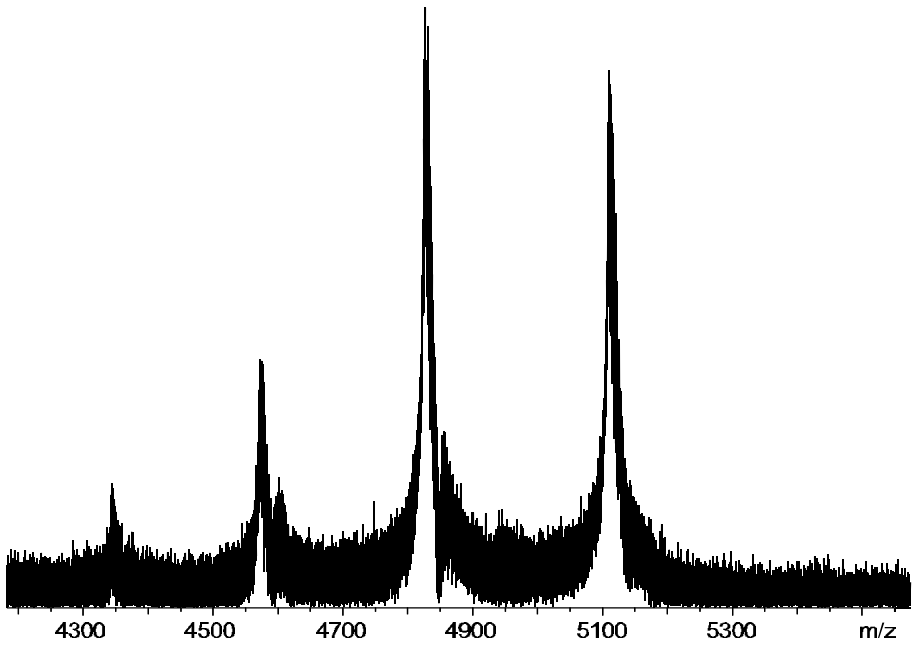

b)

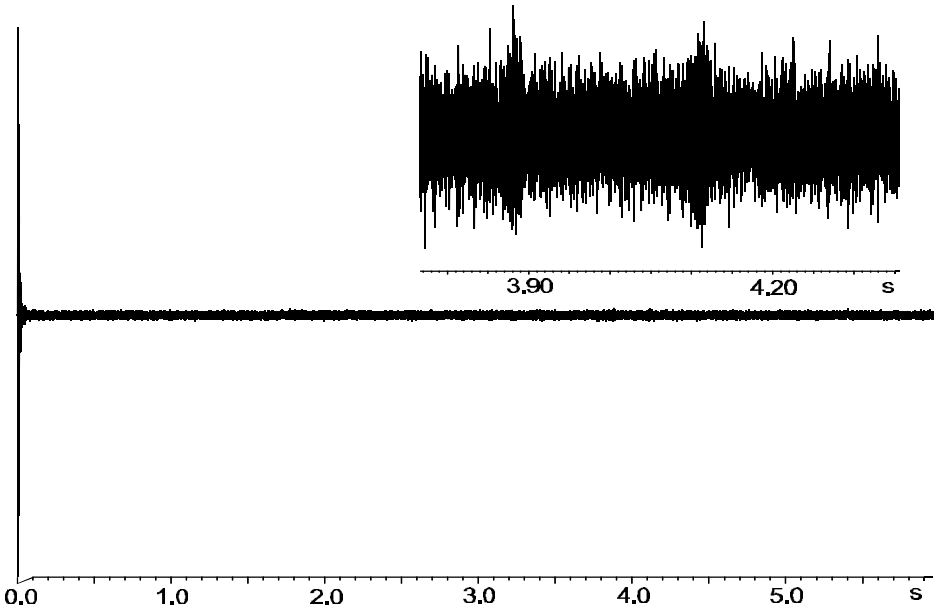

bridged diiron site and has a high amino acid sequence homology to nigerythrin, but unlike nigerythrin, only the tetrameric form has been observed by mass spectrometry.[35] At this high molecular weight, the second beat of the transient occurs at approximately 4 seconds. Achieving isotopic resolution requires that the coherence of the ion packet is maintained for an extended length of time. Rubrerythrin was not able to withstand 200°C capillary temperature without degradation of the complex, so the temperature was reduced to 150°C. Figure 7a shows the mass spectrum of rubrerythrin, and Figure 7b shows its accompanying transient. The inset is an expansion of the 3.8-4.3 second region of the transient, showing a very weak second beat. Although the second beat is apparent in the transient, isotopic structure is not evident in the mass spectrum. From these data, we can obtain an average molecular weight of 86856.5 Da, which agrees well with the calculated value of 86847.6 Da.[59, 64] These data are consistent with an Fe_{12} stoichiometry, as expected for the tetramer. Evidence of the bridging oxygens is not observed in these mass spectra, consistent with high resolution data for the monomer of this protein.[17]

CONCLUSIONS

These data show that multimeric metalloproteins are stable on the time scale of the FTICR experiment. We have obtained mass spectra for multimers ranging in size from 20-90 kDa. Sample purity, particularly for material isolated from biological systems, is a primary concern. Samples obtained from bacterial media contain high quantities of salt as well as buffers which are not compatible with mass spectrometry. Careful and rigorous desalting must be performed in order to remove as much of the adducting species as possible without denaturing the noncovalent complex. Larger metalloproteins are

particularly challenging to desalt, as rigorous methods such as reverse phase HPLC cause loss of the metal center. Sodium contamination is found to be the principle limitation in extending the mass range of this technique. Space charge is a factor, as the closely spaced isotope peaks coalesce more readily as molecular weight increases. Reducing the number of ions to allow isotopes to be observed also reduces the signal to noise ratio, necessitating extensive signal averaging. Finally, the transients of all the multimeric complexes examined to date damp out within five seconds. In order to obtain isotopic resolution of even higher mass noncovalent complexes, it will be necessary to sustain the coherence of the ion packet for more than five seconds, possibly through quadrupolar excitation, although this method can increase space charge effects such as isotope coalescence. Alternatively, higher magnetic fields would aid these studies.

ACKNOWLEDGMENTS

CpFd was graciously donated by Dr. Michael Adams at the University of Georgia. Rubrerythrin and nigerythrin were prepared by Dr. Eric Coulter, Dr. Neeta Shenvi, and Shi Jin. The authors are grateful for generous financial support from NSF (CHE-9974579) and from NIH (GM40388).

REFERENCES

(1) Alberts, B.; Bray, D.; Lewis, J.; Raff, M.; Robert, K.; Watson, J. D. *Molecular Biology of the Cell*, 3rd ed.; Garland Publishing, Inc.: NY, 1994.

(2) Chowdhury, S. K.; Katta, V.; Chait, B. T. *J. Am. Chem. Soc.* **1990,** *112*, 9012-9013.

(3) Ganguly, A. K.; Pramanik, B. N.; Tsarbopoulos, A.; Covey, T. R.; Huang, E.; Fuhrman, S. A. *J. Am. Chem. Soc.* **1992,** *114*, 6559- 6560.

(4) Ganguly, A. K.; Pramanik, B. N.; Huang, E. C.; Tsarbopoulos, A.; Girijavallabhan, V. M.; Liberles, S. *Tetrahedron* **1993,** *49*, 7985-7996.

(5) Strupat, K.; Roginaux, H.; Dorsselaer, A. V.; Roth, J.; Vogl, T. *J. Am. Soc. Mass Spectrom.* **2000,** *11*, 780-788.

(6) Bruce, J. E.; Smith, V. F.; Liu, C. L.; Randall, L. L.; Smith, R. D. *Protein Sci.* **1998,** *7*, 1180-1185.

(7) Cao, P.; Moini, M. *J. Am. Soc. Mass Spectrom.* **1999,** *10*, 184-186.

(8) Chen, R. D.; Cheng, X. H.; Mitchell, D. W.; Hofstadler, S. A.; Wu, Q. Y.; Rockwood, A. L.; Sherman, M. G.; Smith, R. D. *Anal. Chem.* **1995,** *67*, 1159-1163.

(9) Cheng, X. H.; Morin, P. E.; Harms, A. C.; Bruce, J. E.; BenDavid, Y.; Smith, R. D. *Anal. Biochem.* **1996,** *239*, 35-40.

(10) Doktycz, M. J.; Habibigoudarzi, S.; McLuckey, S. A. *Anal. Chem.* **1994,** *66*, 3416-3422.

(11) Espinoza, E. O.; Lindley, N. C.; Gordon, K. M.; Ekhoff, J. A.; Kirms, M. A. *Anal. Biochem.* **1999,** *268*, 252-261.

(12) Fitzgerald, M. C.; Chernushevich, I.; Standing, K. G.; Kent, S. B. H.; Whitman, C. P. *J. Am. Chem. Soc.* **1995,** *117*, 11075- 11080.

(13) Fitzgerald, M. C.; Chernushevich, I.; Standing, K. G.; Whitman, C. P.; Kent, S. B. H. *Proc. Nat. Acad. Sci. USA* **1996,** *93*, 6851-6856.

(14) Ganem, B.; Li, Y. T.; Henion, J. D. *J. Am. Chem. Soc.* **1991,** *113*, 7818-7819.

(15) Goodlett, D. R.; Loo, R. R. O.; Loo, J. A.; Wahl, J. H.; Udseth, H. R.; Smith, R. D. *J. Am. Soc. Mass Spectrom.* **1994,** *5*, 614-622.

(16) Jespersen, S.; Niessen, W. M. A.; Tjaden, U. R.; van der Greef, J. *J. Mass Spectrom.* **1998,** *33*, 1088-1093.

(17) Kulkarni, S. S.; Taylor, K.; Amster, I. J. *Proceedings of the 44th ASMS Conference on Mass Spectrometry and Allied Topics* **1996**, 487.

(18) Lightwahl, K. J.; Springer, D. L.; Winger, B. E.; Edmonds, C. G.; Camp, D. G.; Thrall, B. D.; Smith, R. D. *J. Am. Chem. Soc.* **1993,** *115*, 803- 804.

(19) Lightwahl, K. J.; Schwartz, B. L.; Smith, R. D. *J. Am. Chem. Soc.* **1994,** *116*, 5271- 5278.

(20) Loo, R. R. O.; Goodlett, D. R.; Smith, R. D.; Loo, J. A. *J. Am. Chem. Soc.* **1993,** *115*, 4391- 4392.

(21) Loo, J. A.; Loo, R. R. O.; Andrews, P. C. *Org. Mass Spectrom.* **1993,** *28*, 1640-1649.

(22) Loo, J. A. *J. Mass Spectrom.* **1995,** *30*, 180-183.

(23) Loo, J. A. *Mass Spectrom. Rev.* **1997,** *16,* 1-23.

(24) Raftery, M. J.; Geczy, C. L. *J. Am. Soc. Mass Spectrom.* **1998,** *9,* 533-539.

(25) Robinson, C. V.; Chung, E. W.; Kragelund, B. B.; Knudsen, J.; Aplin, R. T.; Poulsen, F. M.; Dobson, C. M. *J. Am. Chem. Soc.* **1996,** *118,* 8646- 8653.

(26) Sannes-Lowery, K. A.; Mei, H. Y.; Loo, J. A. *Int. J. Mass Spectrom.* **1999,** *193,* 115-122.

(27) Schwartz, B. L.; Lightwahl, K. J.; Smith, R. D. *J. Am. Soc. Mass Spectrom.* **1994,** *5,* 201-204.

(28) Senko, M. W.; Beu, S. C.; McLafferty, F. W. *J. Am. Soc. Mass Spectrom.* **1995,** *6,* 229-233.

(29) Senko, M. W.; Hendrickson, C. L.; Pasatolic, L.; Marto, J. A.; White, F. M.; Guan, S. H.; Marshall, A. G. *Rapid Commun. Mass Spectrom.* **1996,** *10,* 1824-1828.

(30) Smith, R. D.; Lightwahl, K. J.; Winger, B. E.; Loo, J. A. *Org. Mass Spectrom.* **1992,** *27,* 811-821.

(31) Tang, X. J.; Brewer, C. F.; Saha, S.; Chernushevich, I.; Ens, W.; Standing, K. G. *Rapid Commun. Mass Spectrom.* **1994,** *8,* 750-754.

(32) Tolic, L. P.; Harms, A. C.; Anderson, G. A.; Smith, R. D.; Willie, A.; Jorns, M. S. *J. Am. Soc. Mass Spectrom.* **1998,** *9,* 510-515.

(33) Witkowska, H. E.; Shackleton, C. H. L.; Dahlmanwright, K.; Kim, J. Y.; Gustafsson, J. A. *J. Am. Chem. Soc.* **1995,** *117,* 3319- 3324.

(34) Yang, L. Y.; Lee, C. S.; Hofstadler, S. A.; Pasa-Tolic, L.; Smith, R. D. *Anal. Chem.* **1998,** *70*, 3235-3241.

(35) Lei, Q. P.; Cui, X. Y.; Kurtz, D. M.; Amster, I. J.; Chernushevich, I. V.; Standing, K. G. *Anal. Chem.* **1998,** *70*, 1838-1846.

(36) Veenstra, T. D. *Biophys. Chem.* **1999,** *79*, 63-79.

(37) Veenstra, T. D. *Biochem. Biophys. Res. Commun.* **1999,** *257*, 1-5.

(38) Veenstra, T. D.; Tomlinson, A. J.; Benson, L.; Kumar, R.; Naylor, S. *J. Am. Soc. Mass Spectrom.* **1998,** *9*, 580-584.

(39) Ganem, B.; Li, Y. T.; Henion, J. D. *J. Am. Chem. Soc.* **1991,** *113*, 6294-6296.

(40) Katta, V.; Chait, B. T. *J. Am. Chem. Soc.* **1991,** *113*, 8534.

(41) Baca, M.; Kent, S. B. H. *J. Am. Chem. Soc.* **1992,** *114*, 3992- 3993.

(42) Jaquinod, M.; Leize, E.; Potier, N.; Albrecht, A. M.; Shanzer, A.; Vandorsselaer, A. *Tetrahedron Letters* **1993,** *34*, 2771-2774.

(43) Tolic, L. P.; Bruce, J. E.; Lei, Q. P.; Anderson, G. A.; Smith, R. D. *Anal. Chem.* **1998,** *70*, 405-408.

(44) Li, Y. T.; Hsieh, Y. L.; Henion, J. D.; Senko, M. W.; McLafferty, F. W.; Ganem, B. *J. Am. Chem. Soc.* **1993,** *115*, 8409- 8413.

(45) Kleinekofort, W.; Pfenninger, A.; Plomer, T.; Griesinger, C.; Brutschy, B. *Int. J. Mass Spectrom. Ion Process.* **1996,** *156*, 195-202.

(46) Glocker, M. O.; Bauer, S. H. J.; Kast, J.; Volz, J.; Przybylski, M. *J. Mass Spectrom.* **1996,** *31*, 1221-1227.

(47) Przybylski, M.; Glocker, M. O. *Angew. Chem.-Int. Edit. Engl.* **1996,** *35*, 807-826.

(48) Li, Y. T.; Hsieh, Y. L.; Henion, J. D.; Ganem, B. *J. Am. Soc. Mass Spectrom.* **1993,** *4*, 631-637.

(49) Smith, R. D.; Bruce, J. E.; Wu, Q. Y.; Lei, Q. P. *Chem. Soc. Rev.* **1997,** *26*, 191-202.

(50) Bruce, J. E.; Vanorden, S. L.; Anderson, G. A.; Hofstadler, S. A.; Sherman, M. G.; Rockwood, A. L.; Smith, R. D. *J. Mass Spectrom.* **1995,** *30*, 124-133.

(51) Schwartz, B. L.; Bruce, J. E.; Anderson, G. A.; Hofstadler, S. A.; Rockwood, A. L.; Smith, R. D.; Chilkoti, A.; Stayton, P. S. *J. Am. Soc. Mass Spectrom.* **1995,** *6*, 459-465.

(52) Marshall, A. G.; Hendrickson, C. L.; Jackson, G. S. *Mass Spectrom. Rev.* **1998,** *17*, 1-35.

(53) Amster, I. J. *J. Mass Spectrom.* **1996,** *31*, 1325-1337.

(54) Easterling, M. L.; Amster, I. J.; van Rooij, G. J.; Heeren, R. M. A. *J. Am. Soc. Mass Spectrom.* **1999,** *10*, 1074-1082.

(55) Hofstadler, S. A.; Bruce, J. E.; Rockwood, A. L.; Anderson, G. A.; Winger, B. E.; Smith, R. D. *Int. J. Mass Spectrom. Ion Process.* **1994,** *132*, 109-127.

(56) Linnemayr, K.; Rizzi, A.; Josic, D.; Allmaier, G. *Anal. Chim. Acta* **1998,** *372*, 187-199.

(57) Torto, N.; Hofte, A.; van der Hoeven, R.; Tjaden, U.; Gorton, L.; Marko-Varga, G.; Bruggink, C.; van der Greef, J. *J. Mass Spectrom.* **1998,** *33*, 334-341.

(58) Cardenas, J.; Mortenson, L. E.; Yoch, D. C. *Biochimica Et Biophysica Acta* **1976,** *434*, 244-257.

(59) Lumppio, H. L.; Shenvi, N. V.; Garg, R. P.; Summers, A. O.; Kurtz, D. M. *J. Bacteriol.* **1997,** *179,* 4607-4615.

(60) Johnson, K. A.; Verhagen, M.; Brereton, P. S.; Adams, M. W. W.; Amster, I. J. *Anal. Chem.* **2000,** *72,* 1410-1418.

(61) Petillot, Y.; Golinelli, M. P.; Forest, E.; Meyer, J. *Biochem. Biophys. Res. Commun.* **1995,** *210,* 686-694.

(62) Fujinaga, J.; Meyer, J. *Biochem. Biophys. Res. Commun.* **1993,** *192,* 1115-1122.

(63) Taylor, P. K.; Amster, I. J. *submitted* **2000**.

(64) Pierik, A. J.; Wolbert, R. B. G.; Portier, G. L.; Verhagen, M.; Hagen, W. R. *Eur. J. Biochem.* **1993,** *212,* 237-245

CONCLUSIONS

Analysis of metal incorporation during overexpression of *Clostridium pasteurianum* rubredoxin by electrospray FTICR mass spectrometry

ESI-FTICR has been shown to be a useful tool in the examination of numerous forms of metalloproteins, because of its inherent high resolution and high mass accuracy. The uptake of iron and zinc during the overexpression of rubredoxin was monitored at 15-minute increments beginning 30 minutes after induction and ending 180 minutes after induction. Samples were handled with minimal purification. Analysis of the data showed that iron is detected into Rd in the Fe(III) oxidation state, while zinc was detected in the Zn(II) oxidation state. Unless special care is taken to maintain the protein under reducing conditions, the metal center of metalloproteins is detected in its highest biologically relevant oxidation state.[1] Both Zn- and FeRd were observed in the earliest time point sample taken. Both ZnRd and FeRd showed an increase in concentration over time, consistent with protein production throughout the experiment. ZnRd concentration increased at a higher rate than did FeRd, consistent with either a greater rate of Zn^{2+} uptake vs. Fe^{3+} during protein production or displacement of Fe^{3+} by Zn^{2+} from FeRd after biosynthesis. Since no ZnRd has been observed in samples taken directly from the native biological organism, *C. pasteurianum*, it is possible that the organism employs metal sequestration. Future experiments conducted on *C. pasteurianum* cell lysate with a minimal amount of purification could determine the presence or absence of a zinc form of Rd in the bacteria.

Space charge effects on mass accuracy for multiply charged ions in ESI-FTICR

One of the strengths of FTICR is its high mass accuracy. However, space charge effects have been shown to decrease mass accuracy by causing shifts in the cyclotron frequency based on the ion density within the cell. If these frequency shifts can be accounted for, mass accuracy can be increased. Theory has been developed to characterize space charge-induced frequency shifts for singly-charged ions. ESI-FTICR has been used to examine space charge effects for multiply-charged ions. The observed variation in cyclotron frequency has been shown to be independent of charge state, in contradiction to widely accepted theory. In fact, ions of different charge states monitored simultaneously experience the same shift in frequency. This finding makes it possible to perform internal calibration on a charge state distribution without regard for the charge state of either the calibrant or analyte peaks. However, external calibration requires accounting for space charge-induced frequency shifts to attain the highest degree of mass accuracy. A plot can be made of frequency shift vs. signal intensity for a series of standards, and the slope of this plot can be used to account for space charge effects in a sample mass spectrum, lowering the error in mass accuracy by an order of magnitude. The sharpest decrease in mass accuracy error occurred when the calibrant and analyte had similar molecular weights and therefore a similar degree of transient complexity. Future research should explore in greater depth the relevance of charge state to space charge-induced frequency shifts for multiply-charged ions. Quadrupolar excitation has proven to accentuate space charge effects by compressing the ion cloud. Broad-band quadrupolar excitation would serve to axialize a wide range of charge states, increasing the frequency

shifts to a level more accurately measurable, on the order of a few Hz. A high degree of complexity in the transient can affect the intensities of the individual isotope peaks, so that summing the peak intensities may not be a true representation of the ion density. Previous research has shown that proper quantitation can be achieved by collecting for more thn two beats of the transient.[2] Future progress will require that more coherent, longer duration transients be acquired to discern if transients of different complexity can be used for external calibration.

Study of the binding of the substrate oxygen to multimeric hemoglobin by ESI-FTICR and Achieving isotopic resolution for noncovalent complexes of metalloproteins by ESI-FTICR

ESI-FTICR has proven to be a most beneficial technique in the study of noncovalent complexes. In order to obtain accurate mass measurements of noncovalent complexes, isotopic resolution must be achieved, requiring observation of the second beat in the FTICR transient. By using noncovalent complexes of increasing molecular weight, isotopic resolution has been obtained for complexes ranging from 23-64 kDa. Sodium contamination as well as space charge-induced peak coalescence have proven to be barriers to achieving isotopic resolution of high molecular weight noncovalent complexes. *Clostridium pasteurianum* ferredoxin, a 23 kDa dimer, contains a free cysteine per subunit in addition to the four cysteines involved in the iron-sulfur cluster. This free cysteine is involved in the binding of sulfur adducts, increasing the mass spectral complexity. Bovine hemoglobin forms both a 32 kDa dimer and a 64 kDa tetramer in solution. In addition to peaks arising from sodium adducts, low-intensity peaks have been observed in the correct

mass-to-charge range for oxygen binding. After overnight dialysis in oxygen-saturated buffer, the high resolution of FTICR allowed the detection of two molecules of dioxygen to the dimer, as well as four molecules of dioxygen to the tetramer. The second beat of the transient for *Desulfovibrio vulgaris* rubrerythrin has been observed for an 86 kDa transient, although isotopes are not discernable in the mass spectrum due to heterogeneity introduced by multiple sodium adducts. Extension of the capabilities of FTICR for these experiments will continue to prove useful, as high mass accuracy and high resolution studies of noncovalent complexes are able to detect specific binding of other species to the substrate, determine subunit stoichiometry, and identify nonspecific adducts. Further studies will require new methods of desalting to remove all sodium adducts without loss of the metal from metalloprotein noncovalent complexes, as well as mass spectral techniques such as quadrupolar excitation to increase signal-to-noise. Also, a more powerful magnetic field would increase the theoretically achievable resolution.

References

(1) Johnson, K.; Verhagen, M.; Brereton, P.; Adams, M.; Amster, I. *Anal. Chem.* **2000,** *72,* 1410-1418.

(2) Easterling, M. L.; Amster, I. J.; van Rooij, G. J.; Heeren, R. M. A. *J. Am. Soc. Mass Spectrom.* **1999,** *10,* 1074-1082.